TUBE ROW AND DAMPING PARAMETER EFFECTS ON TUBE-ARRAY STABILITY

by

MOHY ELDIN ELKASHLAN, B.Sc. (Math.) Hons., B.Sc. (Eng.) Hons.

A Thesis

Submitted to the School of Graduate Studies

in Partial Fulfilment of the Requirements

for the Degree

Master of Engineering

McMaster University

August 1980

TUBE ROW AND DAMPING PARAMETER EFFECTS ON TUBE-ARRAY STABILITY

MASTER OF ENGINEERING (1980)
(Mechanical Engineering)

McMASTER UNIVERSITY
Hamilton, Ontario

TITLE: Tube Row and Damping Parameter Effects on Tube-array Stability

AUTHOR: Mohy Eldin ElKashlan, B.Sc. (Alexandria University) (Math.) Hons.

B.Sc. (Alexandria University) (Eng.) Hons.

SUPERVISOR: Dr. D. S. Weaver

NUMBER OF PAGES: xii, 147

ABSTRACT

Modern heat-exchangers are susceptible to damage due to the excessive tube vibrations caused by the shell-side fluid flow. The present investigation seeks to further the understanding of flow induced vibrations due to fluid-elastic instability in tube arrays.

A low-speed wind-tunnel having 305 x 305 mm. working-section, was used to conduct the experiments. The tube-array was a parallel-triangle having a pitch/diameter = 1.375. The array was 18 rows deep with 5 tubes in each row. Nineteen elastically mounted movable tubes in the front of the array were especially designed so that natural frequency and damping could be controlled precisely over a wide range of values. Positions for as many as nine rows of fixed tubes in the front of the tube-array were available in order to facilitate studying the effect of tube-bundle size on tube response.

The experiments have indicated that the first tubes to become unstable in a particular tube-bundle are in the first few rows, and that the third and fourth rows are the critical ones. From the fluid dynamic damping-flow velocity results obtained for the array tested, it suggests the use of the static damping measured in still fluid for the estimate of the velocity for the onset of instability. For the first time a fluidelastic stability boundary as a function of the mass ratio has been determined experimentally for the array. This result

along with the result obtained by Grover for the fluid-elastic stability boundary as a function of the damping only, show that the mass ratio and the damping behave independently of each other, i.e., they should not be lumped together in the damping factor.

ACKNOWLEDGEMENTS

The author wishes to express his sincere gratitude to his supervisor Dr. D. S. Weaver, for his able guidance and encouragement during this investigation.

Thanks are due to Departmental technicians, Mr. Frank Drieman, and Mr. Dave Schick for their kind help during this work. The great effort of Ms. BettyAnne Bedell for her excellent typing of this manuscript is highly appreciated.

The financial support provided through the Natural Science and Engineering Research Council Operating Grant A8284 is gratefully acknowledged.

TABLE OF CONTENTS

LIST OF FIGURES

LIST OF TABLES

CHAPTER 1

INTRODUCTION

Flow induced vibration problems in heat exchanger and nuclear reactor tube bundles have become more common in the last few years as performance demands increase. Such vibrations have caused fretting and fatigue damage in the tubes at the tube sheets and baffles as well as mid-span leaks due to tube-to-tube clashing. This damage is very expensive to repair and has caused production loss and several shut-downs in nuclear power plants. Some statistics collected recently by Paidoussis [1] show some of the facts behind the damage and the cost of repair due to flow-induced vibration in heat exchangers in nuclear plants.

Flow-induced vibration problems continue to occur due to the following reasons: (i) flow-induced vibration is usually a secondary design parameter, as compared to the requirements of lower pressure drop and higher heat-transfer rates needed for higher equipment performance; (ii) the state of the art is still far from complete enough to allow fully successful design in all cases; (iii) feedback from the field is sometimes sketchy and insufficient to understand the actual problem; (iv) there is insufficient lateral communication with other engineering fields where the problems of flow-induced vibration are usually encountered.

During the last few years, a considerable technical

literature in the area of flow induced vibration has evolved but the diversity in geometric patterns and tube bundle sizes used in experiments as well as excitation mechanisms proposed left many unanswered questions. Several literature surveys have been done in order to clarify the state of knowledge and identify important areas for future research, Paidoussis [1], Shin and Wambsganss [2], and Savkar [3].

There appear to be four basic mechanisms causing tube vibrations; (1) vortex shedding; (2) turbulent buffeting; (3) acoustic resonance; and (4) fluidelastic excitation.

Fluidelastic mechanisms are those which depend crucially on tube motion. Experimental evidence on the whole seems to favour the whirling mechanism which is a result of the fluidelastic excitation of the tubes. The name was coined from the characteristic oval shaped orbits traced by the tubes. The mechanism was a result of Connors [4] work on a single-row of circular cylinders. As the flow crosses the tubes and the flow velocity exceeds a certain critical value, a large whirling vibration of the tubes is possible. Connors has established a fluidelastic stability boundary based on wind-tunnel test results coupled with quasi-static measurements of fluid forces. This instability was investigated experimentally, after Connors work, by several authors [5-9], using different tube patterns and spacings and fluids other than air.

Blevins [10] recently developed a two-dimensional analytical model for fluidelastic whirling of a tube row in cross flow, based on Connors earlier experimental work. He

assumed that the fluid forces on a tube are only dependent on the relative displacements of the two nearest tubes.

There is little experimental evidence to support the theory of Connors and the extension by Blevins. Weaver and Grover [9] showed that the relative motion of adjacent tubes is not necessary for instability to occur, i.e., a single flexible tube in a rigid tube bank will become unstable. In a subsequent study, Weaver and Lever [11] showed that the effect of detuning adjacent rows of tubes did not have the stabilizing effect predicted by Blevins [10]. Furthermore, the observations by Weaver and Grover [9] suggest that the predicted dependence of the critical flow velocity on the damping parameter is exaggerated. As the fluidelastic excitation in a tube-bundle can be correlated in terms of a dimensionless velocity parameter (V_p/fD) and a damping parameter ($m\delta/\rho D^2$), they raised a question; whether the dimensionless parameter ($m/\rho D^2$) and logarithmic decrement δ should be lumped together or not.

The purpose of the present investigation is to clarify some of the unanswered questions. In particular, it is to determine:

(1) The effect of flow-field velocity on the tube damping,

(2) The effect of tube-bundle size on the fluidelastic stability threshold.

(3) Whether or not the dimensionless parameter ($m/\rho D^2$) and logarithmic decrement δ should be lumped together in the damping factor.

It is hoped that this experimental program will be helpful in understanding the fluidelastic whirling mechanism and in the design of simpler and more meaningful future experiments.

CHAPTER 2

A SURVEY OF FLOW INDUCED VIBRATION

Structures are subjected to flow-induced vibration as a result of the interaction of elastic and inertial forces of the structure with the fluid forces. The amplitudes of such vibrations depend on the damping, mass and the stiffness of the structure as well as on the velocity of the fluid flow and the fluid density.

The physical situation in which flow induced vibration problems arise are extremely diverse and, often the excitation mechanisms are not well understood.

This field finds its greatest applications in the areas of tube vibrations in heat exchangers and steam generators [1], [2], [12], vibrations of hydraulic components and structures [13], [14], and in the areas of marine structures [15] and space science [16]. Ground boundary layer turbulence effects on buildings and structures [17] is another important area encompassed by this field.

Because of the complexity of the phenomena of flow-induced vibration and increasing occurences, the technical literature is expanding rapidly. The papers usually treat very specific problems and are published in diverse journals. Few attempts have been made to classify the hydroelastic instabilities according to the way in which they were affected

by damping [18], or through their common flow instability mechanisms [19]. However, in general, flow induced vibrations can be characterized as forced, self-controlled and self-excited vibrations.

Forced vibrations are induced by turbulence or pressure fluctuations in the flow or fluid impact. These motions are usually random in nature and are called 'forced' since the motion of the structure usually has no appreciable effect on the fluid forces. Some of the problems subjected to this kind of dynamic excitation are complex and difficult to analyze. One of these problems is the loading condition for a marine vehicle which operates at an interface between air and water. Other examples are the dynamic response of spacecraft structures to boundary-layer excitation and dynamic response of pipe transporting fluids. The response of high buildings to ground boundary layer turbulence is a related problem which is of great practical interest. Ship slamming is one of the problems which is associated with hydrodynamic impact. The problem in these kinds of forced vibrations is knowing the force field. Once it is known, the analysis is relatively straight-forward.

Self-controlled vibrations are ones where some periodicity exists in the flow. If this happens to coincide with one of the natural frequencies of the structure, the amplitude of vibration builds up to the point where the magnitude and frequency of the fluid forces are controlled by the motion of the structure and a dynamic feedback mechanism develops. The most common source of this periodicity in the flow is the vortex-

shedding phenomenon. Vortex shedding results also in acoustic resonance which causes noise generation. Vibrations of submarine periscopes, hydraulic-turbine-blade vibration and smokestacks are examples of this class of vibration. It is clear that, addition of stiffening or damping may prevent such oscillations as well as some geometry change which will destroy the periodicity in the flow.

In self-excited vibration, the oscillations of the structure result in periodic forces which amplify the structure's motion. These vibrations are distinguished from those of self-controlled vibrations in that the periodic forces disappear in the absence of structural motion. Self-excited vibrations of submerged vertical lift hydraulic gates, oscillations of gate seals and hydroelastic vibration of swing check valves are some examples of this class of vibration. In such cases, a change in geometry may be the most effective remedy.

Self-controlled and self-excited vibrations are referred to as fluidelastic vibrations (aeroelastic or hydroelastic) and involve the mutual interaction of elastic and inertial forces of the structure with the fluid forces. A necessary condition for such a designation is that the motion of the structure alters the fluid forces acting on it.

The analysis and development of mathematical models for fluid-structure interaction problems draws on four disciplines: (1) theory of elasticity; (2) mechanical vibration; (3) fluid mechanics; and (4) mathematical stability theory.

Flow induced structural vibrations are associated with

the transfer of energy from the fluid to the structure. This energy transfer is the result of non-conservative dynamic forces which appear in the differential equations of motion as terms capable of adding or taking away energy from the system. The adequacy of formulating the differential equations of motion depends on the degree to which the mechanism of excitation is understood. This may be viewed as consisting of the determination of the so-called structural operators, inertial operators, and fluid dynamic operators.

The major difficulty of fluidelasticity centres around the fluid-dynamic operators. This is a result of the often nonlinear and/or stochastic nature of these operators.

Due to complexities of the flow field and the dependence of component vibration characteristics on fluid structural interaction, scale model tests are relied upon to verify design adequacy and for the determination of the fluid-dynamic operators of any future mathematical analysis.

To study the response and stability of these dynamic models, wind-tunnels, water-tunnels, water-loops, and two-phase flow-loops are commonly employed.

Broadly grouped according to flow configuration, the vibration problems in heat-exchangers and nuclear reactors are distinguished as being induced by (a) cross-flow, (b) internal axial (pipe) flow, (c) external axial flow, and (d) annular and leakage flow. The following will be confined to the situation of uniform cross-flow, as this is the concern of the research reported here.

The literature on flow-induced vibrations on circular cylinders in cross-flow is vast, scattered and in the main very inconclusive. Clear results have been obtained mainly for highly idealised situations involving isolated single cylinders or single rows of cylinders. Whilst these are useful for gaining some physical understanding of the processes, their immediate application to the case of bundles remains doubtful, particularly when the motion is allowed. Savkar's [3] major review discusses many of these idealised situations.

The consensus now seems to be that there are four main problems in flow-induced vibrations. These are:

(1) Vortex shedding from the tubes.

(2) Turbulent buffeting; the response of the system to turbulence, i.e., more random excitations than in pure vortex shedding.

(3) Acoustic resonance in the transverse direction in the the shell side fluid.

(4) Fluidelastic mechanisms.

Flow-Induced Excitation Mechanisms in Bundles of Circular Cylinders in Cross-flow

1. Vortex shedding:

In two-dimensional fluid flow across a single cylinder or arrays of parallel cylinders, the tubes are excited by the formation of vorticity in the wake of the cylinders [20]. As vortices are shed, an alternating wake-pressure field is attained and forces the cylinders to vibrate at a frequency f_s, given by:

$$f_s = \frac{SV}{D}$$

where

S = dimensionless frequency or Strouhal number

V = free-stream velocity

D = diameter of circular cylinder

This f_s may match with one of the structural natural frequencies of the tube or tubes, f_n. If this happens, the amplitude of vibration builds up to the point where the magnitude and frequency of the fluid forces are controlled by the motion of the structure. This results in the development of a dynamic fluid-cylinder feedback mechanism. The velocity range over which the fluid forces are controlled by the structural vibration frequency is called the 'lock-in' region. The width of this region depends on the amount of damping in the structure. In the case of a single cylinder, f_s 'locks in' to f_n, when the tube is allowed to vibrate and is not overly damped. This lock-in, appears in the form of resonance, and it may cause destructive oscillations of the tube. Whether or not 'lock-in' occurs significantly in arrays is still in some doubt.

Owen [21] opines that at high Reynolds number, the flow deep in the array is more or less completely turbulent. The energy associated with these turbulent pressure fluctuations rather than being concentrated at a discrete frequency, are normally distributed over a wide range of frequencies. This may not allow 'lock-in' to occur in arrays. For in-line arrays the situation could be different as the open channels between

tube columns may allow laminar flow to be formed deep in the array. However, there are no systematic studies of the turbulence spectra available, and a few streakline visualisations on models of tube arrays have been produced [3], and [31]. Some actual spectral analyses, showing both vortex shedding and turbulence, are shown in Figure 2.1, from a recent paper [11] of Weaver and Lever.

The nature of the vortex shedding is dependent on the Reynolds number. The major regimes of fluid flow across a rigid circular cylinder are shown in Figure 2.2. At extremely low Reynolds numbers (<5), the flow streamlines in the wake of the cylinder are close to each other and the flow does not separate, as shown in Figure 2.2a. As the Reynolds number is further increased, the streamlines widen up and a pair of fixed "Föppl" vortices is formed immediately behind the cylinder at Reynolds numbers in the range 5-15, as shown in Figure 2.2b. Tritton [22] showed and confirmed that at a Reynolds number of about 40, the vortex pair behind the wake of cylinder becomes unstable. At a Reynolds number of about 90, one of the vortices breaks away from the cylinder. This separation causes a wake-pressure field asymmetry and the other leaves. This process repeats itself, and a state of alternating vortex shedding is attained, as shown in Figure 2.2c. For the Reynolds number range below 150, in which the free vortex layers roll up into vortices prior to transition, the resulting vortices are purely viscous. The main body of the fluid in such vortices is laminar, and the vortex street is preserved for many diameters downstream.

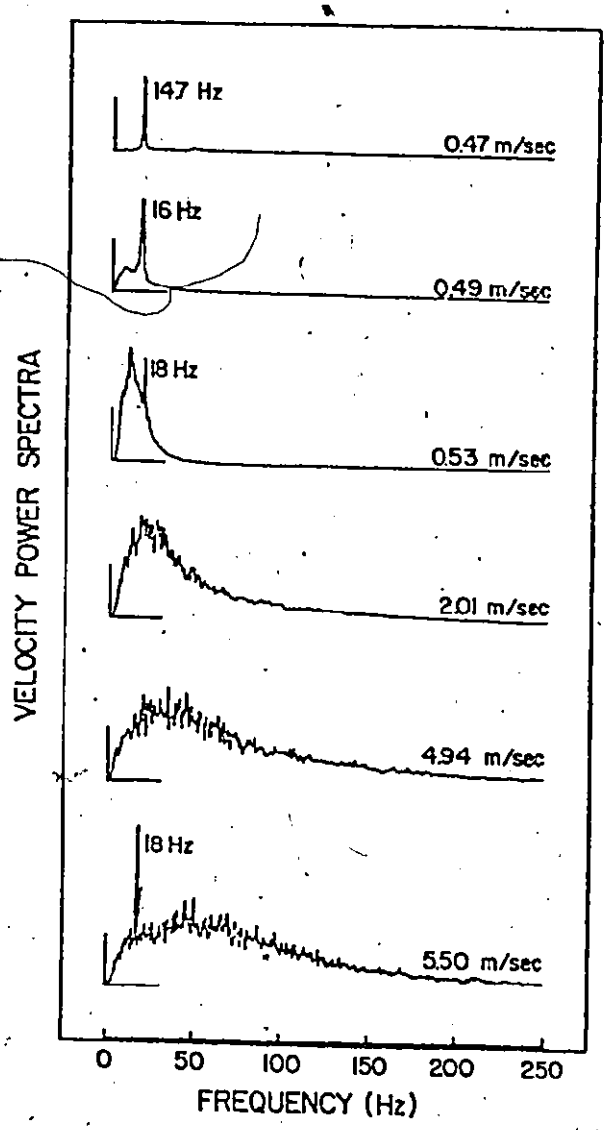

Fig. 2.1 Velocity Power Spectra (from Ref. 11).

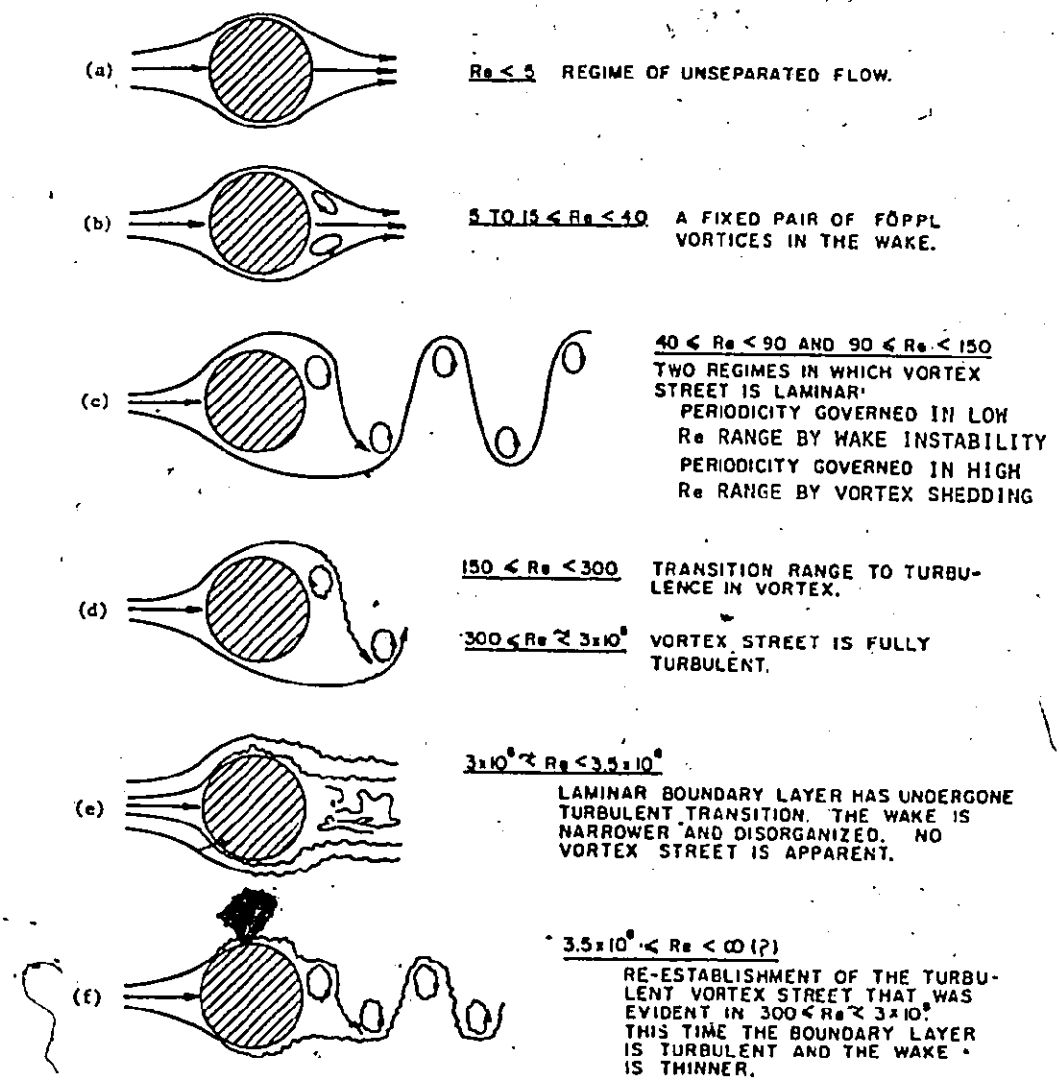

Fig. 2.2 Regimes of Fluid Flow across Rigid Circular Cylinder (from Ref. 25).

As the Reynolds number is increased beyond the vortex-shedding point to the range of 150 to 300, a laminar-to-turbulent transition begins in the free vortex layers before breaking away into the street, as shown in Figure 2.2d. At a Reynolds number of about 300, and continuing up to approximately 3×10^5, the vortex street is fully turbulent. In the Reynolds number range 3×10^5 to 3.5×10^6, the laminar-boundary layer has undergone turbulent transition, the wake is narrower and disorganized, and no vortex street is apparent, as shown in Figure 2.2e. As the Reynolds number is increased beyond 3.5×10^6, the turbulent vortex street forms and the wake is thinner, as shown in Figure 2.2f.

Chen [23] and some other investigators studied the variation of Strouhal number with Reynolds number. In the case of flow crossing an isolated single stationary cylinder, it was found that the Strouhal number remains approximately constant with a value of 0.21 over the range of Reynolds number from 300 to about 2×10^5. As the Reynolds number is further increased to about 3.5×10^5, the Strouhal number increases up to a value of 0.27 due to the narrowing of the wake of the flow. Beyond a Reynolds number of about 3.5×10^6, no further change in Strouhal number seems to occur as the turbulent vortex reestablishes.

The flow approaching a cylinder at an angle other than perpendicular to the longitudinal axis has also been studied. However the flow characteristics within a tube bundle are much more complicated than for an isolated single tube.

Grover [24], refers to arrays, by the names 'square', 'rotated square', 'parallel-triangle', and 'perpendicular triangle' (see Figure 2.3), these being common geometries in actual applications. However, in general, they may be referred to as in-line (square and parallel-triangle arrays) and out-of-line or staggered tube patterns (rotated square and rotated-triangle arrays).

Chen [23] also studied the variation of Strouhal number with tube spacings for in-line and staggered tube arrays. The Strouhal numbers obtained in Chen's experiments are functions of the transverse and longitudinal spacing ratios, T/D and L/D, respectively, of the tube array, as shown in Figures 2.4 and 2.5. In general, for in-line tube arrays the Strouhal number increases with decreasing longitudinal tube spacing ratio and increasing transverse tube spacing ratio. A Strouhal number as high as 0.48 was reported, for a longitudinal tube spacing ratio of 1.25 and a transverse tube spacing ratio of 1.6. For a staggered tube array and a given longitudinal spacing, the Strouhal number peaks at a transverse tube spacing ratio of about 2.1. Strouhal numbers as high as 0.7 were reported, for a longitudinal tube spacing ratio of 1.25.

When flow crosses a cylinder the fluid-dynamic forces acting on the cylinder can be resolved into two types:
(1) drag forces F_D acting in the direction of flow, and
(2) alternating lift forces F_L acting transverse to the flow direction. In turn, the drag force F_D can be resolved into two

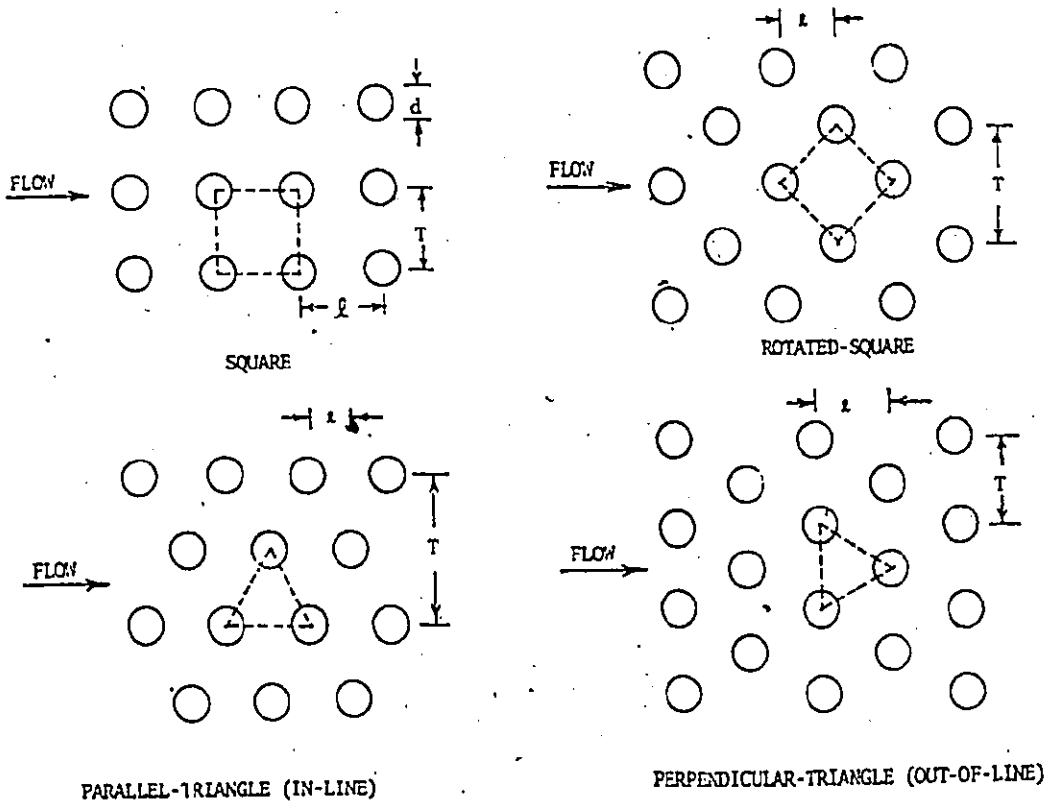

Fig. 2.3 Commonly Used Tube Arrays (from Ref. 24).

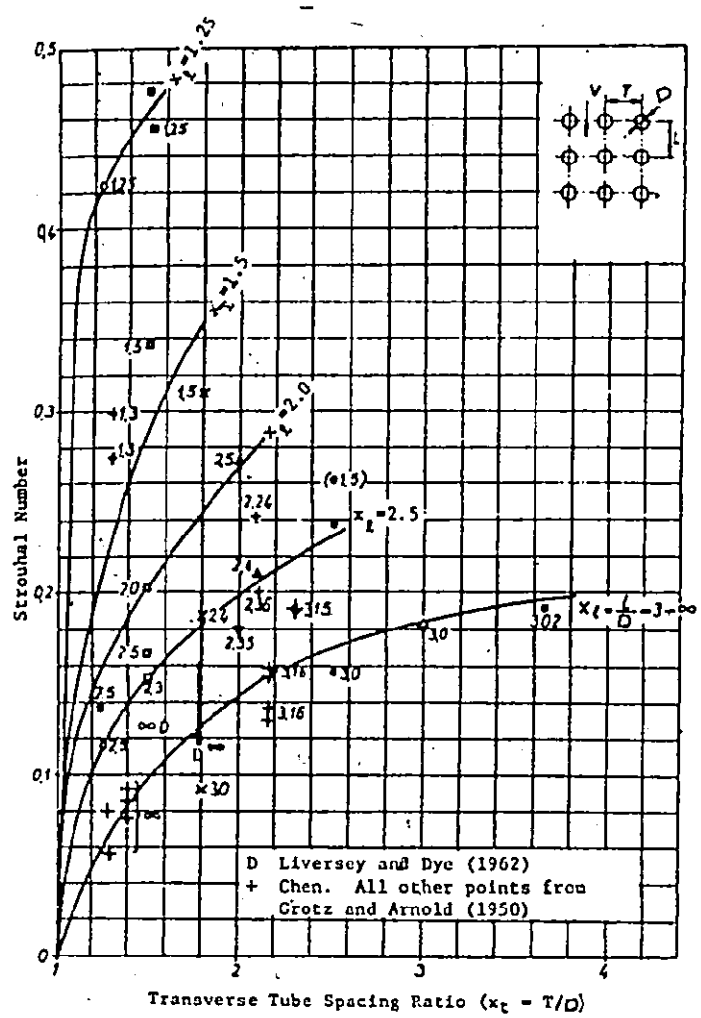

Fig. 2.4 Strouhal Number vs Transverse Tube-spacing Ratio with Longitudinal Tube-spacing Ratio (X_ℓ=L/D) for In-line Tube Branks (from Ref. 23).

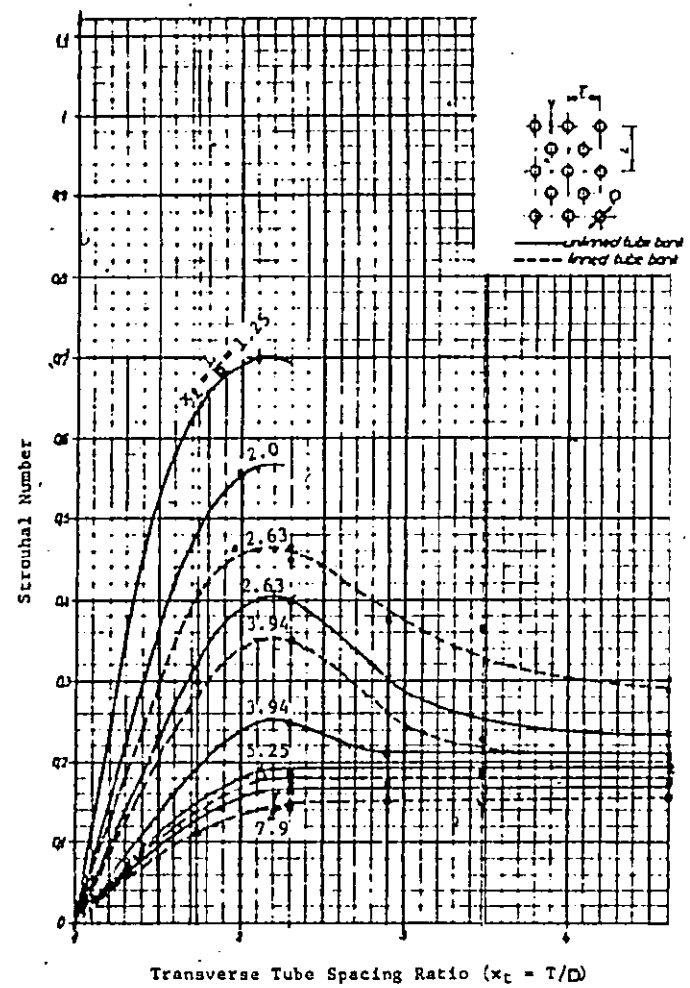

Fig. 2.5 Strouhal Number vs Transverse Tube-spacing Ratio with Longitudinal Tube-spacing Ratio (X_ℓ=L/D) for Staggered Tube Banks (from Ref. 23).

components: pressure drag and frictional drag. The pressure drag results from the pressure distribution over the surface of the cylinder. The frictional drag results from the viscous shear force on the surface of the cylinder. For a given flow velocity, the frictional drag force is relatively constant, while the pressure drag force contains a constant component and an oscillatory component. This oscillatory component is associated with vortex shedding. At very low Reynolds numbers the frictional drag force is dominant. As the Reynolds number is increased, the frictional drag force gradually becomes negligible in comparison with the pressure drag force. The alternating lift force is totally associated with the vortex shedding. However, since the excitation in the lift direction is 5 to 10 times higher than the excitation in the drag direction (because of the greater force coefficient), the lift direction is of primary importance in tube response analysis.

A dimensional analysis by Lienhard [25] shows that the magnitude of the drag and lift forces acting on a cylinder can be expressed in the following forms:

Drag force: $F_D = C_D \frac{1}{2} \rho A V^2$;

Lift force: $F_L = C_L \frac{1}{2} \rho A V^2$.

where

F_D, F_L = time averaged drag force and lift forces respectively,

C_D, C_L = drag and lift coefficients, respectively,

ρ = mass density of fluid

A = projected area per linear length of cylinder (outer diameter of the cylinder)

V = free-stream velocity.

Lienhard also reviewed most of the experimentally determined data on drag and lift forces for an isolated single stationary cylinder, and plotted the values of the drag and lift coefficients over a wide range of Reynolds numbers. His plot indicates that, at the low Reynolds number range 0.5 to 300, the mean drag coefficient C_D varies from 20 to 1. As the Reynolds number increased beyond 300 and up to less than 2×10^5, a nearly constant value of $C_D = 1.1$ is preserved.

Measurement of the mean oscillatory lift coefficients for the Reynolds number range 10^4 to 10^6 was compiled by Chen [26]. The scatter of the data was large compared to the drag coefficient data. Specific values of C_D and C_L cannot be assigned with certainty because of the wide variation in measured values.

The vortex-shedding phenomena of a vibrating cylinder has been studied by Bishop and Hassan [27]. They reported that the transverse lift increased for a vibrating cylinder over that for a rigid cylinder presumably due to improved shedding correlation.

The added mass per unit length which should be used to calculate the natural frequency for the cylinder is still under study. Fitz-Hugh [28] simply uses the classic potential theory. For potential flow, the added mass has long been known to be just the mass of displaced fluid. The effect of

boundary layer separation is still undecided. Savkar [3] reviewed some of the data available for the added mass.

For tube arrays, Chen [26] presented some measured data of the oscillatory lift coefficient as a function of the longitudinal-tube spacing ratio L/D and the transverse-tube spacing ratio T/D. The data indicated that the oscillatory lift coefficient depends on tube spacings as well as Reynolds number. However, in closely packed tube arrays, a vortex street in the usual sense has no room to form. The constant Strouhal number periodic forces are not understood and have become known as "vorticity shedding" to distinguish them from von Karman vortex streets.

2. Turbulent buffeting

Turbulent pressure fluctuations occurring in the wake of a tube or carried to it from an upstream disturbance was suggested by Owen [21] as providing a mechanism of excitation.

The energy associated with turbulent pressure fluctuations are considerably distributed over a wide range of frequencies, and the tube selects for its response primarily that portion of the energy spectrum that is close to a natural frequency. The turbulent excitation mechanism gives rise to a behavior associated with a randomly forced, damped vibration. The amplitudes of vibration will be very small at low flow velocities and are expected to increase in direct proportion to the dynamic head ($1/2\ \rho U_o^2$), as long as the motion of the tube does not effect the turbulent fluid forces.

For closely-packed tube arrays, as the vortex shedding becomes less distinct, and the wakes more turbulent, turbulent buffeting becomes increasingly important. Owen is of the opinion that this is in fact the only mechanism of importance, due to the cummulative growth of random motions as one progresses deep into the tube array. Owen conducted his experiments with heavy, stiff tubes, for which turbulent buffeting is the more important excitation. Owen explained the tube vibrations sufficiently deep inside the tube array by the randomly fluctuating pressure turbulent forces as follows.

Starting with a simple hypothesis that the dominant frequency of the pressure turbulent fluctuations is identifiable with the dominant frequency of the fluctuating force on the tubes, the former is proportional to the average flow velocity through the tube array. As this velocity is increased from zero, two resonant conditions may arise, one when the dominant frequency matches with a natural frequency of the tube, the other is an acoustic resonance when the shell side fluid is gaseous. Theoretical considerations led to the equation:

$$\frac{f_b L}{U} \frac{T}{D} = K \left(1 - \frac{D}{T}\right)^2,$$

where

f_b = dominant turbulent buffeting frequency,

L = distance between centerlines of successive tube rows (see Figure 2.6)

T = transverse spacing of tube (see Figure 2.6)

D = outer diameter of tube

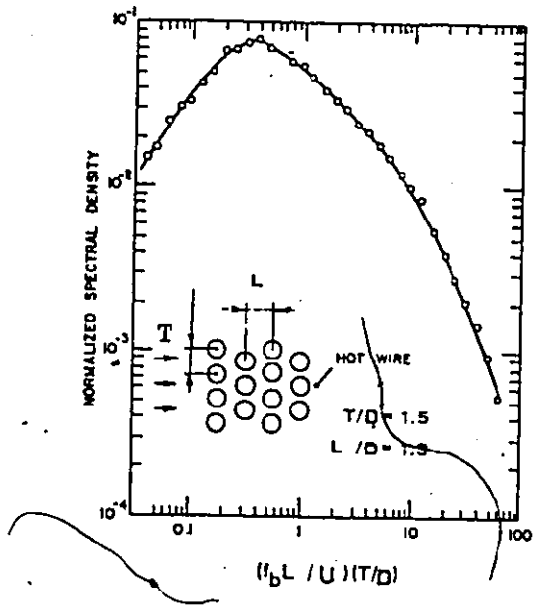

Fig. 2.6 Typical One-dimensional Turbulent-energy Spectrum Determined Experimentally (from Ref. 21).

U = mean flow velocity between adjacent tubes,

and

K = constant.

Based on experimentally determined data, Owen suggested a value for $K = 3.05$. Owen also proposed a rule for estimating f_b in the form: the dominant frequency of the vibration in a bank of tubes, for which the ratio of the diameter to the lateral spacing lies between 0.2 and 0.6, is equal to the interstitial flow velocity divided by twice the distance between successive rows, i.e.,

$$f_b = \frac{U}{2L}$$

When both sides of this equation are multiplied by $\frac{D}{U}$, this yields the Strouhal-number relationship:

$$\frac{f_b D}{U} = \frac{D}{2L}$$

Owen also included an experimentally determined one-dimensional turbulent-energy power spectrum, reproduced in Figure 2.6.

This figure indicates that the pronounced peak occurs near $(f_b L/U)(T/D) = 0.4$ for tube spacings $T/D = 1.5$ and $L/D = 1.3$. However, the data discussed by Owen, having been measured downstream of the array, is strongly dominated by the effect of the free wake of the last row and is certainly not indicative of the bulk of the array.

Brunn and Davies [29] reported some useful quantitative

data for isolated cylinders, concerning the point of buffeting of the array. Their observations showed that there is little influence of the upstream turbulence on the wake region. This therefore backs up Owen's observations that any buffeting, deep within a tube array, is due to wake interaction rather than any upstream turbulence carried to the wake.

Weaver and Grover [9] showed that Owen's predictions may be improved for closely packed tube arrays by using the velocity in the minimum gap rather than the transverse spacing of tubes in a row.

The results shown in Figure 2.1 (Weaver and Lever [11]) for some velocity power spectra show how vortex shedding goes over to turbulence in tube arrays.

3. Transverse acoustic resonance in the shell-side fluid:

This type of flow-induced vibration manifests itself as an intense noise radiating into the surroundings. The steady cross-flow in the inlet and outlet zones of shell-side fluid over tube arrays of steam generators can also induce a standing pressure wave perpendicular to both tubes and flow which can cause extensive structural damage to the shell, and a large pressure drop along the shell-side fluid. This problem increases when the fluids are dense liquids or heavily compressed gases.

This type of excitation can be caused by vortex shedding. Chen [23], [26], [30] and Funakawa [31] treat the

acoustic resonance excitation as an aspect of vortex shedding in tube arrays. Whether instances arise where it is due to fluidelastic excitation of the tubes still is unknown. It is very dangerous when a resonant frequency of the shell coincides with a natural frequency of the tubes since a coupling between vortex shedding, tube vibration, and transverse acoustic oscillation will arise.

Morse [32] gives the transverse acoustic standing-wave resonant frequency f_a, for a cylindrical shell, in the form:

$$f_a = \pi \alpha_m \frac{c}{d_s},$$

where

c = velocity of sound in fluid,

d_s = inner diameter of the cylindrical shell,

and α_m = constant depending on the mode excited (for modes from 1 to 8, Morse reported the corresponding values of α_m).

For tube arrays, Chen [33] gives the threshold criterion for excitation as:

$$\frac{R_e}{S} \frac{(L-D)^2}{L} \frac{D}{T} \geq 600,$$

where

R_e = Reynolds number,

S = dimensionless frequency or Strouhal number,

L = distance between centerlines of successive tube rows,

D = outer diameter of tube,

and

T = transverse spacing of tubes.

To avoid a coupling between the transverse acoustic oscillations and the tube vibration, Chen suggested that the flow velocity should be increased past the critical velocities exciting the acoustic resonances sufficiently fast that the acoustic mode does not have time to build up. Chen also recommended the insertion of detuning baffles along the flow direction in heat exchangers. The baffle length should be large compared with the sound wave length expected, but not so long that local resonances, which may be obtained, are no longer local.

Funakawa [31] also investigated the locked-in shedding frequencies as a function of Reynolds number and the geometry of the array. The results obtained by Funakawa supported that of Chen's work.

Zdravkovich [34] reported that, acoustic resonance can be minimized by omitting some tubes in a tube array to disturb the regular flow pattern.

4. Fluidelastic mechanism:

Vibration of aircraft-wing flutter and transmission-line galloping are the most familiar examples of fluidelastic vibration. The vibration in such cases involves single bodies essentially isolated in a uniform flow field. The excitation

mechanism is mainly due to the change in the angle of attack which results in a change of the lift force exerted by the body. Since the change in the angle of attack is a direct result of the vibrational motion, the oscillations are clearly self-excited. Although isolated cylinders of non-circular cross section can, under certain conditions, develop plunging oscillations (galloping) associated with a changing angle of attack, the symmetry of an isolated circular cylinder rules out such a mechanism for it [4].

In single and multi-row arrays of circular cylinders, the situation is quite different from that for a single isolated cylinder, and other types of fluidelastic excitation not based on angle of attack are possible. It seems that the most important of this kind of excitation for tube arrays is the fluidelastic whirling where most of the research during the last few years lies.

When a flow crosses single- and multi-row tube arrays, and the flow velocity exceeds a certain critical value, a large whirling vibration of the tubes is expected. The vibrations are of a self-excited or fluidelastic nature in that, once initiated, the vibration amplitude will grow sufficiently to cause tube-to-tube clashing and extensive tube damage. These vibrations were observed by Connors [4]. Connors explained this fluidelastic excitation mechanism as the momentary displacement of one tube in a row from its normal equilibrium position, altering the flow field, thereby upsetting the force balance on neighboring tubes and causing them to also

change their positions in a vibratory manner. If, during a cycle of vibration, the energy extracted from the flowing fluid by the tubes exceeds the energy dissipated by damping, a fluid-elastic vibration is established. Connors also established a fluidelastic stability threshold, based on wind-tunnel test results from a single row of tubes, coupled with quasi-static measurements of fluid forces. He showed the stability boundary above which fluidelastic instabilities occur to be defined by the empirical relationship,

$$\frac{U}{f_o D} = 9.9\sqrt{\frac{m_o \delta_o}{\rho D^2}}$$

where

U = mean flow velocity between adjacent tubes,

f_o = natural frequency of tube,

D = outer diameter of tube,

m_o = virtual mass of tube per unit length (equals the mass of the tube itself, plus the added mass of the displaced fluid),

δ_o = logarithmic decrement of damping of tube in still fluid, dimensionless,

and ρ = mass density of fluid.

His stability diagram for the array tested is shown in Figure 2.7.

Several other authors [5-9] also investigated this instability experimentally, using different geometric patterns

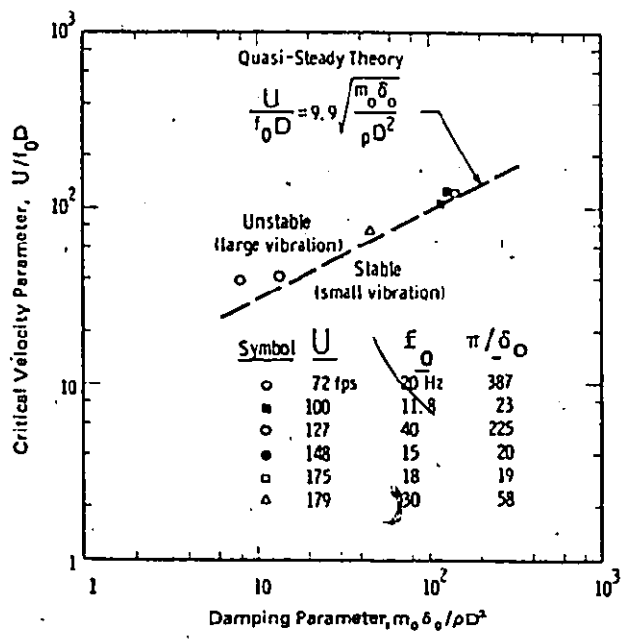

Fig. 2.7 Stability Diagram for Single-row Arrays Having a Pitch-to-Diameter Ratio of 1.41 (from Ref. 4).

and tube bundle sizes and fluids other than air. Much of the available experimental data on critical flow velocities for tube arrays has been compiled by Shin and Wambsganss [2] in the form of a stability diagram and is reproduced in Figure 2.8. The experimental results obtained by Hall et al. [8] from air flow tests on overhung spans of finned U-tubes simulating a sodium-to-air heat exchanger, seems to be in a good agreement with that obtained by Connors. Also shown are the results obtained by Pettigrew and Gorman [5], Hall and Lawrence [6] and Mirza and Gorman [7] for liquid flow. The only results obtained for a two-phase flow are those obtained by Pettigrew and Gorman [5], as shown in Figure 2.8. The effect of Reynolds number is included only implicitly in these plots, hidden in the value of the proportionality constant which is 9.9 for Connors' experiments and which depends also on array geometry. Figure 2.8, also shows that the fluidelastic instability in liquid flow is overlapping that for vortex shedding. In this overlap region, it may not be possible to detect two distinct mechanisms in practice.

Hartlen [35] pointed out that the factor $(f_oD)^{-1}$ in Connors' fluidelastic stability boundary is approximately proportional to tube-span-to-diameter ratio, which does not vary greatly for typical designs; thus, the dimensionless factor (U/f_oD) depends primarily on the shell-side velocity. Schematic stability maps of Hartlen are shown in Figure 2.9. The regions for low, medium and high shell-side fluid densities can be seen as well as the vortex shedding region.

Blevins [10] developed a two-dimensional analytical

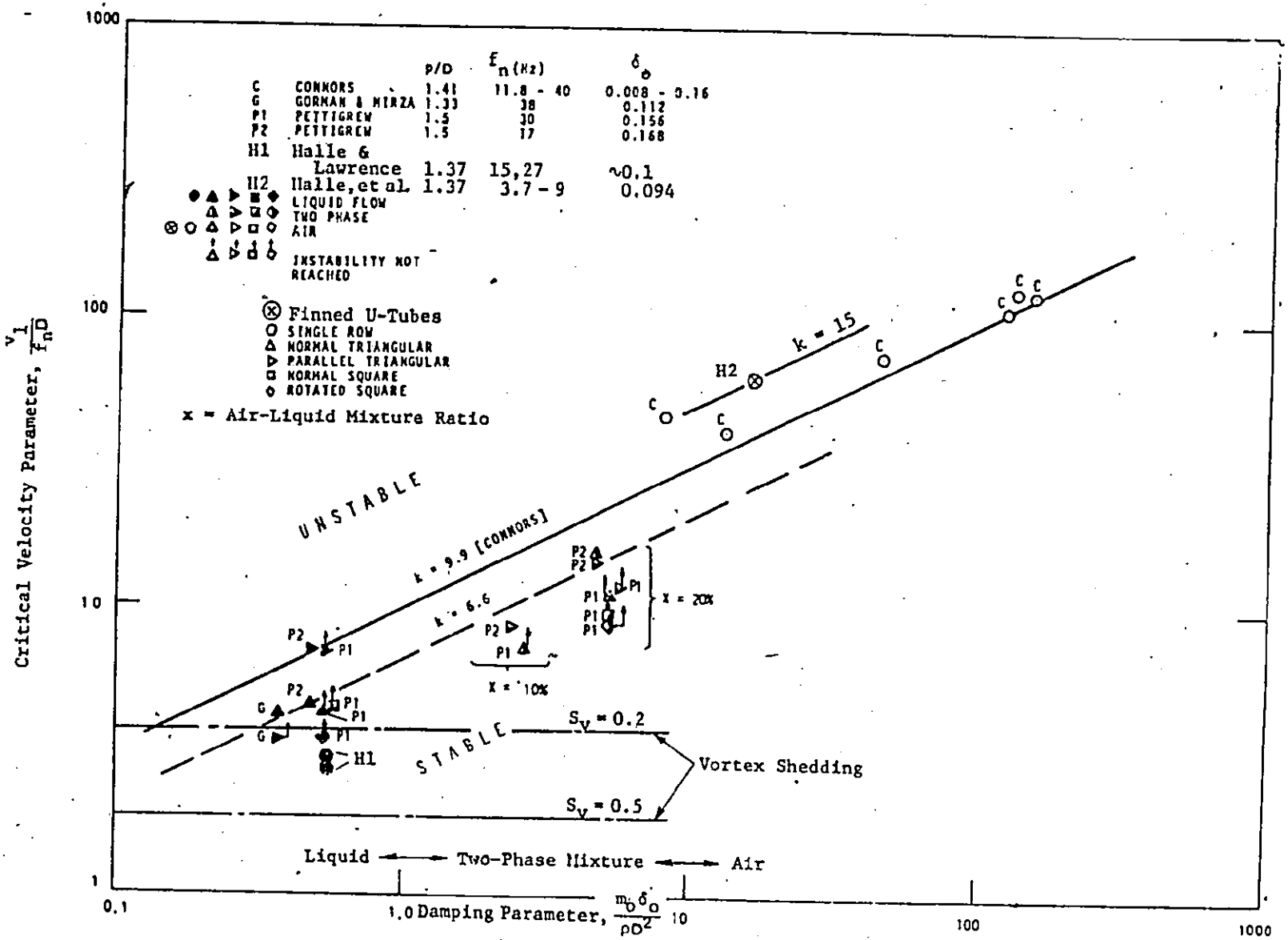

Fig. 2.8 Stability Diagram for Tube Arrays (from Ref. 2).

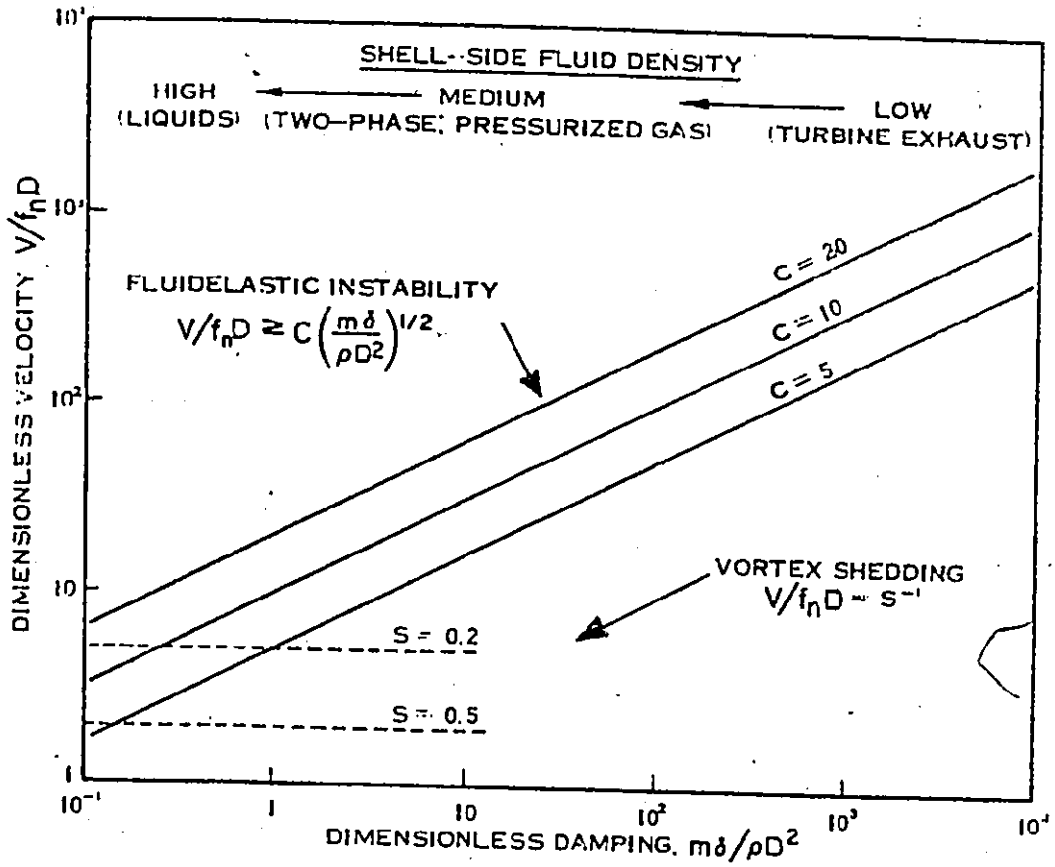

Fig. 2.9 Conceptual Boundaries of Flow-induced Vibration (from Ref. 35).

model for fluidelastic whirling of a tube row in cross flow, based on Connors' earlier experimental work. He assumed that the tubes are not excited by vortex-shedding and jet-switching mechanisms which Connors had verified. Blevins reported the following results:

a.) The critical flow velocity is a function of both the natural frequencies and damping factors of tubes in both co-ordinate directions,

b.) The critical flow velocity increases sharply with increasing the separation of the natural frequencies of adjacent tubes.

c.) The critical flow velocity increases as the number of tubes in the row decreases.

d.) A tube row bounded on one side by a wall and on the other side by a fixed tube can have a lower critical flow velocity than if the same tube row were bounded by fixed tubes.

The result quoted in part (b) is the one which prompted the research of Weaver and Lever [11]. Their results showed that, in the case of arrays, detuning by up to 3% increases the critical flow velocity, but increasing the difference beyond this brings the critical velocity down again. Blevins' theoretical predictions are quite different.

Recent results of Weaver and Grover [9] suggest that $\delta^{0.21}$ is more reasonable for the prediction of the onset of instability than $\delta^{0.5}$ as suggested by Connors' work. They point out that there is no reason, on purely dimensional grounds,

of lumping the dimensionless parameters ($m/\rho D^2$) and logarithmic decrement of damping δ together, and suggest a fluid-elastic stability boundary in the form:

$$\frac{V_p}{fD} = \left[\frac{m}{\rho D^2}\right]^{1/2} \delta^{0.21}$$

They also warn of the dangers of non-conservative stability predictions if $\delta^{0.5}$ is used to extrapolate test results from low δ models to higher δ prototypes.

Roberts [36] observed a jet-switching mechanism in a single-row tube array. When a flow crosses a closely packed tube array, the fluid forms jets as it issues from the gap between the tubes. Later, Connors [4] also investigated the mechanism in connection with fluidelastic whirling of tubes. Connors noted that the jet switching mechanism is of secondary importance in the self-excited vibration of tube arrays.

Savkar [3] discussed the possibility of two other fluidelastic mechanisms, a negative stiffness mechanism which is quasi-steady (position dependent) and an aerodynamic flutter instability mechanism (time velocity dependent). There do not appear to be any publications showing these as possible mechanisms in tube arrays.

In summary, it can be said that the possible mechanisms causing tube vibration in an array appear to be vortex-shedding, turbulence, acoustic resonance and fluidelastic mechanisms. The amplitudes of vibration reported experimentally due to fluid-elastic excitation show that it could be the principle mechanism causing tube damage in practice. The general trend for critical

velocities seems to be in the order:

Single rows > staggered arrays > in-line arrays

Connors' stability boundary is still used widely as a design guide. However, there appears little evidence to verify that the exponent in such a boundary should be 0.5 for tube arrays. The theory of Connors and Blevins, showing the 0.5 power law of the damping factor, is only an approximation for the experimental result obtained by Connors using a single row of circular tubes. In reality, a straight line with a 0.4 power of the damping factor comes much closer as shown by Savkar [37]. Also there is no sound reason for lumping the dimensionless parameters $(m/\rho D^2)$ and δ in the damping factor.

CHAPTER 3

EXPERIMENTAL EQUIPMENT

In the existing wind-tunnel (designed by Grover [24]), both vortex shedding and fluidelastic tube vibrations can occur distinctly in the same tube array. The developed rig was used to achieve the following parameter ranges:

Damping parameter ($m\delta/\rho D^2$): 2 to 62

Velocity parameter (Vp/fD) : 3 to 100

Such a damping parameter range usually corresponds to two-phase shell side flow in heat exchangers.

Piano-wire movable tubes were used, so both the damping and natural frequency could be varied over a wide range of values without changing the diameter, length or mass of the tube. However, as the purpose of part of this study was to change the damping parameter by varying the tube mass while keeping the damping constant, the design of the test section allowed the tubes to be changed without changing the test section. Also, a facility of adding tube-rows upstream was available.

3.1 The Wind-tunnel

The low speed wind-tunnel used for this study is shown schematically in Figure 3.1.

The contraction section of the wind-tunnel is made of 3.2 mm. birch plywood mounted on oak bulkheads. The length of

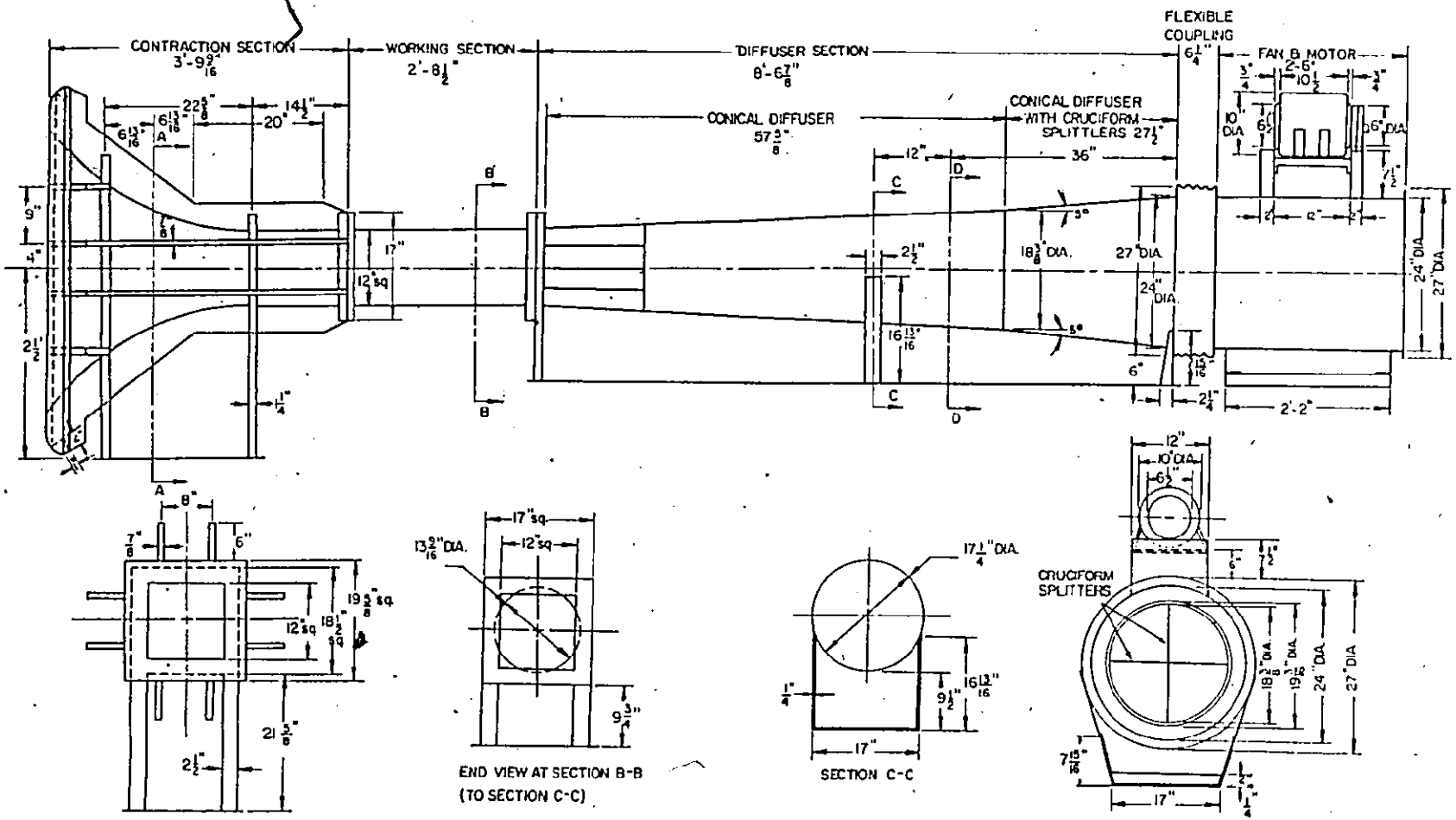

FIGURE 3.1 SCHEMATIC OF THE WIND - TUNNEL

the section is approximately 1.14 m. and contraction takes place from 1.45 m. square at the inlet to 0.31 m. square at the exit (a contraction ratio of about 22:1). The use of a contraction section upstream of the working section considerably reduces spatial irregularities in the velocity distribution and also results in low turbulence levels at the working section.

The skeleton of the working section is a box type structure made up of four perspex plates (13 mm. and 19 mm. thickness) bolted together. The front and back plates (sides) are easily removable. The nominal internal dimensions of the working section are 0.31 m. square by 0.76 m. long.

The diffuser section which is 2.59 m. long is made of 12 gauge mild steel sheet . A square-to-round transition is at the front of the diffuser. The included angle for the main body of the diffuser is 6°. Cruciform splitters installed at the end of the diffuser afford an increase in the included angle to 10°. The principal action of a diffuser is to decelerate the flow. Diffuser efficiency depends on wall angle, inlet and outlet velocity profiles.

The fan and motor assembly are installed at the end of the wind tunnel as shown in Figure 3.1. A 0.61 m. vaneaxial fan having a maximum rating of 3.8 m^3/sec. at 0.038 m. static pressure is used. A D.C. motor is employed to drive the fan. Speed control is obtained by employing a D.C. motor speed control arrangement. Over the operating range of 0-2500 R.P.M. the motor speed could be kept constant within $\pm$ 2 R.P.M. at

lower speeds and within $\pm$ 5 R.P.M. at high speeds. Two different sizes of pulleys are used at the motor shaft to obtain the desired range of fan speeds.

A flexible sleeve is fitted between the diffuser and fan unit to reduce the fan vibration reaching the test section.

3.2 Piano-wire Tubes

To obtain damping parameter ($m\delta/\rho D^2$) values as low as 2 and velocity parameter (V_p/fD) values as low as 3, tubes sprung on a piano-wire are used, in which:

a) the tube itself is effectively rigid, but elastically mounted.

b) for small displacements the elastic constraint is linear (i.e., restoring action is proportional to tube displacement), and can be varied over a range of values.

c) the damping is viscous (i.e., dissipative action is proportional to cylinder velocity), and can be readily controlled and varied.

The tension in the piano-wire could be used to regulate the natural frequency of the tubes. Wire material damping and windage will give the necessary low damping values required whereas high damping values could be obtained by using various fluids such as different grades of motor oil. The arrangement used to control the damping consists of a small cup and paddle assembly on the working section walls at the top and bottom of the tube.

A schematic of a model of these tubes is shown in Figure 3.2. A tube 30.48 cm. long, 2.54 cm. O.D. and 0.38 mm. wall thickness (this wall thickness was for the first set of tubes used to establish a datum with previous results) was mounted on a 1.04 mm. diameter piano-wire. The free length of the wire was 60.96 cm. and it passed through two 15.9 mm. steel plates at each end. The bottom of the wire passed through a concentric hole in a 6.4 mm. brass bolt and was bent at the end for light tubes or held by a nut and bolt for heavy tubes. The movement of the brass bolt and hence wire tension was regulated by a nut. A compression coil spring was installed for fine adjustment control as shown in Figure 3.2. (The springs were chosen according to the stiffness required, see Appendix B). Two damping cup-and-paddle assemblies were also mounted at the top and bottom walls of the working section.

The tension in the piano-wire could be varied in order to obtain the desired translational natural frequencies of the tube.

3.3 The Test Array

A parallel-triangular array having a pitch/diameter ratio of 1.375 was used to conduct tests because of its use in actual heat exchangers. The array had 18 rows of tubes with five tubes in each row as shown in Figure 3.3. Half tubes were installed at the ends to reduce wind-tunnel wall effects. Only the 19 numbered tubes were mounted flexibly. The design of each of these movable tubes was similar to the piano-wire tube described

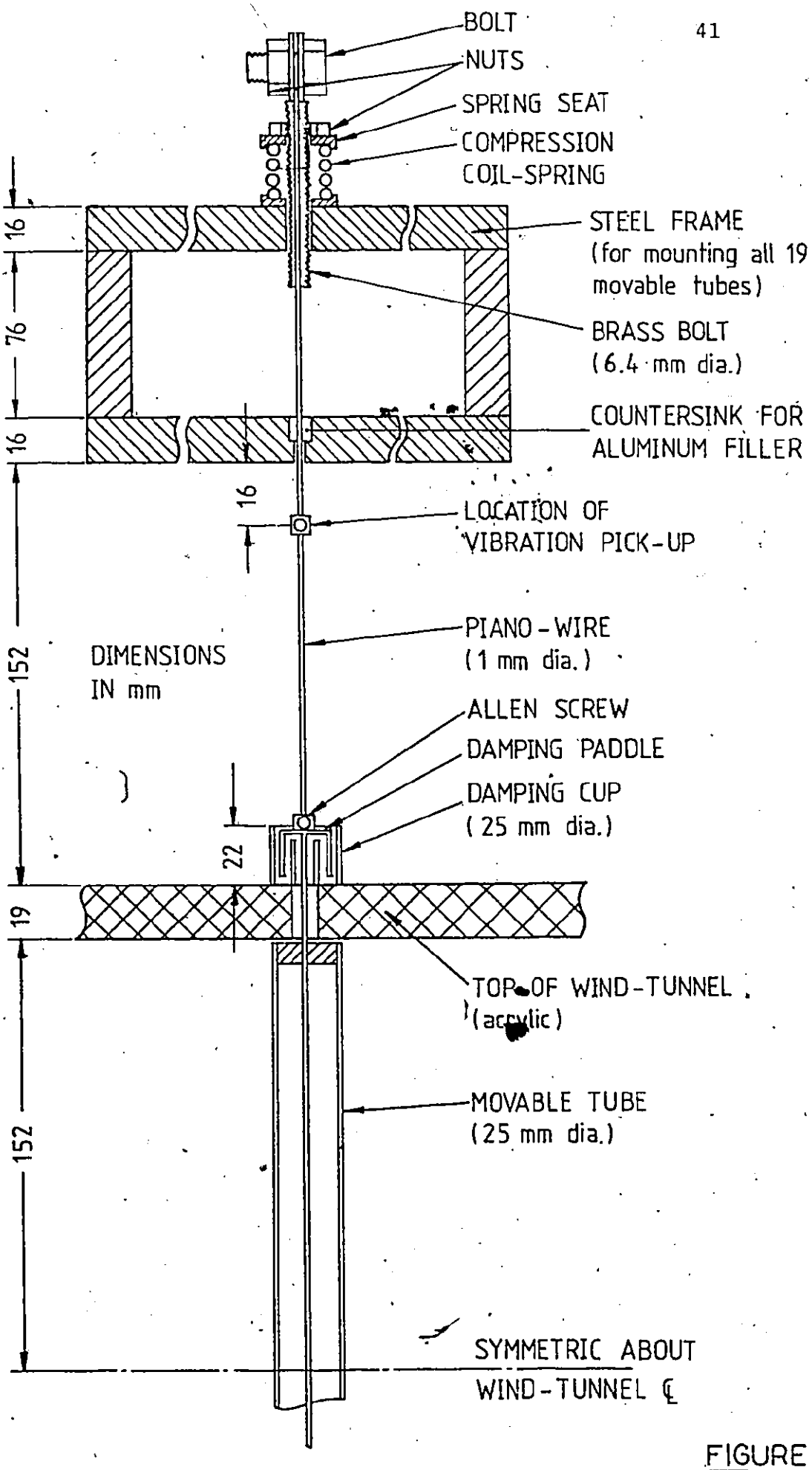
BOLT
NUTS
SPRING SEAT
COMPRESSION
COIL-SPRING
STEEL FRAME
(for mounting all 19
movable tubes)
BRASS BOLT
(6.4 mm dia.)
COUNTERSINK FOR
ALUMINUM FILLER
LOCATION OF
VIBRATION PICK-UP
PIANO-WIRE
(1 mm dia.)
ALLEN SCREW
DAMPING PADDLE
DAMPING CUP
(25 mm dia.)
TOP OF WIND-TUNNEL
(acrylic)
MOVABLE TUBE
(25 mm dia.)
SYMMETRIC ABOUT
WIND-TUNNEL ℄
DIMENSIONS
IN mm
16
76
16
16
152
22
19
152

FIGURE 3.2

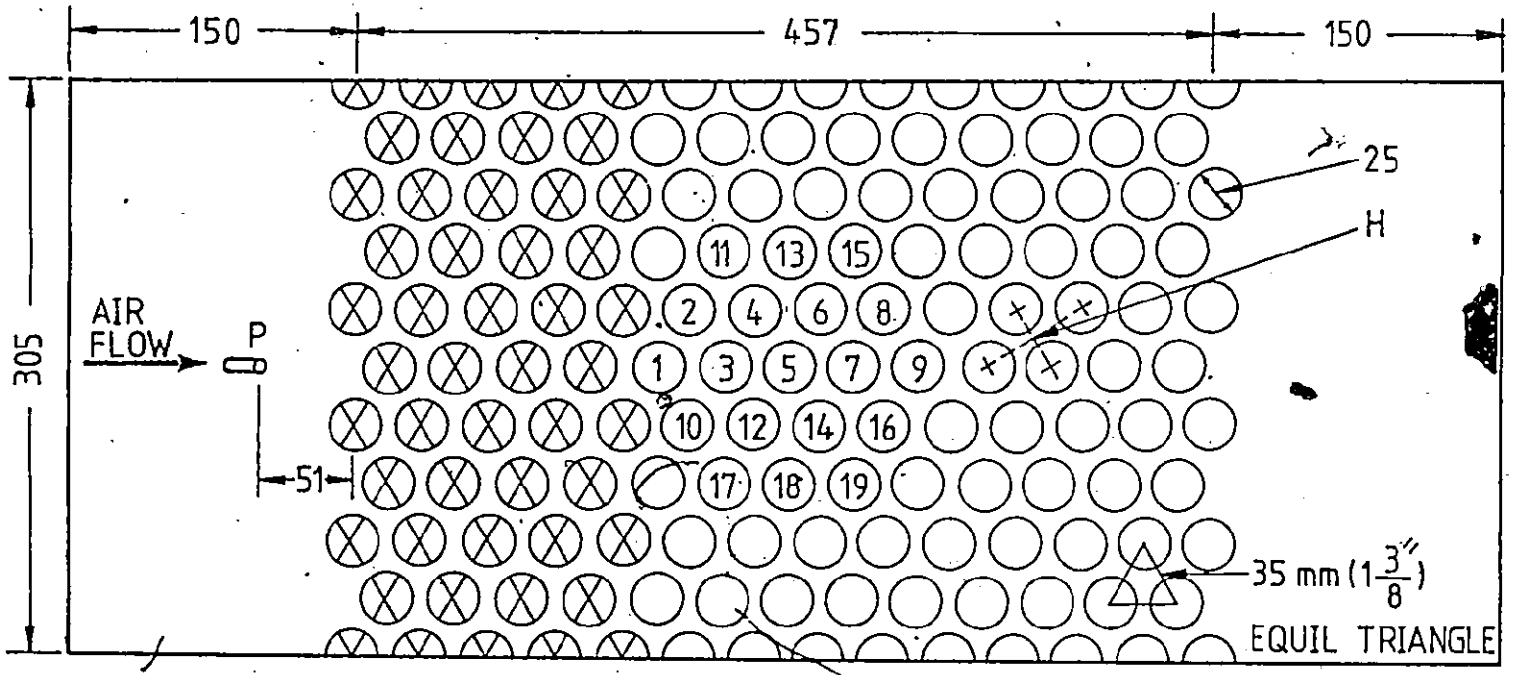

DIMENSIONS IN MM

TUBES MARKED 1-19 ARE MOVABLE TUBES (REST ARE FIXED)
TUBES MARKED 'X' ARE POSITIONS FOR ADDITIONAL UP-STREAM TUBES
P – LOCATION OF PITOT-PROBE
H – LOCATION OF HOT-WIRE PROBE

Cross-section of wind-tunnel test section

FIGURE 3.3

in the previous section. Not all of the tubes in the array were tuned as this was demonstrated to be unnecessary (Weaver and Grover [9]). The rigid upstream tubes were made easily removable to allow determination of the effect of number of tubes in the array on stability behavior.

A steel frame was used for mounting the 19 movable tubes. The frame consisted of 16 mm. steel plates and 64 x 64 x 5 mm. square steel tubing and was bolted together. The steel frame was installed around the middle of the working section as shown by the photograph in Figure 3.4. Two reinforcement steel plates were installed in each of the two hollow box-type components of the steel frame. The maximum deflection at the middle of the box due to maximum tension in all piano-wires taken together was not more than 0.015 mm. The structure was thus very rigid and no change in the tuned natural frequencies of the tubes would result from the tuning of subsequent tubes. A view of the top of the test section with 19 movable tubes in place is also shown in Figure 3.4. The space between the steel frame and the working section (both at the top and the bottom) was enclosed by four 13 mm. acrylic plates so as to form an enclosure for the 19 piano-wires. This arrangement prevented leakage of air into the working section.

The flow velocity at location 'H' in the array as shown in Figure 3.3 was recorded by a hot-wire probe and designated 'pitch velocity' (V_P). The corresponding upstream velocity at location 'P' was also recorded with a pitot-static probe and designated 'upstream velocity' (V_U). The ratio of V_P/V_U

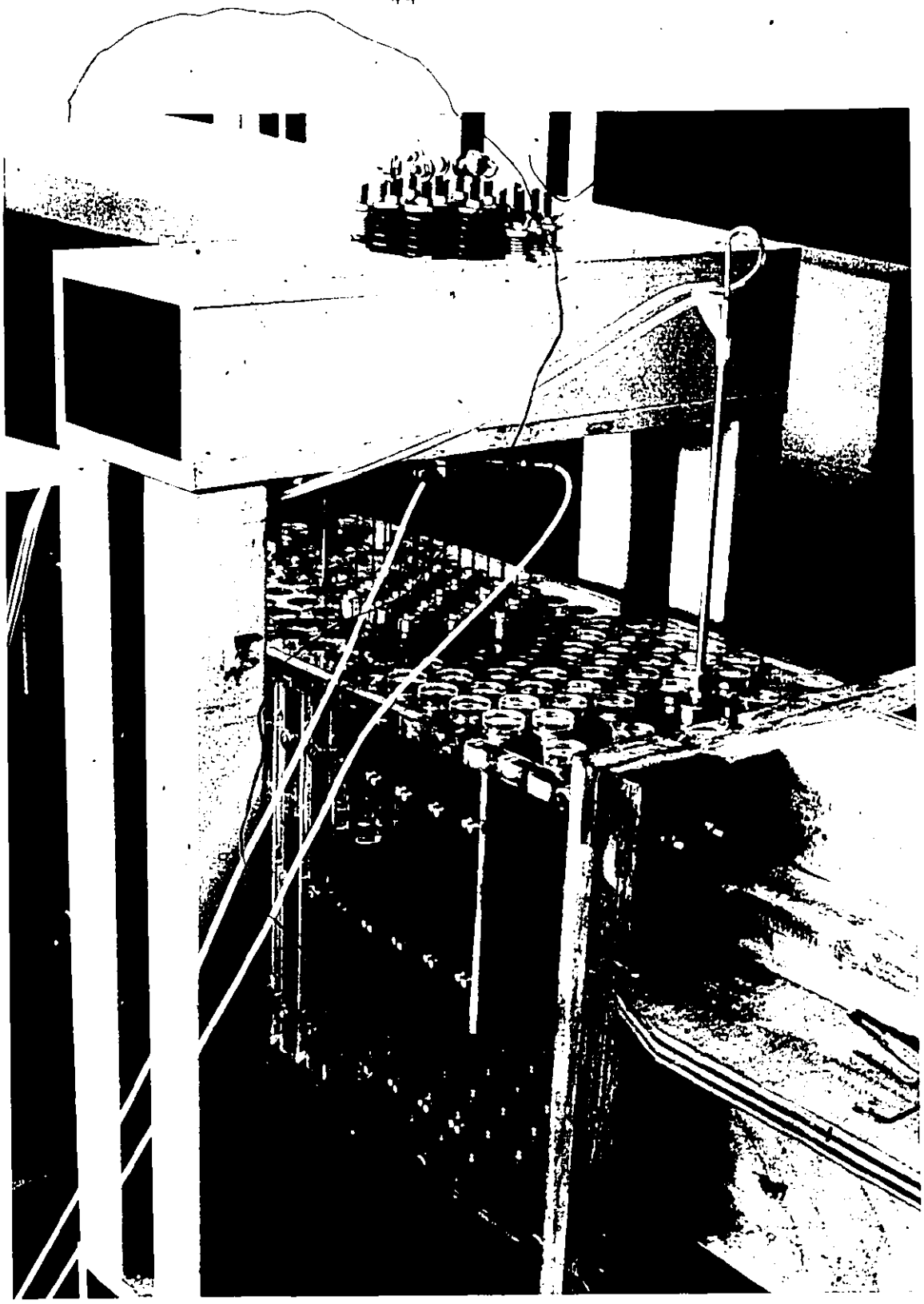

Figure 3.4

was found to be a constant equal to 3.69.

The translational natural frequency of a movable tube was obtained by releasing the tube after displacement from its static equilibrium position and viewing the frequency count on a electronic digital counter. A capacitive probe was used for displacement pick-up. The tension in the piano-wire was adjusted in order to obtain a desired value of tuned frequency for the tube. The procedure was repeated for each of tube No. 4 and its surrounding movable tubes including tube No. 1 til they were all tuned to a natural frequency of 20 Hz. The rest of the movable tubes were tuned to above 30 Hz, so no coupling or interference would occur between them and the tuned tubes. No relaxation or creep was noticed during the period of tests, i.e., the tubes maintained their tuning throughout the tests.

The logarithmic decrement of free vibration was measured by releasing the movable tube after displacement from its static equilibrium position and recording the subsequent amplitude decay on a U.V. recorder. The number of free vibration cycles required for the amplitude to decrease from a particular amplitude to a selected lower amplitude were counted. A certain amount of impact damping was observed in many tubes due to inevitable manufacturing tolerances among clearance holes drilled in the steel for the piano-wires. The problem was corrected by pouring aluminum filler in the grooves in the steel plates around the wires as shown in Figure 3.5. It was noticed that

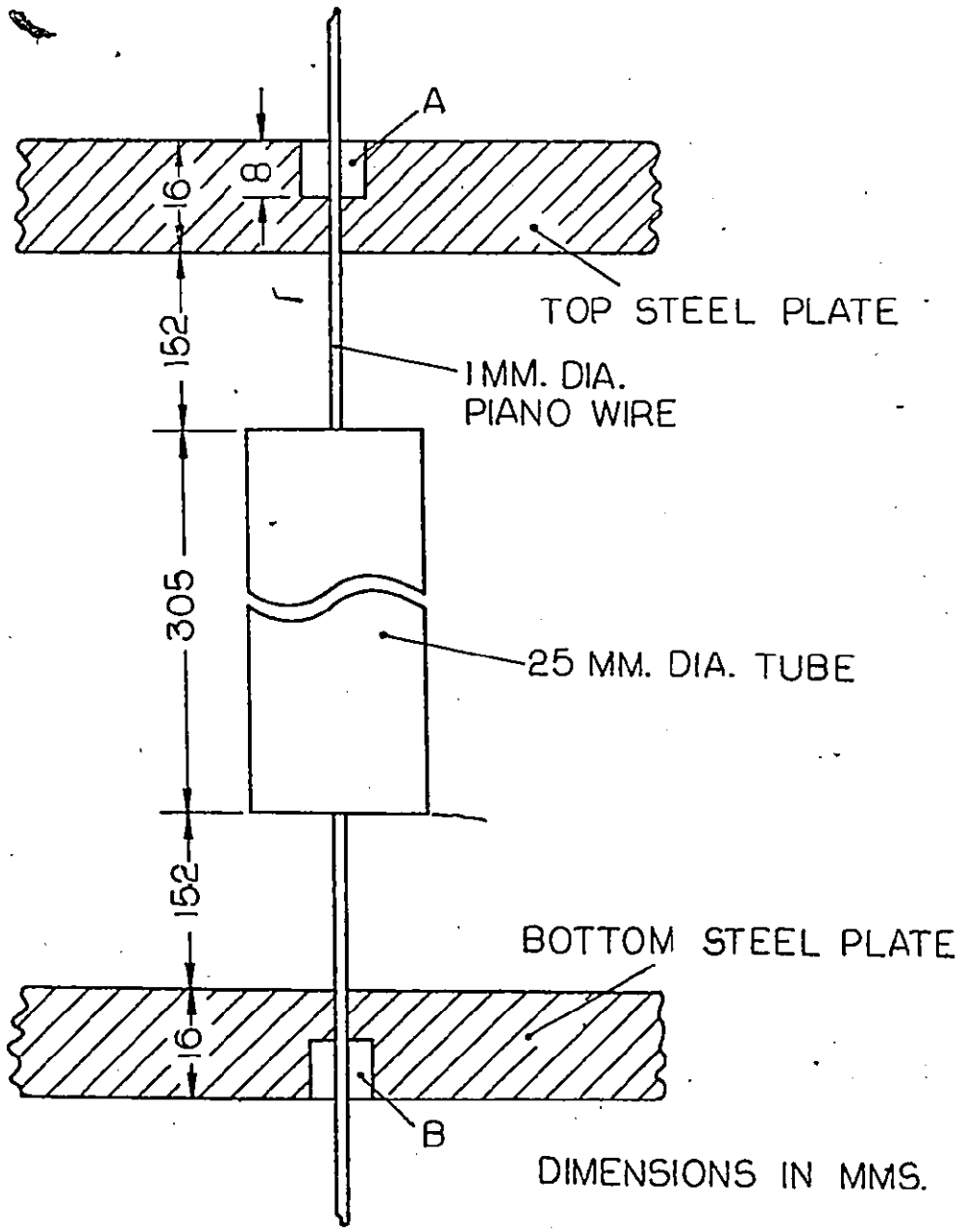

ALUMINUM FILLER WAS POURED IN GROOVES A&B

FIGURE 3.5

using the aluminum filler will reduce the logarithmic decrement of damping by about 30%.

Oil damping was obtained by using SAE-10, 20 and 30 motor oil. Using water in the damping cups was considered inappropriate due to the problems encountered with evaporation. Typical amplitude decay traces recorded for air damping and oil damping are shown in Figure 3.6.

The average weight, wall thickness and the corresponding damping parameter for different sets of tubes used in the tests are given in Table 3.1.

3.4 Instrumentation

Upstream flow velocity was measured using a pitot-static probe and a Betz manometer. The pitch velocity was recorded by a 90° miniature hot-wire probe using a DISA constant-temperature anemometer and the output was displayed on a digital voltmeter. Two MTI capacitive probes (Type ASP-10 used in conjunction with distance and vibration meter AS 1000) were employed to observe tube displacements on an oscilloscope and the signals were also viewed on a Spectrascope Real Time Analyzer (Model SD 335) to measure the amplitude of vibration.

The probes were installed at 90° to each other and 45° to the direction of flow as shown in Figure 3.7. The output of a capacitive probe was also recorded on a U.V. recorder and this record was used to compute the natural frequency and logarithmic decrement of damping of movable tubes. A schematic of the complete instrumentation is shown in Figure 3.8.

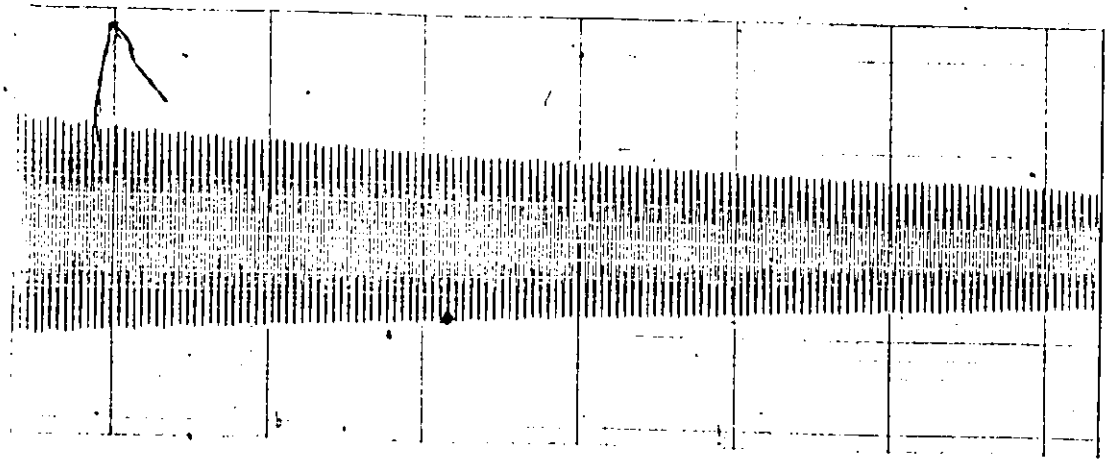

Air Damping

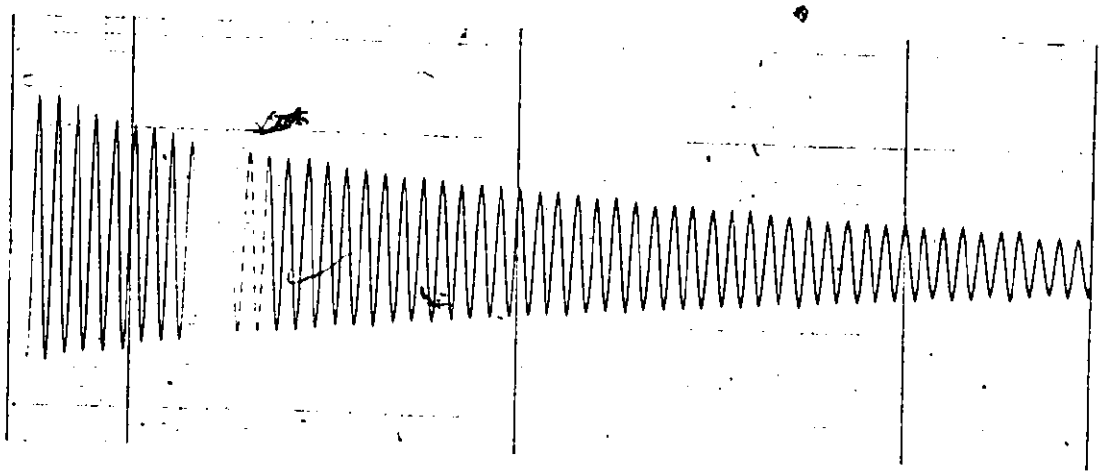

Oil Damping

Fig. 3.6 Typical Amplitude-decay Traces of a Movable Tube.

TABLE 3.1

ALL MATERIAL ARE 25.4 MM. OUTER DIAMETER SEAMLESS TUBING

SET NO.	MATERIAL	WALL THICKNESS (MM.)	TOTAL MASS (GM.)	DAMPING PARAMETER
1	Aluminum	0.380	48.0	5.00
2	Aluminum	1.651	99.1	10.42
3	Steel (cold drawn)	1.245	270.6	28.62
4	Brass	1.651	361.1	38.21
5	Steel (cold drawn)	2.413	461.5	48.89
6	Steel (cold drawn)	3.048	544.4	57.58

NOTE: (1) The tubes are all 30.48 cm. in length.

(2) These damping parameters assume a $\delta = 0.025$.

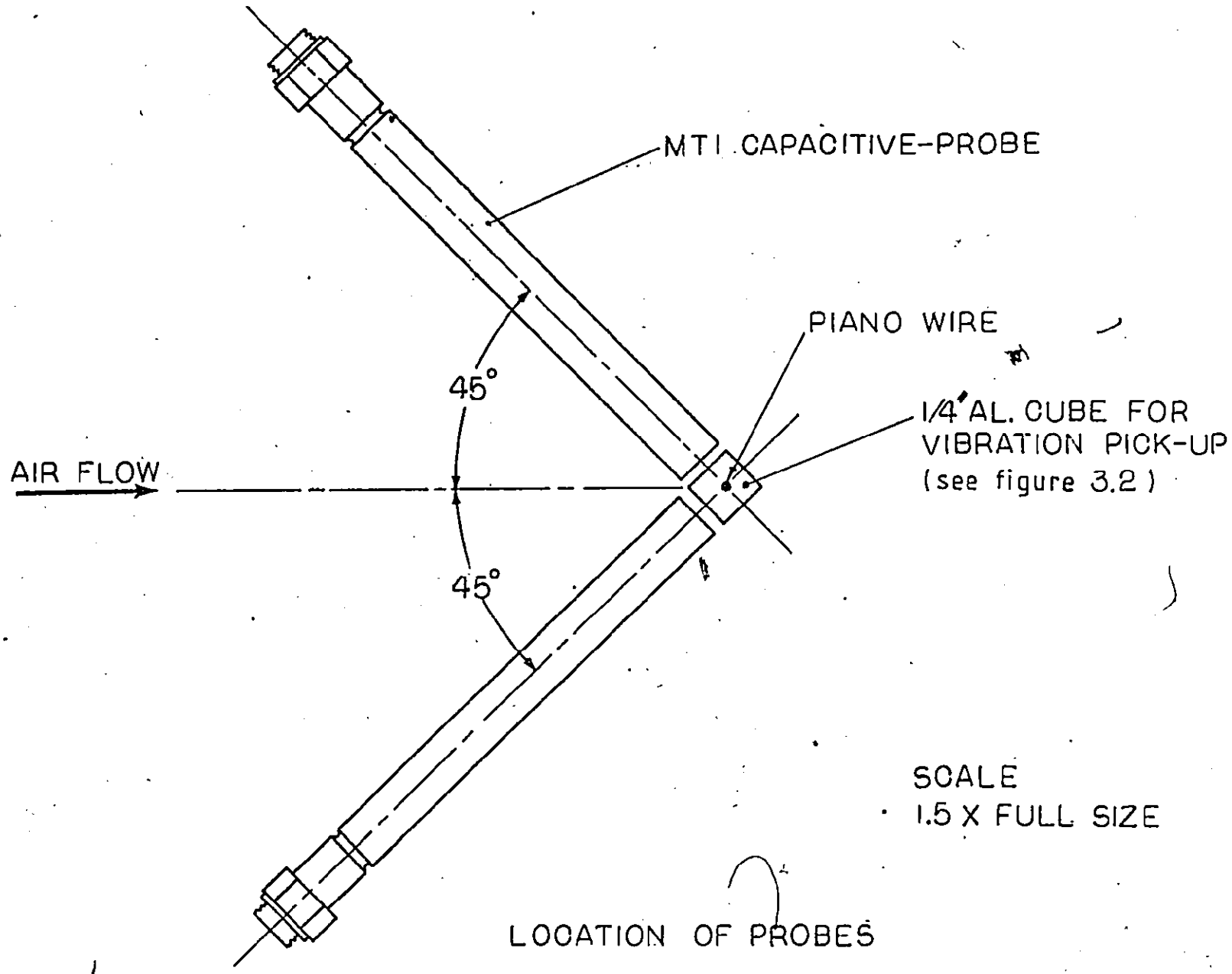
MTI CAPACITIVE-PROBE
PIANO WIRE
1/4" AL. CUBE FOR
VIBRATION PICK-UP
(see figure 3.2)
45°
45°
AIR FLOW
SCALE
1.5 X FULL SIZE
LOCATION OF PROBES

FIGURE 3.7

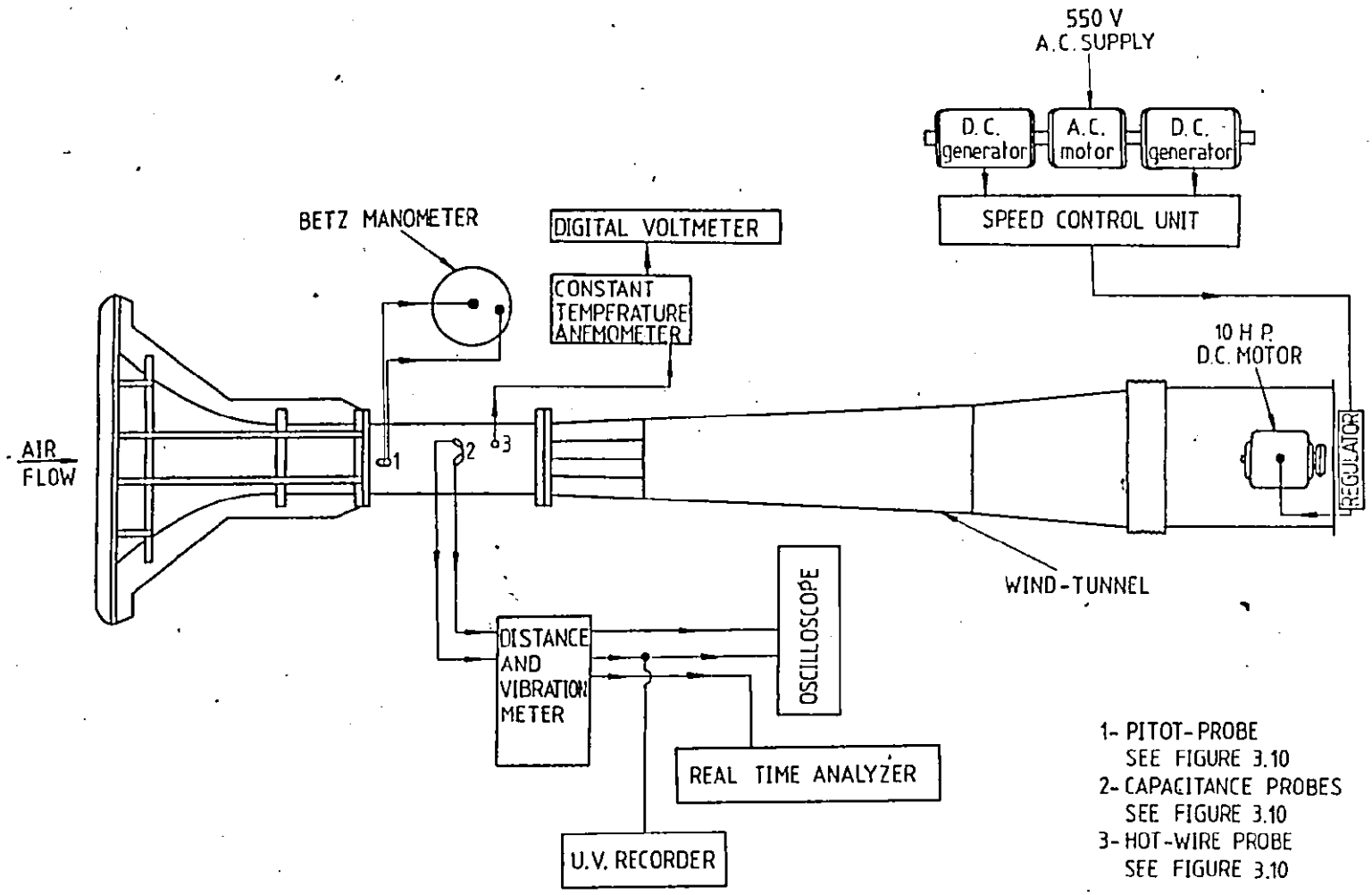

OVERALL LAYOUT OF THE WORK AREA

FIGURE 3.8

A detailed description and specifications of all instruments and probes are given in Appendix C and the calibration curves for the capacitive probes and hot-wire probes have been included in Appendix A.

A photograph showing various instruments in the general work area of wind tunnels is shown in Figure 3.9. Another photograph of a pitot-static probe, a MTI capacitive probe, and a DISA 90° miniature hot-wire probe is shown in Figure 3.10. The front of the wind-tunnel with part of the test section and the instrumentation is shown in Figure 3.11.

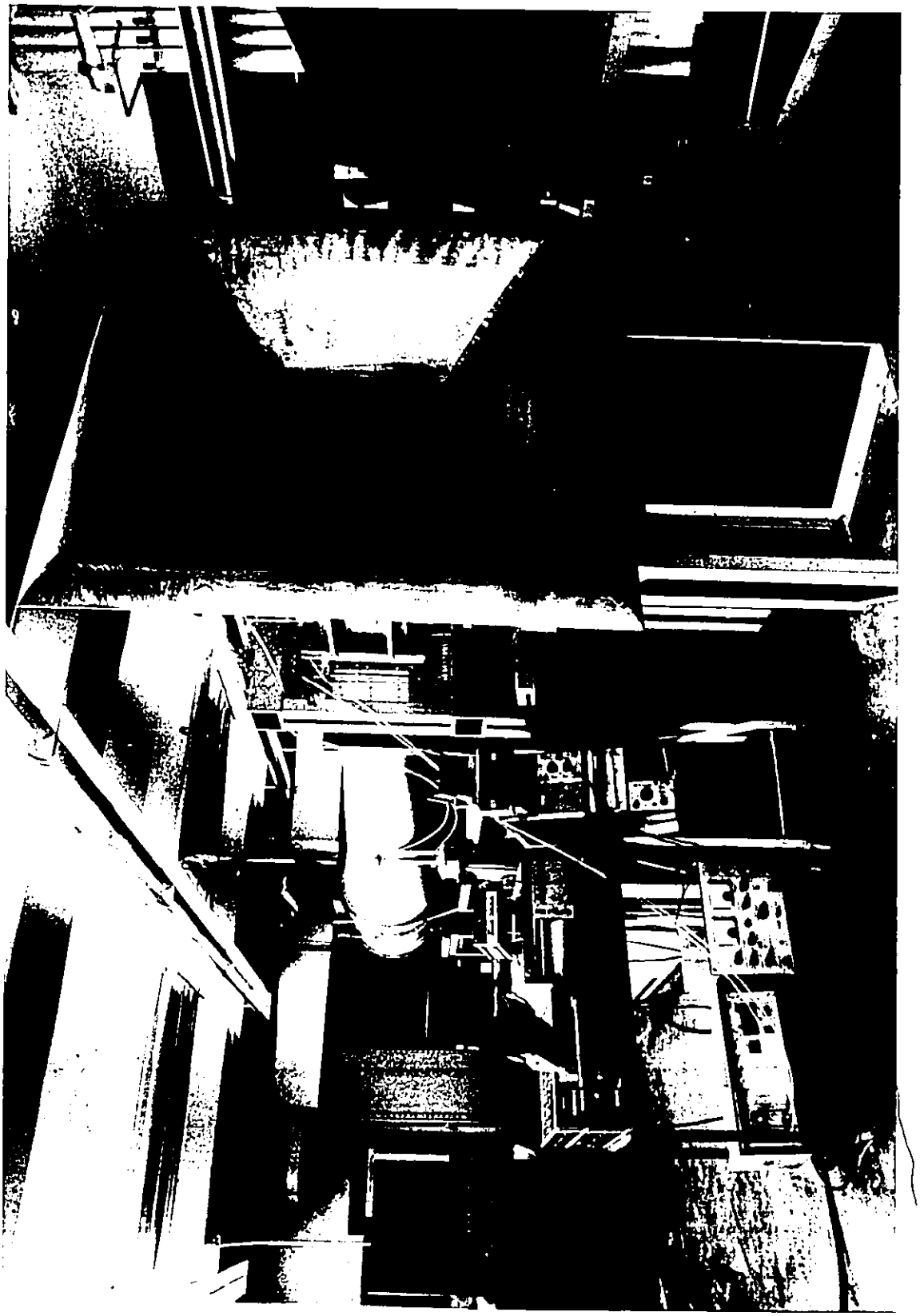

Figure 3.9

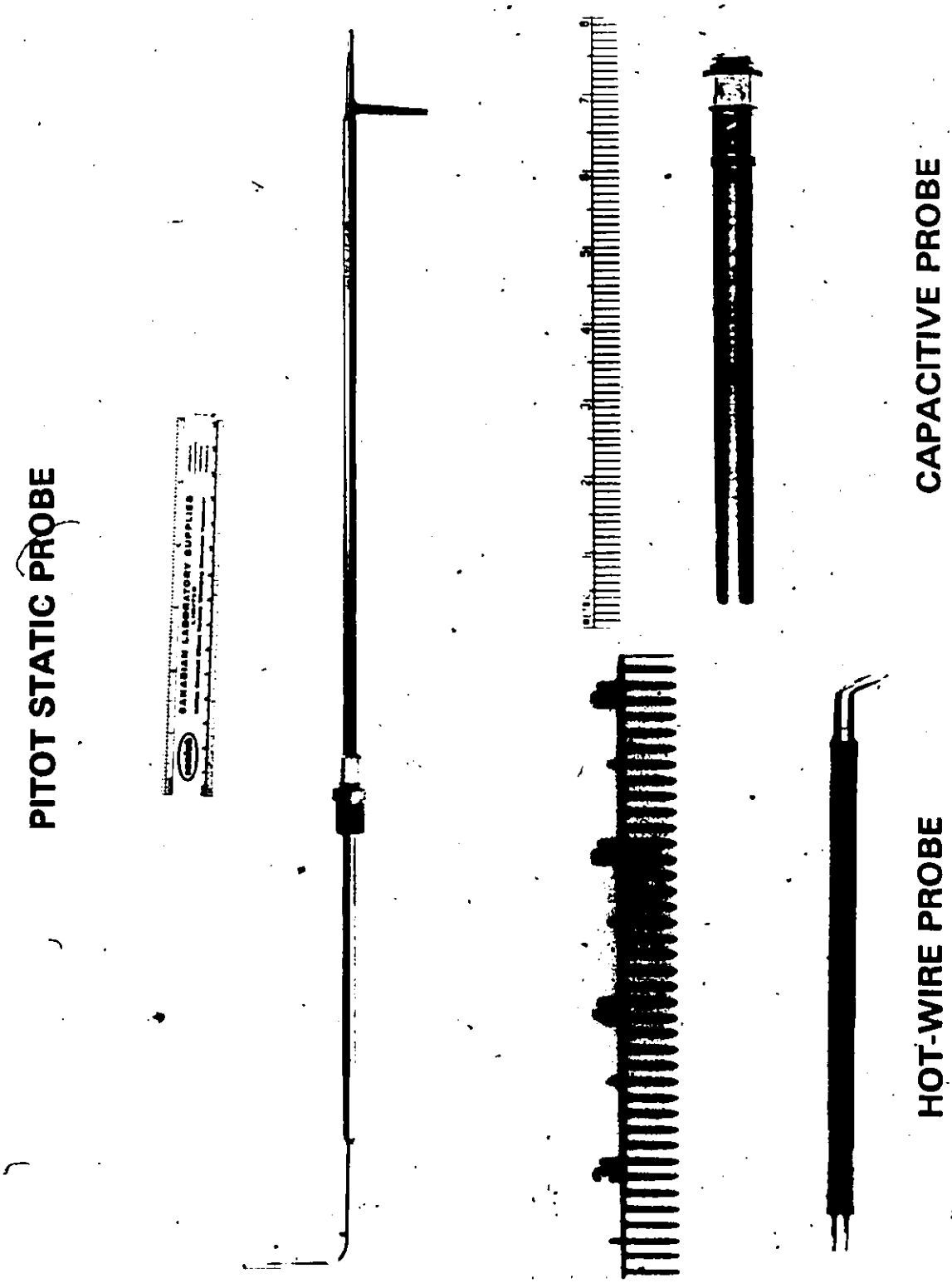

Figure 3.10

Figure 3.11

CHAPTER 4

EXPERIMENTAL RESULTS

The parallel-triangular (in-line) tube array, with pitch/diameter = 1.375, described previously, was used to conduct the experiments. As shown in Figure 4.1, the array was 18 rows deep with 5 tubes in each row. Nineteen identical tubes in the front of the array were movable and their natural frequency and damping could be controlled independently. Positions for as many as 9 rows of fixed tubes in the front of the tube-array, were available in order to facilitate studying the effect of tube-bundle size on tube response.

The experimental program was in three parts:

1) To study the effect of flow velocity on the damping of the tubes, the experiments were conducted with air and material damping only, for two different tubes.

2) The relative positions of these two tubes were changed by adding tube rows upstream, and the effect on the stability threshold was studied.

3) Finally, the effect of changing the tube mass, while keeping its natural frequency, diameter, and damping constant was examined. A new stability criterion has been obtained as a result of this study.

The results obtained are considered separately below. However, before proceeding to a discussion of these new results, a general description of the tube response as a function of flow

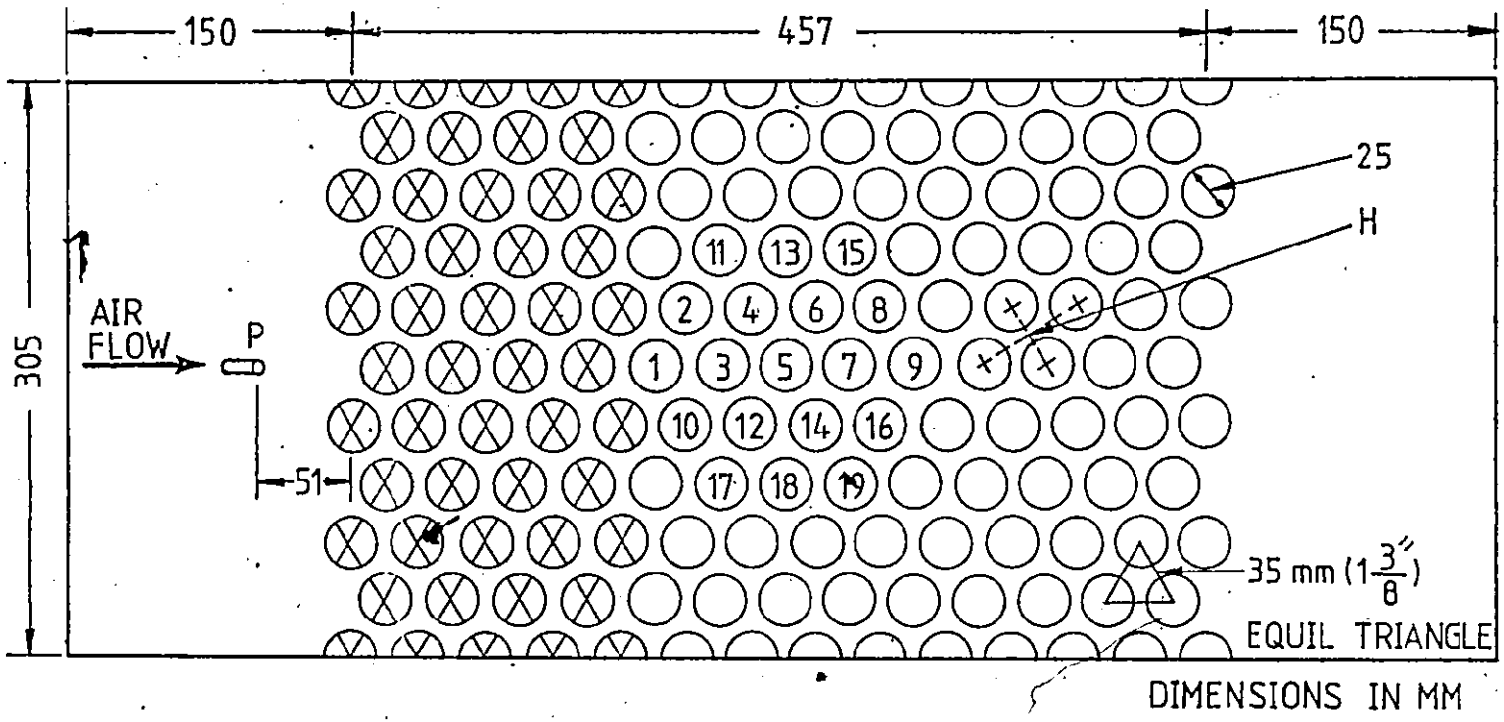

TUBES MARKED 1-19 ARE MOVABLE TUBES (REST ARE FIXED)
TUBES MARKED 'X' ARE POSITIONS FOR ADDITIONAL UP-STREAM TUBES
P - LOCATION OF PITOT-PROBE
H - LOCATION OF HOT-WIRE PROBE

Cross-section of wind-tunnel test section

FIGURE 4.1

velocity will be given.

4.1 Effect of Flow Velocity on Tube Response

The response of the tubes at different flow velocities was determined. A typical tube response as seen on the oscilloscope screen was photographed at a number of flow velocities and has been reproduced in Figure 4.2. For small velocities the amplitude was very small and the response was random in character. As the flow velocity increases, the response becomes more regular and the tube moves in an oval-shaped orbit at its natural frequency, from which it was named "tube-whirling" by Blevins [10]. The output was also displayed on the screen of the spectra-scope and the overall RMS amplitude was measured in decibels. The RMS amplitude rather than the maximum amplitude was computed, because it was found by Weaver and Lever [11], that the stability boundary as defined by the rapid change in slope of the amplitude velocity curve, will be the same using a RMS amplitude or peak-to-peak tube amplitude. Moreover, the overall RMS amplitude could be obtained easily and considerable time saved in the process.

The RMS tube amplitudes (see Appendix A for tube deflection calibration) have been plotted against the hot-wire probe velocities measured in the gap between two tubes in Figure 4.3. The hot-wire probe velocity was found to be approximately equal to the pitch velocity V_p defined in the literature as,

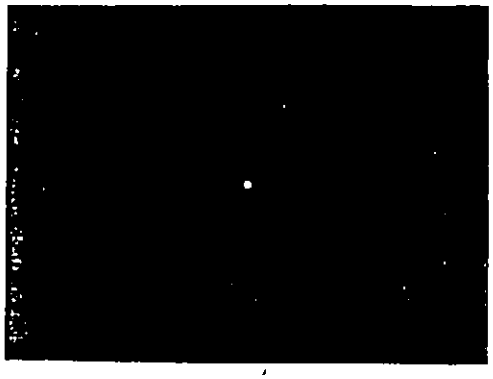

V_P = 0.0 M/sec.

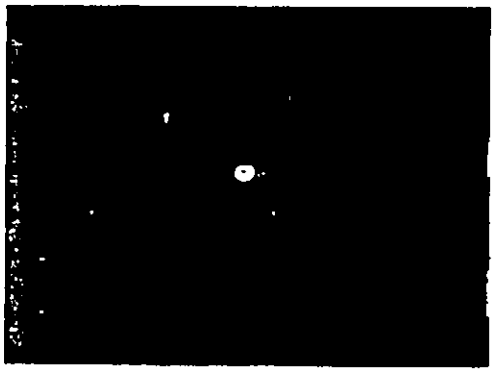

1.73

2.52

3.49

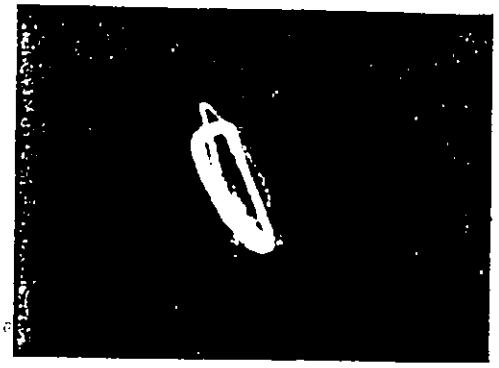

3.97

4.18

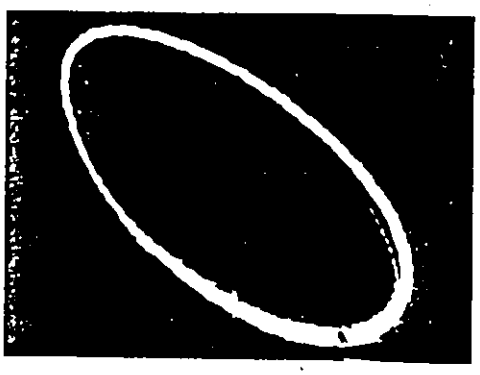

4.40

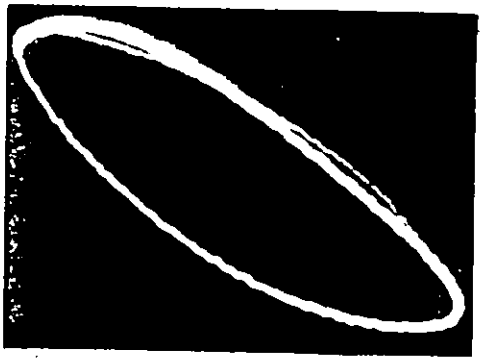

4.45

Fig. 4.2 Tube Response as Seen on Oscilloscope.

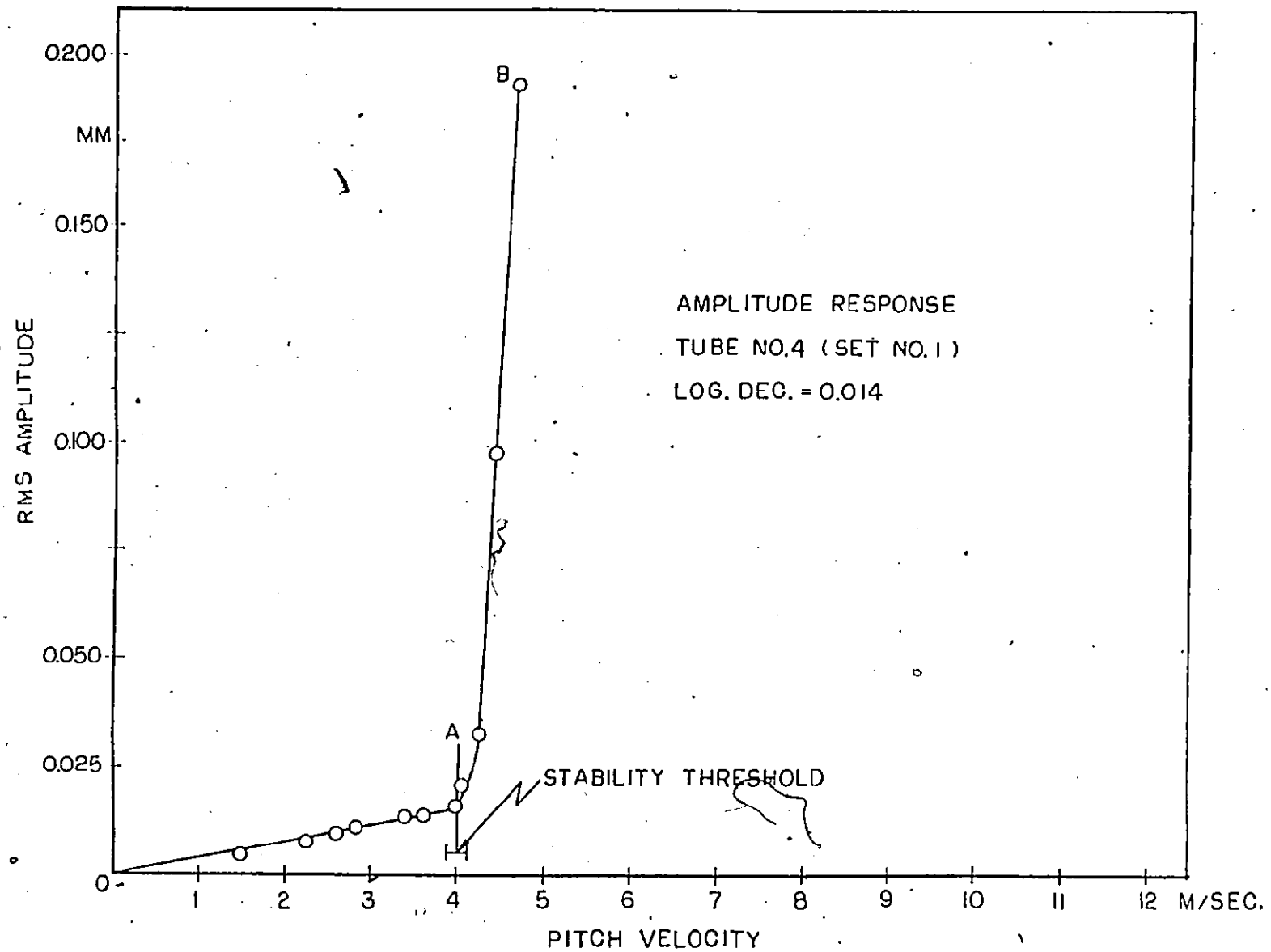
0.200
MM
0.150
0.100
0.050
0.025
0
RMS AMPLITUDE
B
A
AMPLITUDE RESPONSE
TUBE NO.4 (SET NO.1)
LOG. DEC. = 0.014
STABILITY THRESHOLD
1
2
3
4
5
6
7
8
9
10
11
12 M/SEC.
PITCH VELOCITY

FIGURE 4.3

$$V_P = \frac{P}{P-D} V_U \simeq V_{HWP}$$

where

P = pitch (distance between centerlines of tubes),

D = outer diameter of the tube,

and, V_U = upstream flow velocity

and not equal to the gap velocity V_G defined from the array geometry as:

$$V_G = 3.19\ V_U$$

The difference between the hot-wire probe velocity, V_{HWP}, measured in the gap between the two tubes and the gap velocity, V_G, is the difference between measuring the peak of the velocity profile and an assumed rectangular profile, respectively. The tube response obtained was different over two regions. Region OA of the tube response curve represents the random response of the tube to turbulent buffeting. It is seen that the RMS amplitude is directly proportional to the pitch velocity. This linear response was also observed by Weaver and Grover [9]. Southworth and Zdrawkovich [38], reported that the maximum amplitude due to turbulence, from their experiments on only one-two and three-row in-line arrangements, is proportional to the square of flow velocities. However, most work on tube bundles shows a linear increase in RMS tube amplitude with flow velocity.

No vortex shedding response was recorded in this region

of the tube response. However, previous researchers have indicated that vortex shedding is not a dominant response in air.

For further increase in velocity the tube responded in an elliptical orbital regular pattern (see Figure 4.2) at larger amplitudes. The tube motion was predominantly in the transverse direction of the flow, shifting to within $\pm 45^{o}$ of this direction and occasionally to the streamwise direction. As the flow velocity was further increased the overall RMS amplitude kept on building up rapidly. This represents the unstable "fluidelastic whirling" region shown from A to B in Figure 4.3.

The vibration amplitudes are modulated considerably in this region, especially at the lower velocities. The reason for this behaviour is not well understood, but it is undoubtedly associated with nonlinear fluid coupling effects with the surrounding tubes which are vibrating at the same frequency.

The tube response is similar to that observed by Connors [4], except for the mode shapes which appears to be primarily in the transverse direction rather than alternating tubes vibrating in streamwise and transverse orbital patterns.

The pitch velocity at which the slope of the amplitude response curve changes is defined as the fluidelastic "stability threshold" for the tube. As it is often difficult to determine precisely where the change of slope occurs, a certain band of pitch velocities, as shown in Figure 4.3, has been designated as the region of the stability threshold and is an indication

of the uncertainty involved in determining precisely the critical flow velocity. Because of the problem involved in precisely locating the stability threshold, other investigators have defined this point as the intersection between a tangent to the curve AB and the abssica or as the intersection between the line OA and the tangent to AB. Others have even used simply visual observations of tube response. The difficulty with these methods is that the transition to instability may be gradual and considerable velocity in excess of the critical required to cause very large amplitudes. The severity of the stability threshold is affected by the tube pattern as well as damping which generally will vary from tube to tube and may be nonlinear. Thus visual determination of the stability threshold may be unconservative while the tangent method may be too conservative (not to mention the difficulties when the displacement-velocity curve is not a straight line). It was felt that the best compromise is achieved by using the point at which the slope of the displacement-velocity curve changes while noting that the general tube response changes from random to regular. This indicates at least some organized energy transfer mechanism is taking place.

An amplitude power-spectrum was computed from the output of the capacitive probe and is shown in Figure 4.4. The sharp peak at the natural frequency of the monitored tube (20 Hz) indicates the excellent linear characteristics of the movable tube. Figure 4.5 shows two amplitude power-spectra, one at a low flow velocity and the second above the critical velocity.

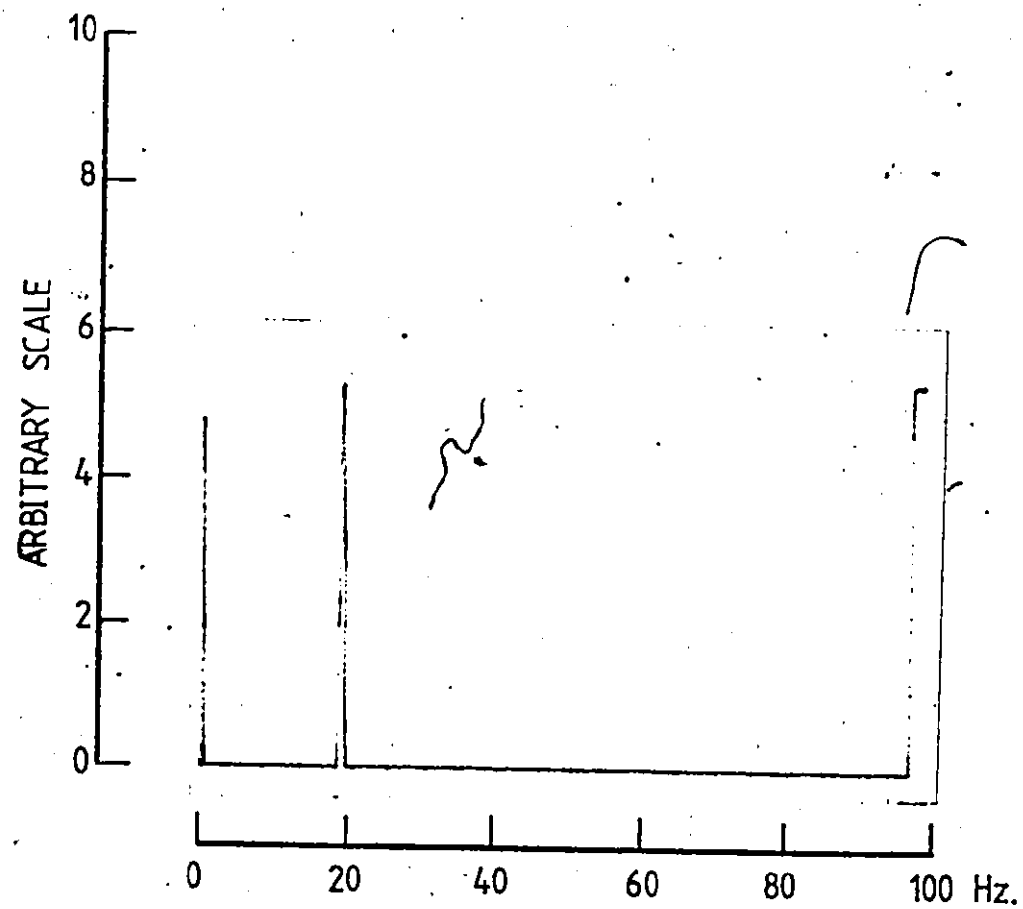

Fig. 4.4 Amplitude-power Spectrum of Tube Response (Tuned Natural Frequency of Tube = 20 Hz).

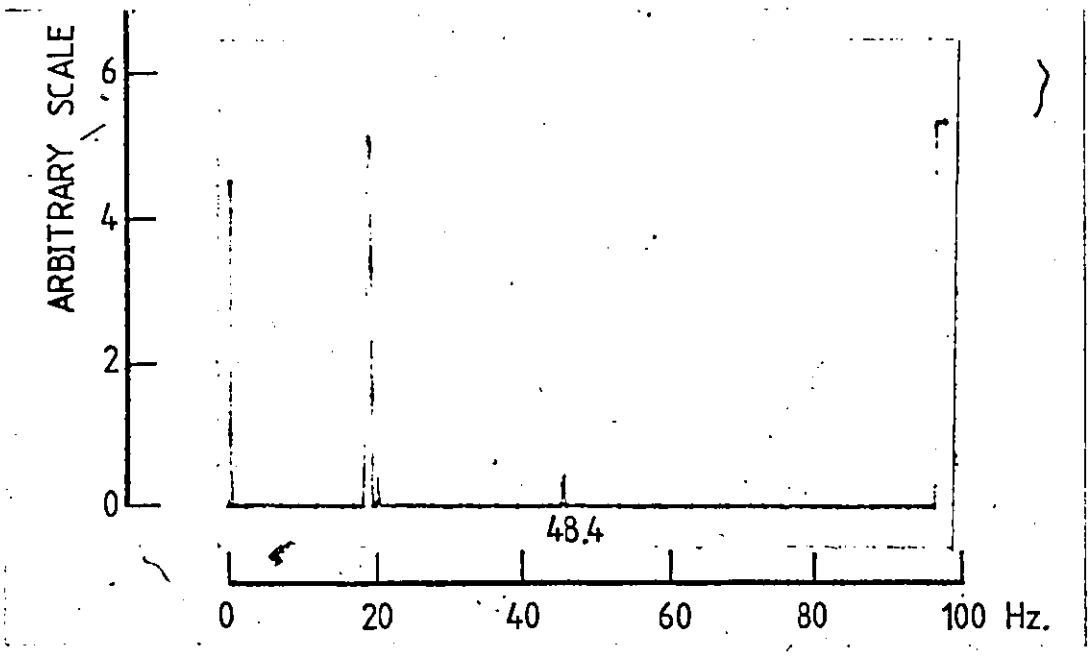

V_p = 1.43 M/Sec.

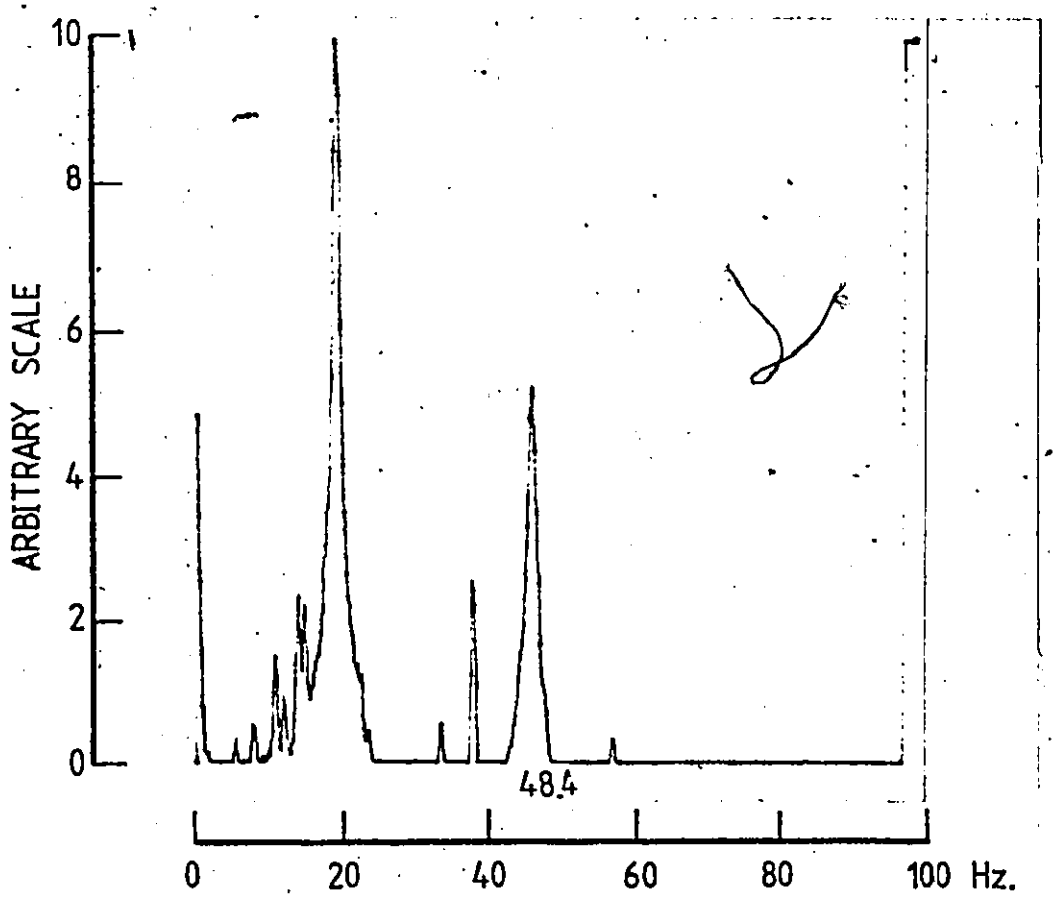

V_p = 4.54 M/Sec.

Fig. 4.5 Amplitude Power Spectrum of Tube Response at a Low Flow Velocity and Above the Critical Velocity.

The second diagram shows the increase in amplitude with flow at the tube natural frequency and excitation of a rocking mode with smaller amplitude at 48.4 Hz.

It was observed that the vibrations always started at a higher flow velocity when the velocity was increasing and ceased at a lower flow velocity when the velocity was being reduced. This hysteresis indicates that the vibrations are of a self-excited nature in which the flow periodicity is caused by the motion of the structure.

4.2 The Effect of the Flow Velocity on the Fluid Damping

The total tube damping consists of the structural and aerodynamic damping measured in a still fluid and fluid dynamic damping resulting from the flow. As a tube vibrates in a steady-cross flow, part of the vibratory energy of the tube is dissipated in fluid dynamic damping. The effect of flow velocity on the fluid dynamic damping is studied in this section. For the purpose of this study, the movable tubes marked from 1 to 6 and 10 to 13 (see Figure 4.1) were tuned to 20.0 Hz. These tubes were chosen so that the monitored tubes will be surrounded by tubes having the same conditions. The rest of the movable tubes were tuned to above 30.0 Hz., so that they would not interfere with the monitored tubes. The static damping for the movable tubes no. 2 and no. 4 (see Figure 4.1) in the second and fourth row respectively, was measured with no rows of stationary tubes upstream. The wind-tunnel was turned on and the flow velocity was increased slowly and the corresponding value

of total damping was measured starting at the same amplitude on the resultant amplitude decay trace for every flow velocity. Great care was taken to obtain consistent amplitude decay traces. This was done so that the different values of total damping measured could not be attributed to amplitude effects. The constant value was chosen to be approximately equal to the amplitude at which the tubes start to take off (i.e., the amplitude corresponding to the threshold velocity) so that the total damping measured at each flow velocity could be related finally to the total damping at the critical flow velocity. The static damping was then subtracted from the total damping measured at every flow velocity and the resultant fluid dynamic damping was plotted versus the flow velocity measured in the gap between two adjacent tubes as shown in Figure 4.6 and Figure 4.7. The complete experiment was repeated adding one row of stationary tubes to the front of the tube-bundle at a time, until the movable tube no. 2 was in the fourth row. The results obtained are also plotted in Figures 4.6 and 4.7. Tables 4.1 and 4.2 show the static damping, the fluid dynamic damping and the corresponding flow velocity for tube no. 2 and no. 4 respectively, for different tube locations obtained from these experiments and used to plot Figures 4.6 and 4.7. In portion OA (Figure 4.6) of the fluid dynamic damping-flow velocity curve, the total damping was increased by about 33% when the flow velocity was about 52% of the critical velocity (these ratios are based on the results obtained with no rows of stationary tubes upstream). The band representing the critical flow velocity

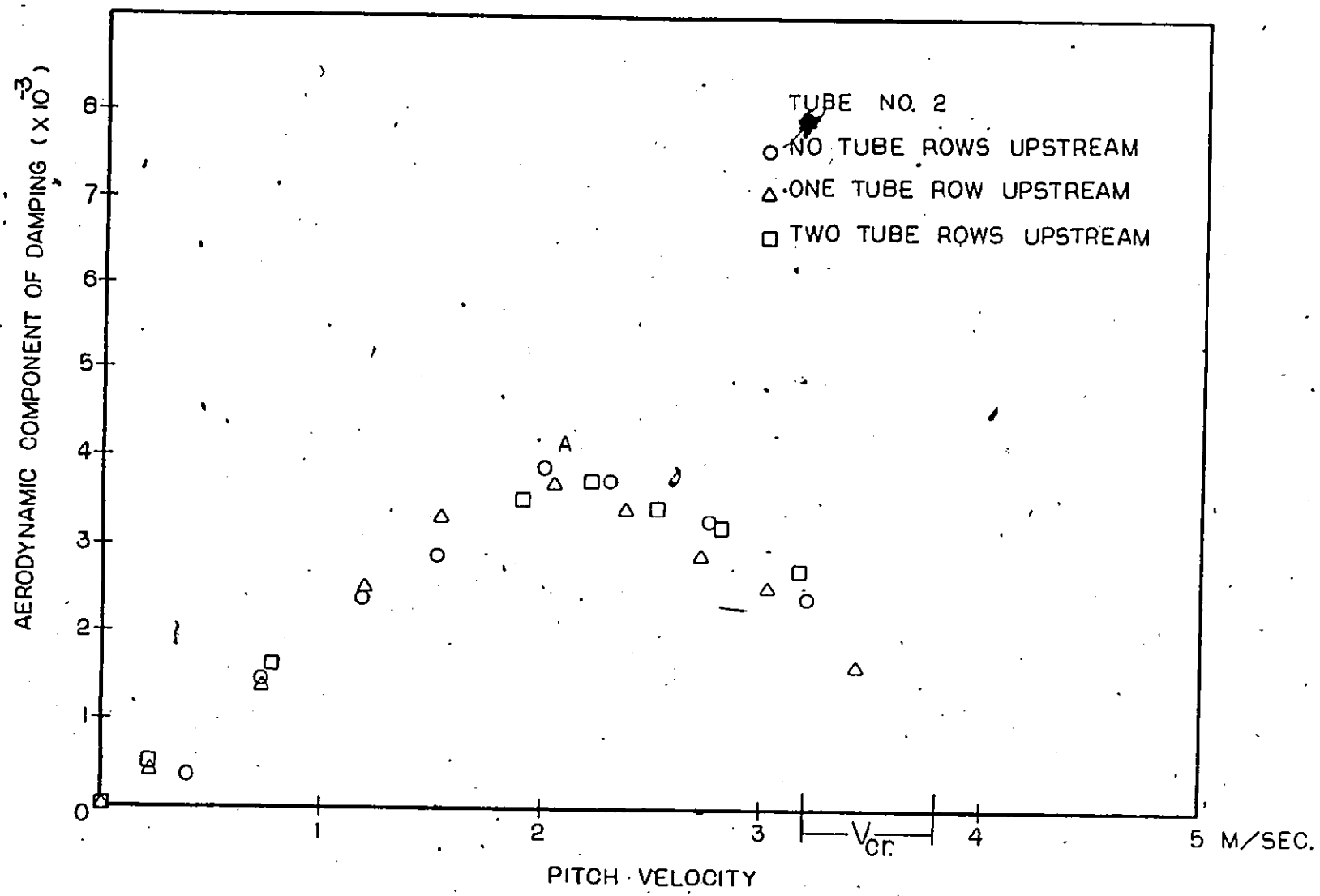

FIGURE 4.6 THE EFFECT OF FLOW VELOCITY ON THE AERODYNAMIC COMPONENT OF DAMPING

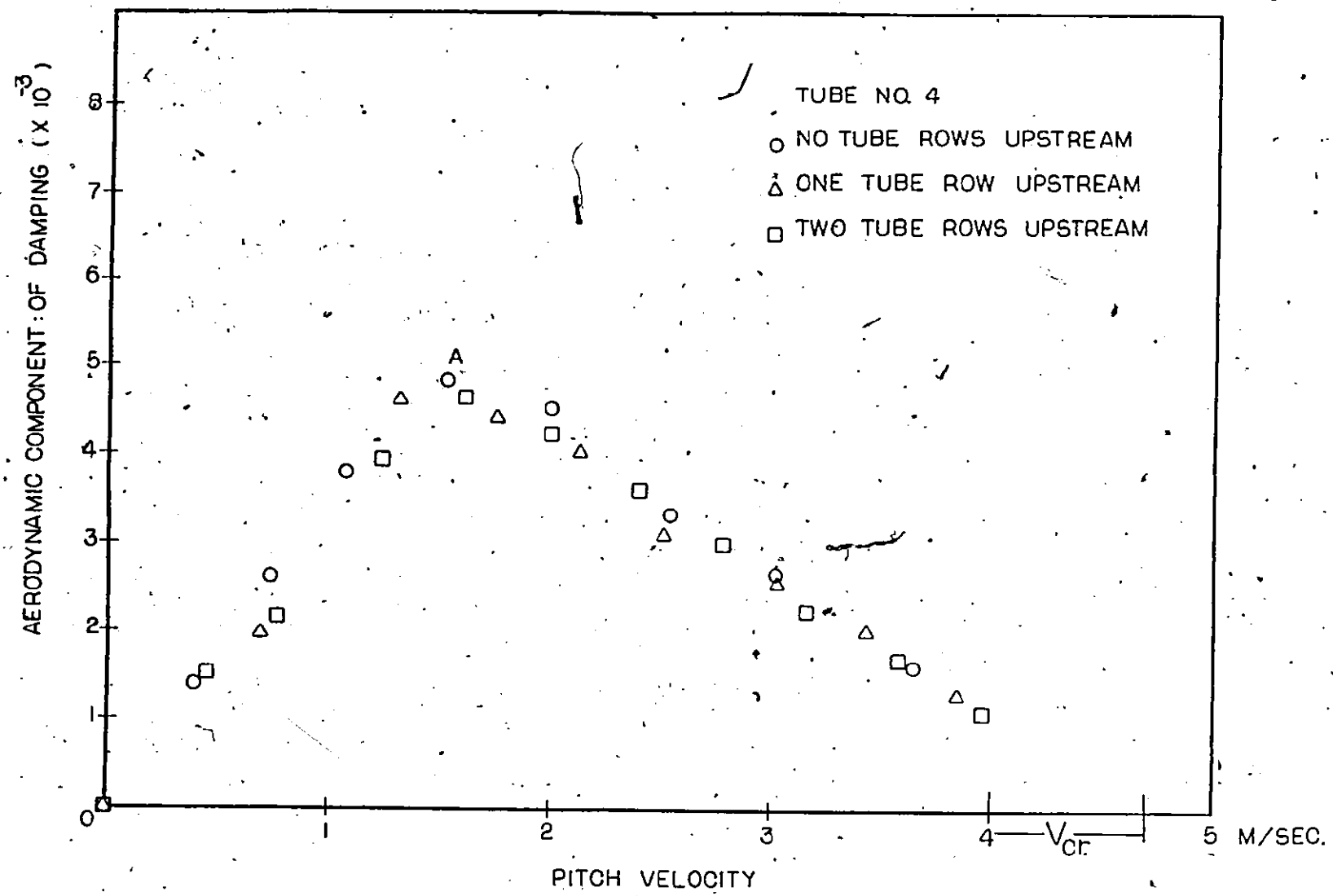

FIGURE 4.7 THE EFFECT OF FLOW VELOCITY ON THE AERODYNAMIC COMPONENT OF DAMPING

TABLE 4.1

Fluid Dynamic Damping for Tube No. 2
for Different Tube Location

No Tube Rows Upstream		One Tube Row Upstream		Two Tube Rows Upstream	
Static Damping=0.0078		Static Damping=0.0107		Static Damping=0.0096	
Flow Velocity m/sec.	δ_d	Flow Velocity m/sec.	δ_d	Flow Velocity m/sec.	δ_d
0.00	0.0000	0.00	0.0000	0.00	0.0000
0.38	0.0003	0.22	0.0004	0.24	0.0005
0.71	0.0014	0.72	0.0014	0.76	0.0016
1.18	0.0024	1.18	0.0025	1.90	0.0035
1.51	0.0029	1.52	0.0033	2.21	0.0037
2.00	0.0039	2.04	0.0037	2.52	0.0034
2.29	0.0037	2.36	0.0034	2.80	0.0032
2.74	0.0033	2.71	0.0029	3.16	0.0027
3.20	0.0024	3.02	0.0025		
4.20	0.0005	3.43	0.0016		

TABLE 4.2

Fluid Dynamic Damping for Tube No. 4
for Different Tube Location

No Tube Rows Upstream		One Tube Row Upstream		Two Tube Rows Upstream	
Static Damping=0.014		Static Damping=0.0167		Static Damping=0.0168	
Flow Velocity m/sec.	δ_d	Flow Velocity m/sec.	δ_d	Flow Veloctiy m/sec.	δ_d
0.00	0.0000	0.00	0.0000	0.00	0.0000
0.39	0.0014	0.69	0.0020	0.46	0.0015
0.74	0.0026	1.31	0.0046	0.76	0.0022
1.07	0.0038	1.75	0.0044	1.23	0.0039
1.53	0.0048	2.13	0.0040	1.60	0.0046
2.00	0.0045	2.52	0.0031	1.99	0.0042
2.55	0.0033	3.03	0.0026	2.40	0.0036
3.04	0.0027	3.43	0.0020	2.78	0.0030
3.65	0.0016	3.85	0.0013	3.16	0.0022
				3.58	0.0017
				3.96	0.0011

seems wide in both figures because it includes the range of uncertainty involved in determining precisely the critical flow velocity for both tubes in different tube locations as seen in the next section. In Figure 4.7 the total damping was increased by about 26% when the flow velocity was about 38% of the stability threshold. This increase in dynamic damping is believed to be due to some correlation between the forces upstream and in the wake of the tube which are trying to hold the tube from vibrating around its equilibrium position. As the flow velocity further increases, the total effective damping starts to decrease. The mechanism involved in this behaviour is not understood, but it seems that the energy fed from the fluid to the tubes increases over that dissipated by the fluid dynamic damping. Around the stability threshold the total effective damping disappears. The difference between the results obtained from the movable tube no. 2 in the second row and the movable tube no. 4 in the fourth row was believed possibly to be due to the difference in the turbulence intensity between the second and fourth rows. However, the difference persisted for tube no. 2 when two tube rows upstream were added.

Blevins [39] reported that for small amplitude vibrations in a high Reynolds number cross flow, the viscous damping increases linearly with the flow velocity, and that parallel to the free stream direction has double the slope of that measured in a direction perpendicular to the free stream. If the same relation holds for small Reynolds number cross flow, this may explain the difference between the slope of portion OA obtained for tube no. 2 and that for tube

no. 4. As the damping was measured for tube no. 2 in a direction transverse to the flow, while that measured for tube no. 4 was in a direction making 45° with the flow, so the slope for tube no. 4 is less than double the slope obtained for tube no. 2.

This increase in fluid dynamic damping was also similar to that recorded by Chen [40]. However, his experiments were limited to the onset of vortex induced vibration.

The drop in the fluid dynamic damping to a negligible value at the stability threshold is very important. It suggests the use of the static damping measured in still fluid for the estimate of the velocity for the onset of instability.

4.3 Effect of Tube-Bundle Size on the Fluidelastic Stability Threshold

The effect of number of tube rows upstream on the critical velocity of the monitored tube was determined. As shown in Figure 4.1, tubes marked from 1 to 19 were the movable tubes. Positions marked X were for additional stationary tube rows upstream. The movable tubes were kept at the same conditions as in the previous section. Due to problems with the movable tube no. 1 (see Figure 4.1), in obtaining a good decay record for damping, the movable tubes no. 2 and no. 4 in the second and fourth rows respectively, were examined. The damping of the monitored tube was measured before each run of the experiment. Some slight variation in damping values was noticed after each run of a single experiment due to the end supports and the aluminum filler was used again to keep the damping constant. The amplitude response of the monitored tube was recorded with

no tube rows upstream by following the same procedure described in section 4.1. The stability threshold (critical velocity) was determined and plotted in Figure 4.8. For the purpose of comparing these new values with the old values obtained by Weaver and Grover [9], which started from the seventh row, the new values are plotted using the following relation,

$$V_{corr.} = V_{cr.}\left(\frac{24}{20}\right)\left(\frac{0.007}{\delta}\right)^{0.21}$$

This is Grover's stability equation which was established using a 24 Hz monitored tube with a fixed value of damping equal to 0.007. This procedure was repeated adding one row of stationary tubes to the front of the tube-bundle at a time, until the movable tube no. 4 was in the tenth row. The same experiment was repeated removing one row of stationary tubes from the front of the tube-bundle at a time, until the movable tube no. 1 was directly facing the upstream flow. Because of the difference noticed between the new results and Grover's results in the nineth and the tenth rows, the complete experiment was repeated four times. The results obtained are plotted in Figure 4.8. The stability threshold for the first row was obtained by removing the movable tube no. 1 and its row of stationary tubes from the first row and this value was recorded for the movable tube no. 2 while it is in the first row. Also, although there is some doubt about the measured damping for tube no. 1 its results are presented as shown in Figure 4.8. These results are reasonably consistent with those of tube no. 2 especially in the third row.

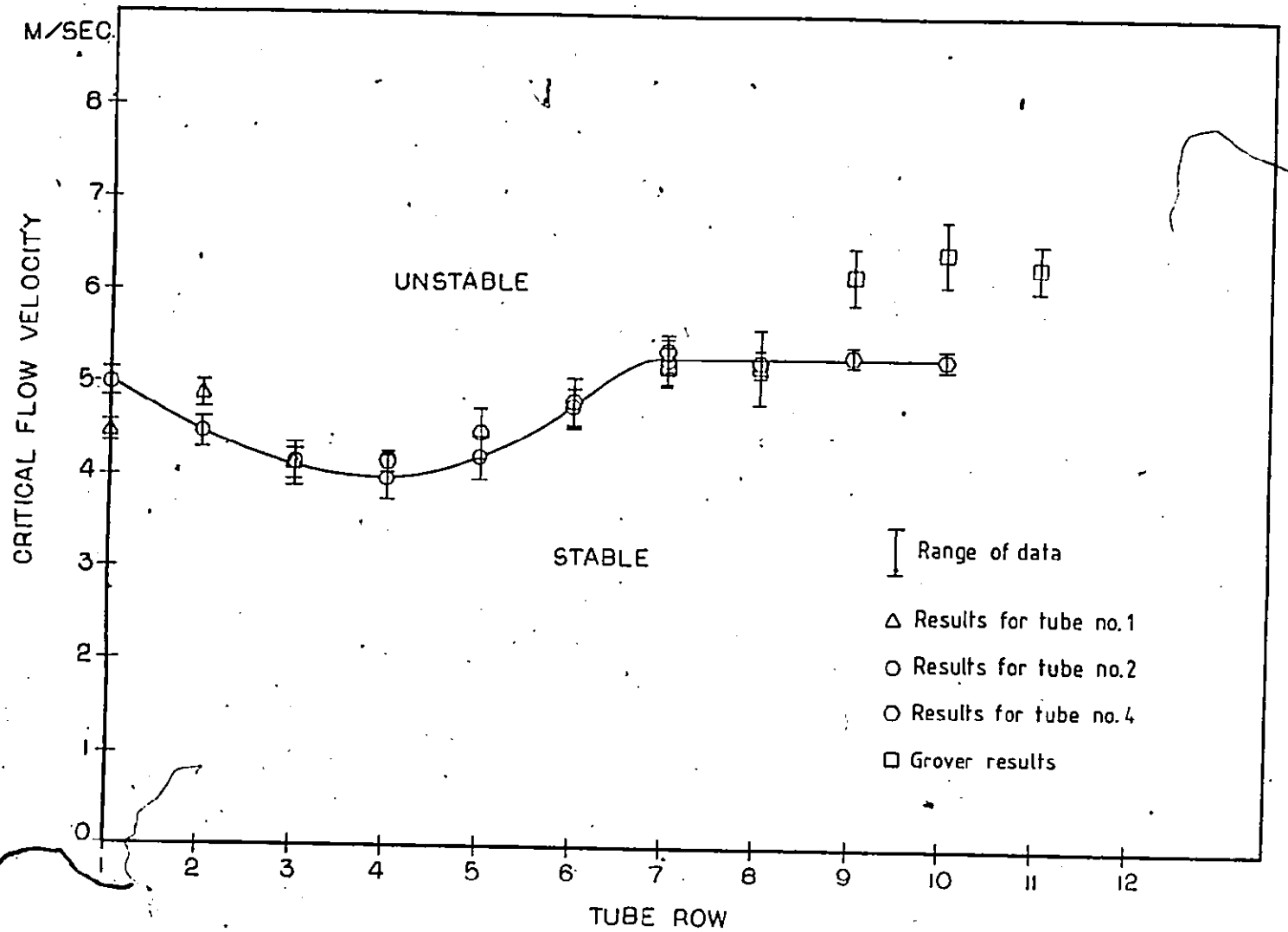

FIGURE 4.8 THE EFFECT OF TUBE - BUNDLE SIZE ON THE CRITICAL FLOW VELOCITY

A smooth curve was drawn through the bands representing experimental uncertainty. The data obtained from the complete set of experiments are given in Table 4.3. The figures respresenting these results are given in Appendix D.

The result obtained is not a surprising one, in that the critical flow velocity varies with the size of the tube-bundle. The stability threshold is lowest when the tubes are in the third or fourth rows. This result was recorded for movable tube no. 2 with two rows of stationary tubes in the front of the tube-bundle. Close agreement was recorded for movable tube no. 4 in the fourth row with no rows of stationary tubes upstream. The highest value for the critical velocity was recorded in the seventh row and subsequent rows showed no further change.

The 21% drop in the stability threshold between the first and the fourth row was believed to be due to a good spanwise correlation of forces on the tubes and a weak turbulence intensity. Between the fourth and the seventh row, the critical flow velocity was increased by about 26%. This increase could be explained due to an increase in the turbulence intensity level which resulted in a delay of large amplitude vibrations to higher flow velocities. Once the interstitial flow is well established, no change occurs deeper inside the tube bundle.

Similar observations for the turbulence intensity level for the first few rows were recorded by Savkar [3]. In addition, most of the damage for tubes in heat exchangers have been reported for the third and the fourth rows. The difference of a maximum value of about 17% between the new results and Weaver

TABLE 4.3

Row No.	Critical Velocity Tube No. 1 (m/sec)	LOG. DEC. δ	Corres-ponding Velocity (m/sec)	Critical Velocity Tube No. 2 (m/sec)	LOG. DEC. δ	Corres-ponding Velocity (m/sec)	Critical Velocity Tube No. 4 (m/sec)	LOG. DEC. δ	Corres-ponding Velocity (m/sec)
1	4.55	0.0185	4.46	4.76	0.0134	4.99			
2	5.04	0.0200	4.85	3.80	0.0079	4.45			
3	4.19	0.0182	4.12	3.54	0.0080	4.13			
4				3.40	0.0082	3.95	4.00	0.0140	4.15
5				3.54	0.0074	4.21	4.60	0.0190	4.48
6				4.05	0.0078	4.75	4.63	0.0142	4.78
7				4.38	0.0072	5.23	5.15	0.0140	5.35
8							5.25	0.0168	5.25
9							5.15	0.0142	5.33
10							5.10	0.0142	5.28

$$V_{corr.} = V_{cr.} \left(\frac{24}{20}\right)\left(\frac{0.007}{\delta}\right)^{0.21}$$

and Grover's results [9] from the nineth to the eleventh row was believed to be due to the value of damping used by Grover. A constant value of 0.0070 for damping was used by Grover over about 45 runs of the experiment. Although the damping does not appear explicity in Figure 4.8, its effect on the critical flow velocity can be seen from the stability equation.

These results were very important for the rest of the experiments. It appears that the first tubes to become unstable in a particular tube-bundle will be in the first few rows particularly in the third and fourth rows. That is, experiments on a tube-bundle with only five rows of tubes should be adequate for establishing the critical fluidelastic stability boundary for that array.

4.4 Fluidelastic Stability Boundary for the Array

The fluidelastic stability boundary for the array may be plotted in the form of a velocity parameter against a damping parameter. The location of this boundary is a function of tube pitch and the geometry of the tube-array. The concept of the fluidelastic boundary was coined by Connors [4], from his experiments which were conducted on a single row of tubes only. It was unclear if Connors' results would be applicable to tube-arrays. Many researchers [5-8] conducted their experiments on tube-arrays, but their results were plotted using Connors' relationship. Weaver and Grover [9] conducted similar experiments on a tube-array, which resulted in a new slope for the stability boundary. His experiments were carried on with a

fixed tube mass and variable damping. As the damping parameter is the product of two dimensionless parameters (mass ratio and damping), the present experiments were conducted to study the effect of changing the mass ratio while keeping the damping constant. The design of the test section allowed the tubes to be changed without causing any damage. As seen in the last section, tubes in the third or fourth rows have the lowest thresholds. For this reason, the movable tube no. 4 was chosen as the monitored tube. Tube no. 4 (see Figure 4.1) and its surrounding neighbours (nos. 2, 3, 5, 6, 11 and 13) were tuned to 20.0 Hz. The rest of the movable tubes were kept above 30.0 Hz so that they behaved essentially like rigid tubes.

As described in the previous chapter, the test section was provided with discrete damping devices to maintain any desired value of damping. These devices consisted essentially of a small cup and paddle assembly installed one each at the top and bottom of the movable tubes. Different grades of motor oil in varying quantities could be poured into the damping cups to vary the damping.

Many experiments were conducted with the movable tube no. 4 and its surrounding neighbours, from which a value of 0.025 for the logarithmic decrement of damping was decided to be used as the fixed value of damping.

The procedure for tuning any of these seven movable tubes to this value of damping was as follows:

(1) The type of oil required (SAE 10 or 20) to obtain the desired value of damping was selected and then poured into the

top and bottom cups of the movable tube. The approximate level of this oil in the cups was noted.

(2) The tube was instrumented to record its motion on a U.V. recorder.

(3) The tube was then plucked and released from its static equilibrium position and the resultant amplitude decay trace was obtained from the U.V. recorder.

(4) From this trace the logarithmic decrement of damping was computed.

(5) Oil was then added or taken out from the damping cups depending on whether the computed value of logarithmic decrement was lower or higher than the desired value of damping. A new amplitude-decay trace was then recorded and another value of damping was similarly computed. This procedure was repeated until the desired value of damping had been obtained.

(6) Steps (1) - (5) were repeated for each of the seven movable tubes until they had all been tuned to the desired value of damping.

The amplitude-decay traces obtained showed excellent linear characteristics of the tube behaviour. These seven movable tubes were changed six times in order to determine the tube response for different tube mass ratios. Great care was taken to prevent any damage to the tubes. The springs on the top of the test section were changed twice in order to maintain fine tuning for the piano-wire tension. The calculations made are given in Appendix C. The natural frequency of these seven

movable tubes always tuned to a fixed value of 20.0 Hz. The aluminum filler was poured into the end holes of each of the movable tubes before adjusting their damping. Steps (1) - (6) were repeated for each set of the movable tubes to adjust the logarithmic decrement of damping to the desired value of 0.025.

4.4.1 Tube Response for Different Tube Mass Ratios

The amplitude-response of the monitored tube (the movable tube no. 4) was recorded for various values of tube mass by following the same procedure described in section 4.1.

The amplitude-response for the original set of tubes (set no. 1, see Table 4.4) is shown in Figure 4.9. The amplitude-response again consisted of two regions, region OA where the tube responded to turbulence in the flow and the unstable region above A. The turbulence excited motion of the tube as seen on the screen of the oscilloscope was random in charater. This region was followed by fluidelastic response of the tube with larger amplitudes and the tube motion becomes periodic. The transition region from turbulence response to fluidelastic response defines the 'stability threshold'.

The tubes were then replaced by set no. 2 and the amplitude-response was similarly plotted as shown in Figure 4.10. The monitored tube responded again to turbulence followed by a change in the slope of the curve defining the stability threshold and a fluidelastic response at the natural frequency of the tube. The amplitude build-up was less than when the tubes were lighter and a considerable increase in the critical

TABLE 4.4

SET NO.	MATERIAL	TUBE MASS (Kgs.)	TENSION REQUIRED TO GET 20.0 HZ. TUNING (Kgs.)
1	Aluminum	0.0480	5.80
2	Aluminum	0.0991	11.97
3	Steel (cold-drawn)	0.2706	32.67
4	Brass	0.3611	43.61
5	Steel (cold-drawn)	0.4615	55.72
6	Steel (cold-drawn)	0.5444	65.74

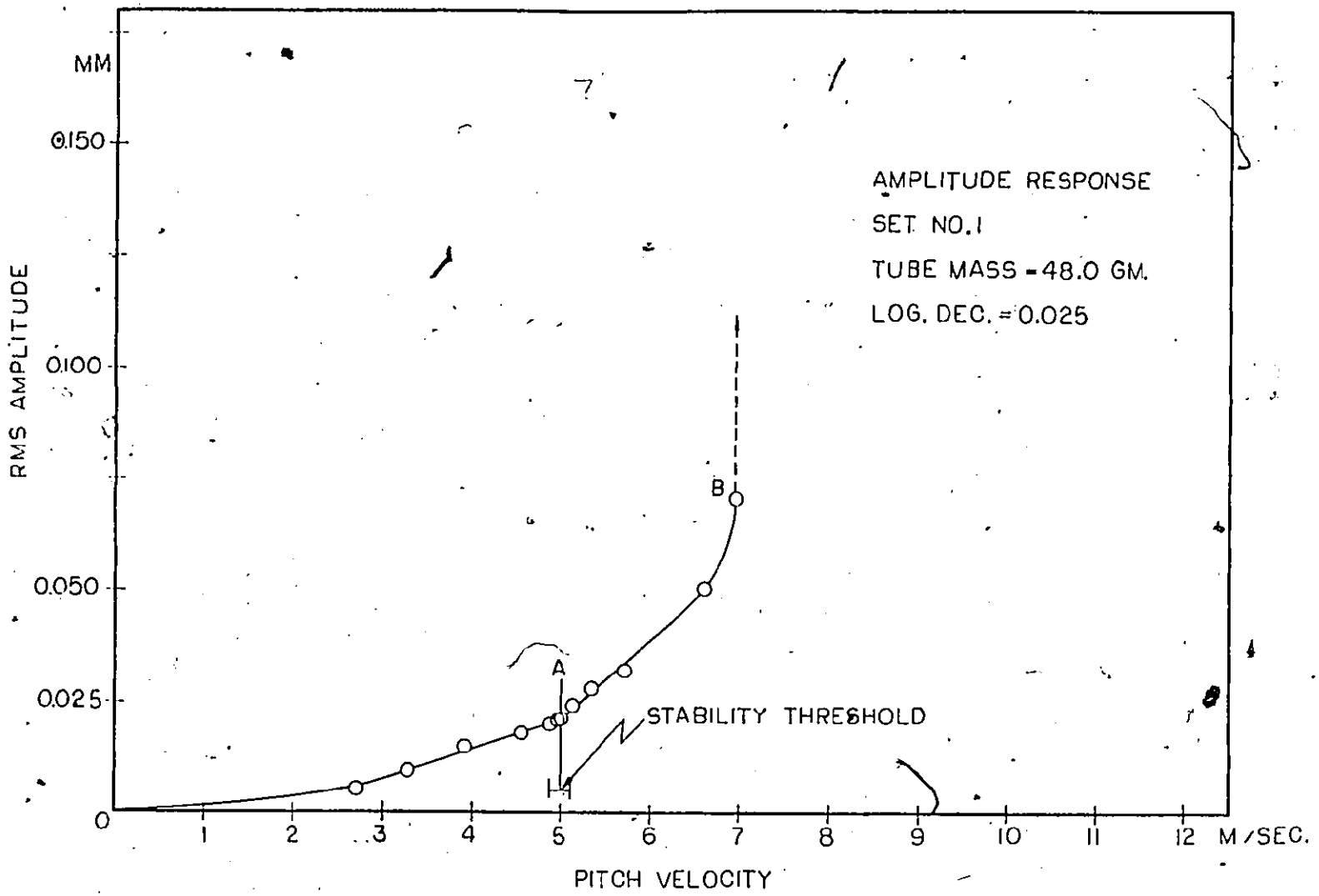
MM
0.150
0.100
0.050
0.025
0
RMS AMPLITUDE
AMPLITUDE RESPONSE
SET NO. I
TUBE MASS = 48.0 GM.
LOG. DEC. = 0.025
A
B
STABILITY THRESHOLD
1
2
3
4
5
6
7
8
9
10
11
12
M/SEC.
PITCH VELOCITY

FIGURE 4.9

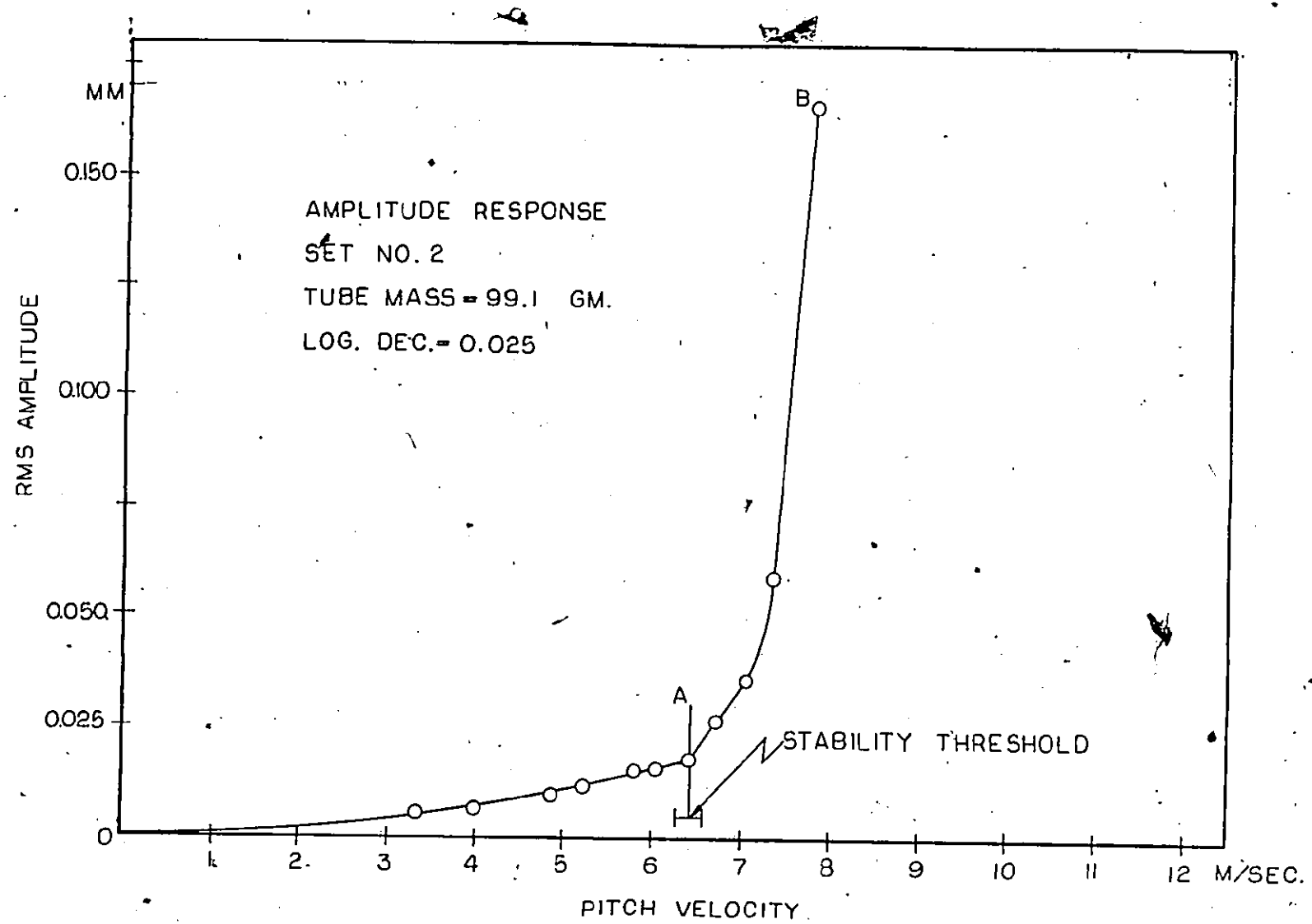
MM
0.150
0.100
0.050
0.025
0
RMS AMPLITUDE
AMPLITUDE RESPONSE
SET NO. 2
TUBE MASS = 99.1 GM.
LOG. DEC. = 0.025
A
B
STABILITY THRESHOLD
1
2
3
4
5
6
7
8
9
10
11
12 M/SEC.
PITCH VELOCITY

FIGURE 4.10

velocity is recorded.

The tubes were again replaced by heavier ones (set no. 3) and the amplitude-response of the instrumented tube was computed and has been plotted in Figure 4.11. The basic character of the tube response remains the same, viz., turbulence response region followed by fluidelastic region. The transition region does not seem to be dependent on the tube mass as compared with the case of changing the damping. It was recorded by Weaver and Grover [9], that as the damping increases, the transition region becomes wider and more gradual.

The amplitude-response for set no. 4 was similarly computed and has been plotted in Figure 4.12. After the stability threshold was determined, the logarithmic decrement of damping was increased to a value of 0.04, following steps (1) - (6) given early in this section. The amplitude-response was then computed and plotted in Figure 4.13. As a result of increasing the damping the amplitudes of vibration decreased in both the turbulence and fluidelastic regions. The transition region is more gradual. This result was similar to that recorded by Weaver and Grover [9] for higher values of damping. A considerable increase in the critical velocity was also noted.

The paddles were then taken from the oil cups at the top and bottom of the test section and the logarithmic decrement of damping in air was measured. The amplitude-response was then computed and plotted as shown in Figure 4.14.

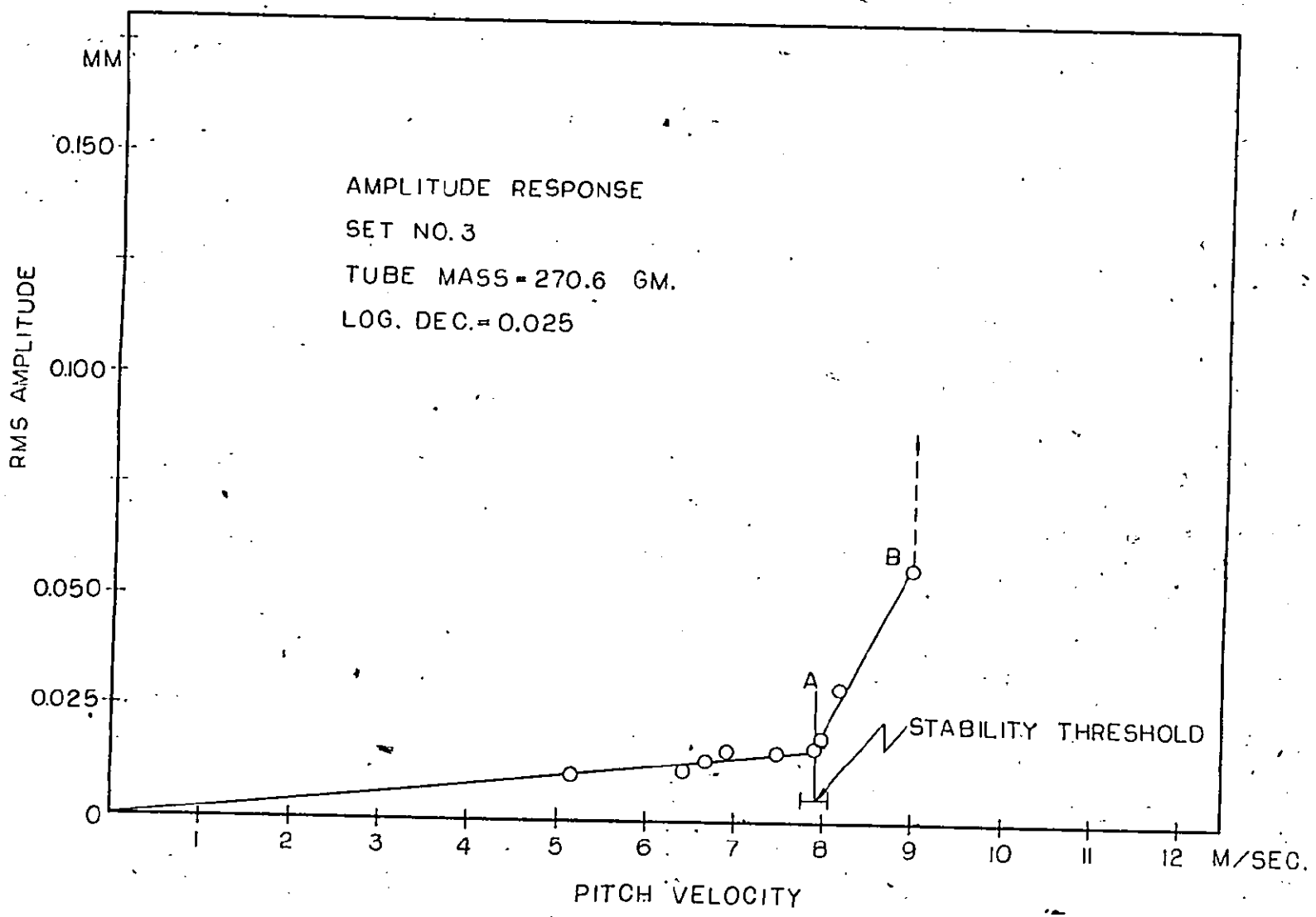
MM
0.150
0.100
0.050
0.025
0
RMS AMPLITUDE
AMPLITUDE RESPONSE
SET NO. 3
TUBE MASS = 270.6 GM.
LOG. DEC. = 0.025
A
B
STABILITY THRESHOLD
1
2
3
4
5
6
7
8
9
10
11
12
M/SEC.
PITCH VELOCITY

FIGURE 4.11

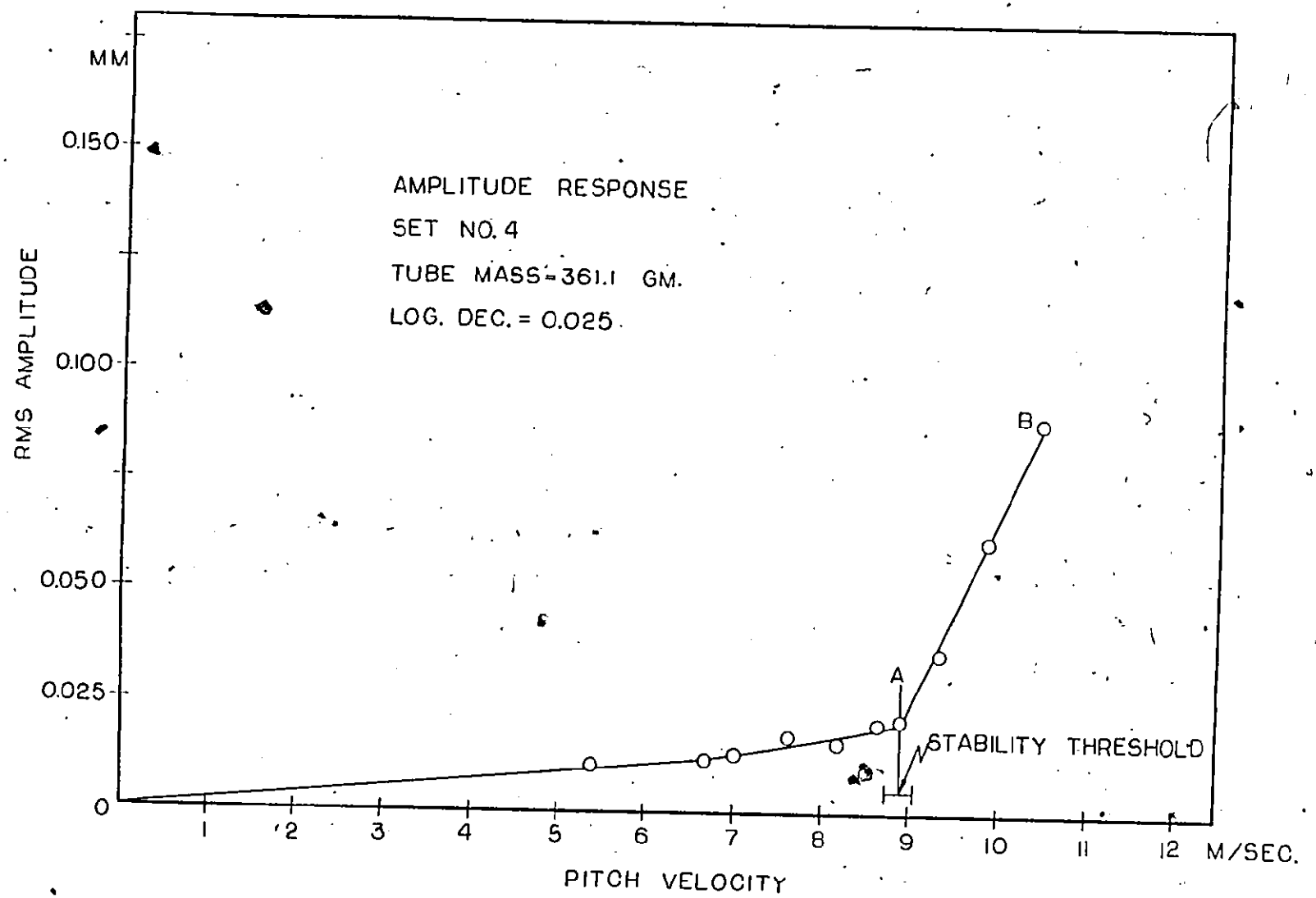
MM
0.150
0.100
0.050
0.025
0
RMS AMPLITUDE
AMPLITUDE RESPONSE
SET NO. 4
TUBE MASS = 361.1 GM.
LOG. DEC. = 0.025
A
B
STABILITY THRESHOLD
1
2
3
4
5
6
7
8
9
10
11
12
M/SEC.
PITCH VELOCITY

FIGURE 4.12

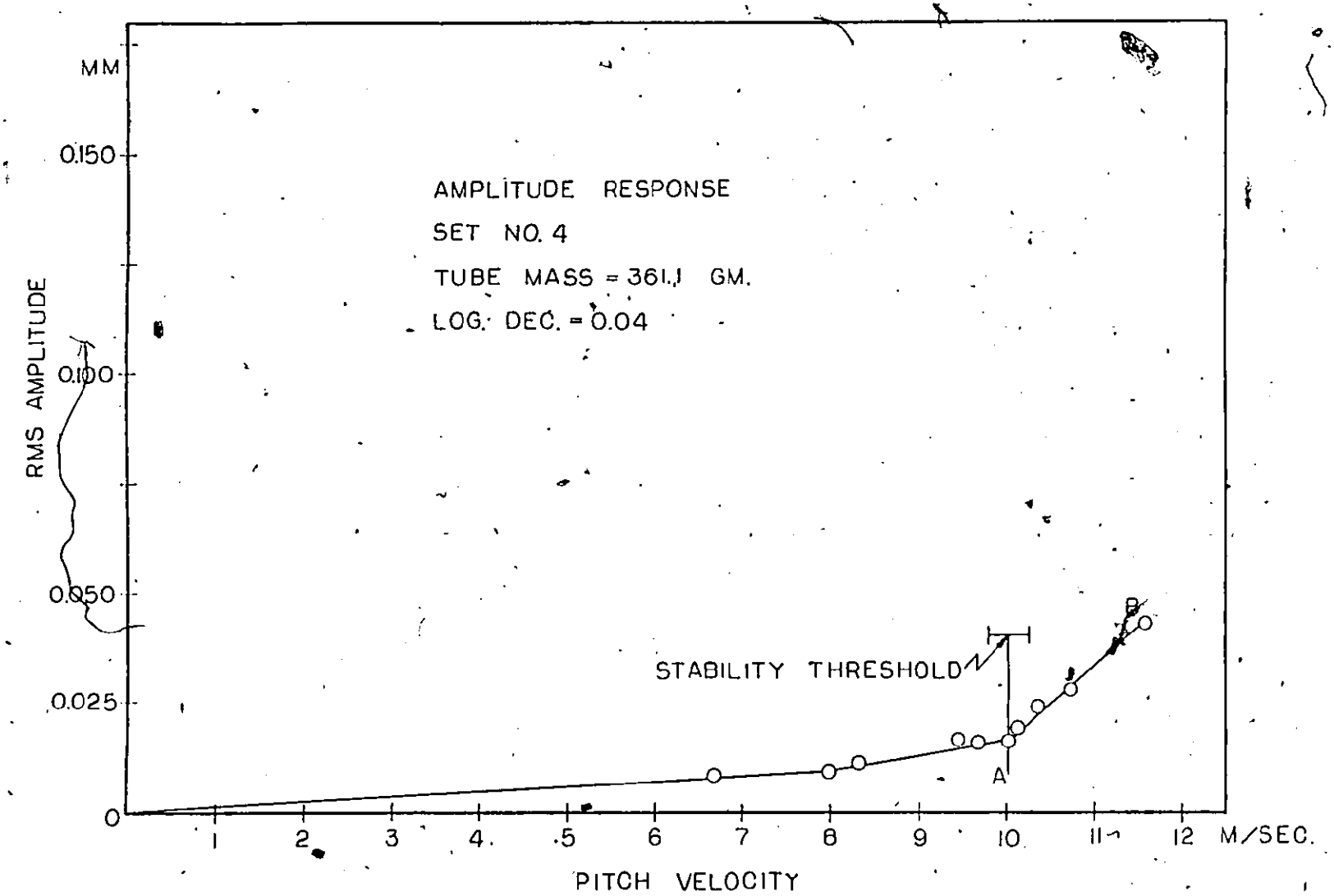
MM
0.150
0.100
0.050
0.025
0
RMS AMPLITUDE
AMPLITUDE RESPONSE
SET NO. 4
TUBE MASS = 361.1 GM.
LOG. DEC. = 0.04
STABILITY THRESHOLD
A
B
1
2
3
4
5
6
7
8
9
10
11
12
M/SEC.
PITCH VELOCITY

FIGURE 4.13

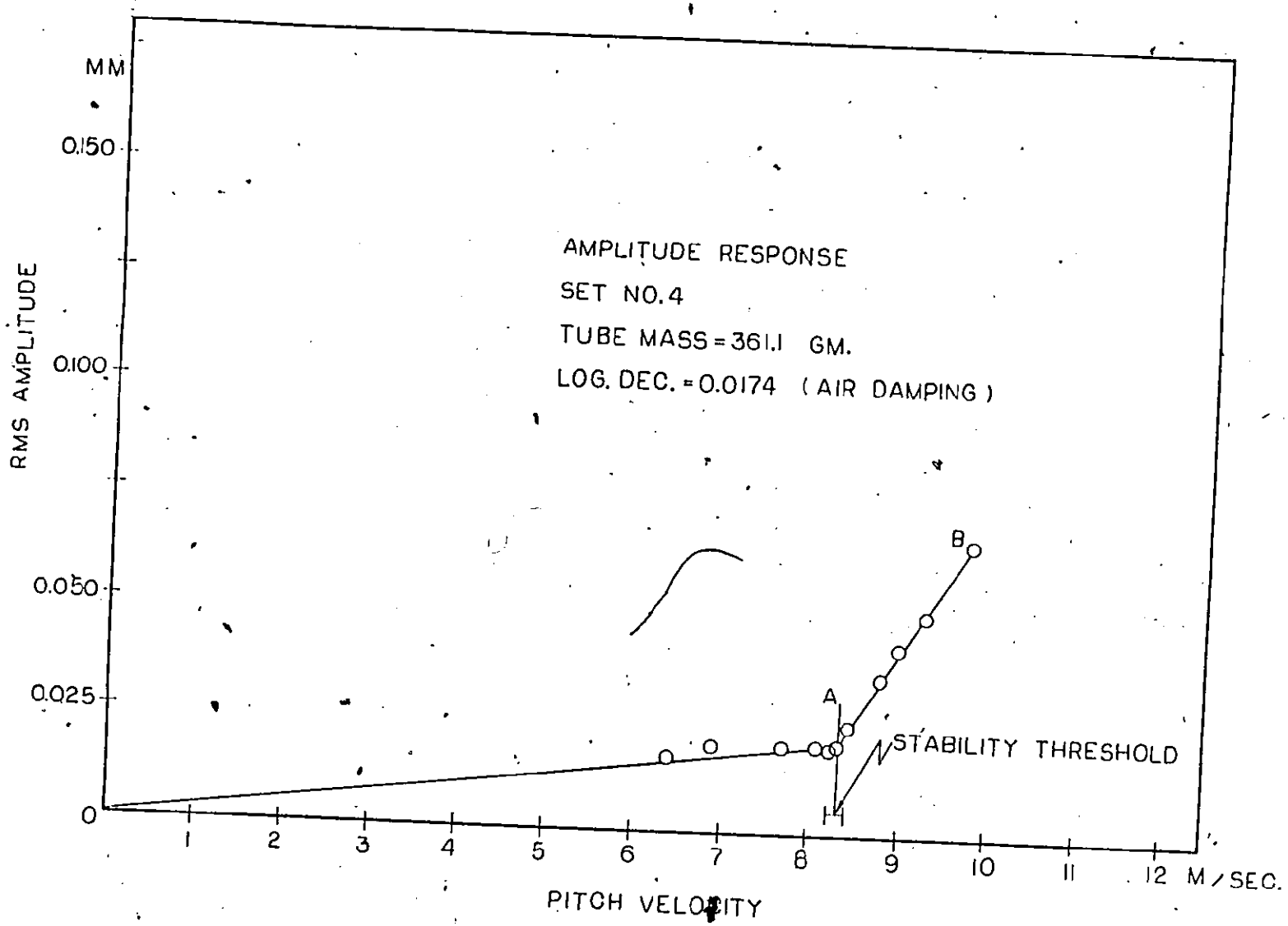
MM
0.150
0.100
0.050
0.025
0
RMS AMPLITUDE
AMPLITUDE RESPONSE
SET NO. 4
TUBE MASS = 361.1 GM.
LOG. DEC. = 0.0174 (AIR DAMPING)
A
B
STABILITY THRESHOLD
1
2
3
4
5
6
7
8
9
10
11
12 M/SEC.
PITCH VELOCITY

FIGURE 4.14

As before, it is noticed that the amplitude of the tube vibration does not stay constant. However, the transition region was smaller giving greater certainty in properly locating the 'stability threshold'.

The results obtained from this set of tubes as a result of keeping the mass ratio constant and varying the damping were similar to that obtained by Weaver and Grover [9] for the stability boundary. The representation of these results is given later in this chapter.

The tube sets nos. 5 and 6 were then replaced one at a time and the damping was adjusted to the required value. The amplitude response of the instrumented tube was computed for each set and then plotted as shown in Figures 4.15 and 4.16. The amplitudes of vibration were smaller than when the tubes were lighter in both the turbulence region and the fluidelastic region.

Apparently, the RMS amplitude at which instability occurs decreases slightly as the tube mass increases. The change in the RMS amplitude at instability were between 0.0210-0.0126 mm. depending on the tube mass. It is noticed as well that the critical flow velocity for fluidelastic instability increases considerably with the increase in tube mass.

4.4.2 The Stability Boundary as a Function of Mass Ratio

The results obtained for the 'stability threshold' for different tube mass were then nondimensionalized to reduced velocity or the velocity parameter in the form V_p/fD where

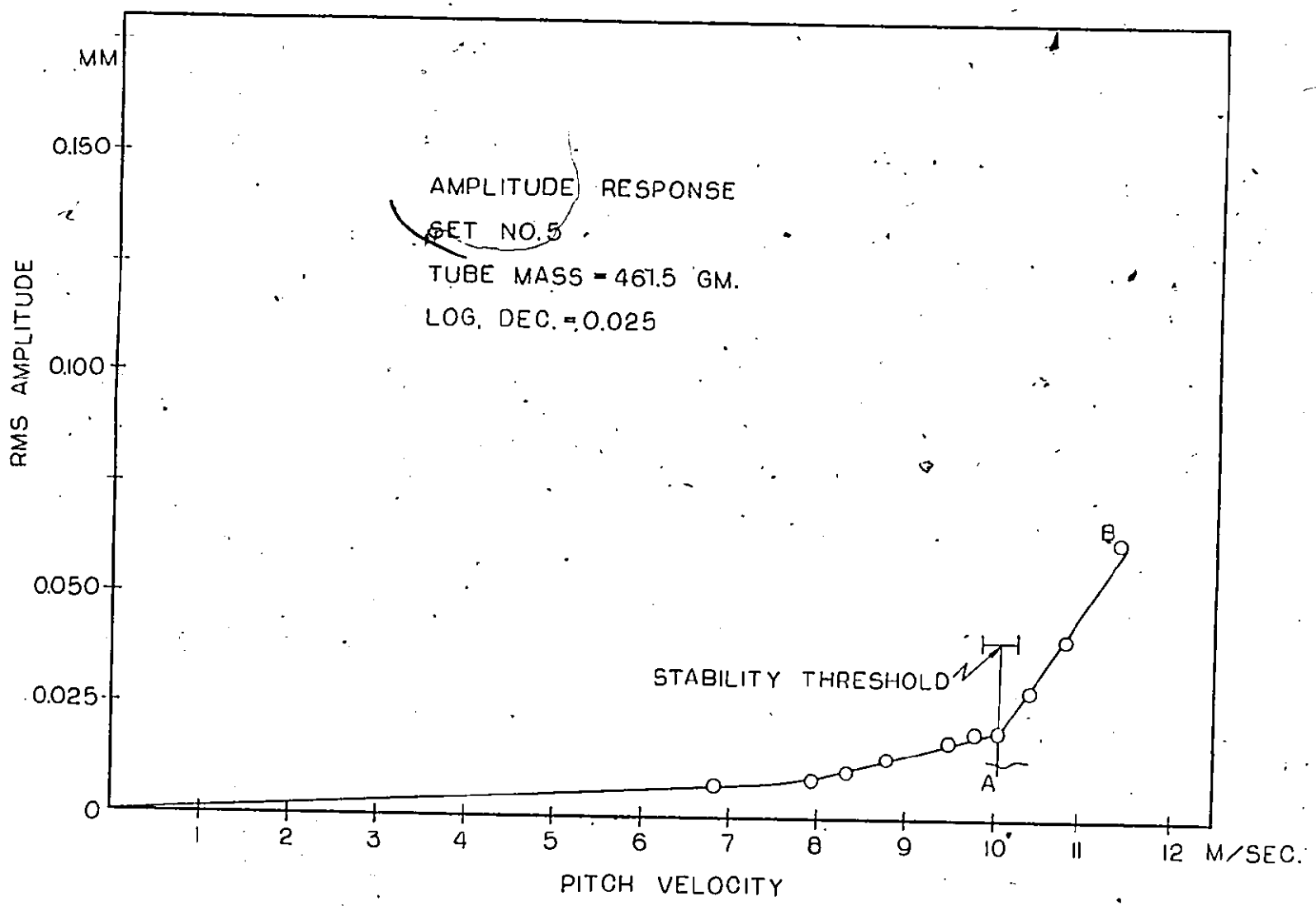
MM
0.150
0.100
0.050
0.025
0
RMS AMPLITUDE
AMPLITUDE RESPONSE
SET NO. 5
TUBE MASS = 461.5 GM.
LOG. DEC. = 0.025
STABILITY THRESHOLD
A
B
1
2
3
4
5
6
7
8
9
10
11
12 M/SEC.
PITCH VELOCITY

FIGURE 4.15

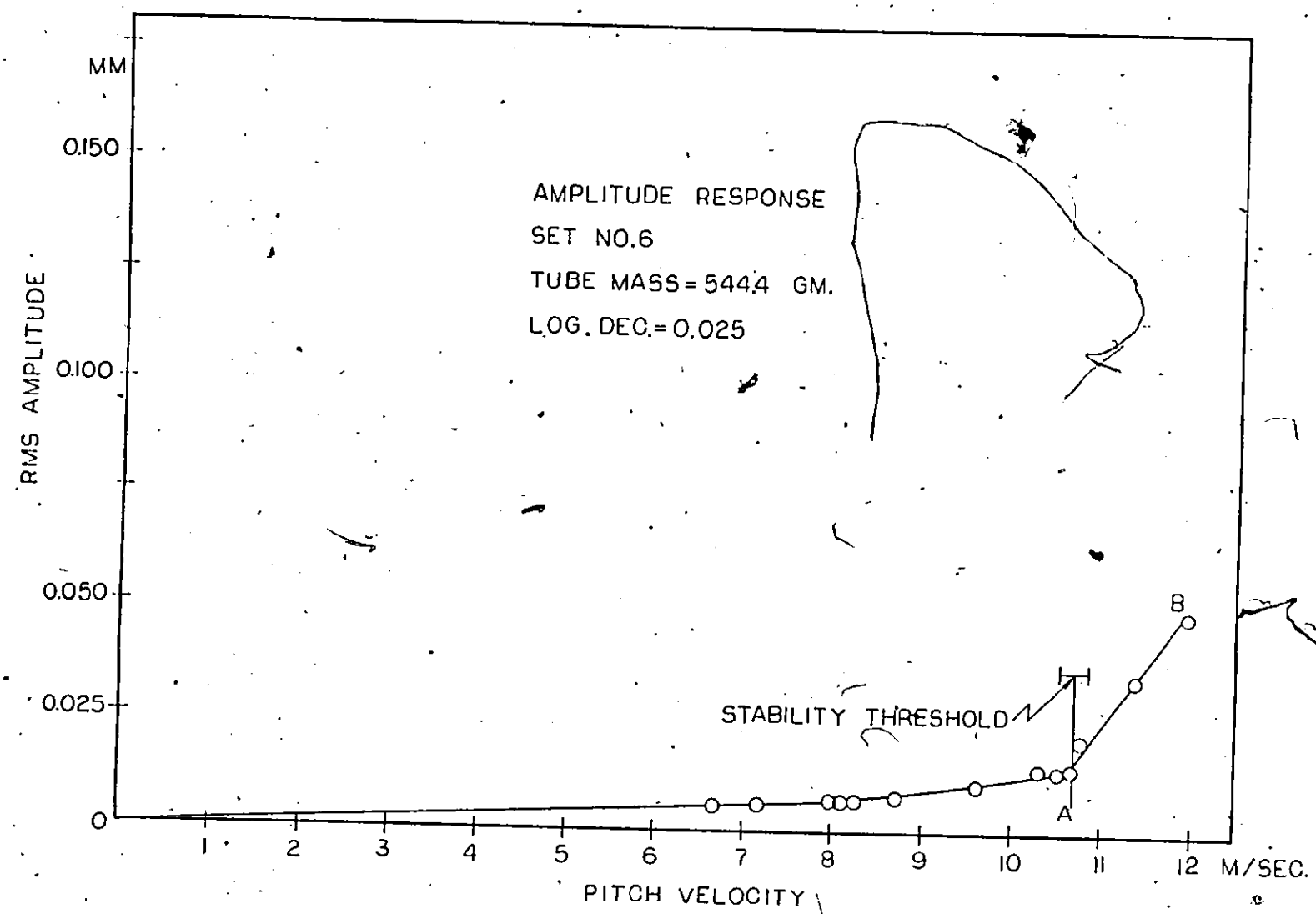
MM
0.150
0.100
0.050
0.025
0
RMS AMPLITUDE
AMPLITUDE RESPONSE
SET NO.6
TUBE MASS = 544.4 GM.
LOG. DEC. = 0.025
STABILITY THRESHOLD
A
B
1
2
3
4
5
6
7
8
9
10
11
12
M/SEC.
PITCH VELOCITY

FIGURE 4.16

V_p is the critical flow velocity, f is the natural frequency of the tube and D is the tube diameter. The computed reduced velocity was then plotted against the damping parameter as shown in Figure 4.17.

A least square straight line fit through these points was computed and is drawn as shown in Figure 4.17. The range of uncertainty for properly locating the stability threshold was also nondimensionalized to reduced velocities and plotted as shown in Figure 4.17.

The least-squares fit to a straight line drawn in Figure 4.17 represents the 'stability boundary' for the tube-array used to conduct the present experiments. The stability boundary has the form

$$\frac{V_p}{fD} = 6.2 \left(\frac{m\delta}{\rho D^2}\right)^{0.29}$$

This boundary is obtained by keeping the tube damping constant while changing the tube mass, with f, ρ, and D are constants.

The constant 6.2 is applicable only to this tube-array and varies from one tube-array to another depending on the array geometry and damping.

In the region below this boundary the tubes are stable and respond randomly to small vibrations due to the turbulence in the flow. Above this boundary large amplitude vibrations of the tube occur at its natural frequency due to fluidelastic mechanism and the tube is said to be unstable.

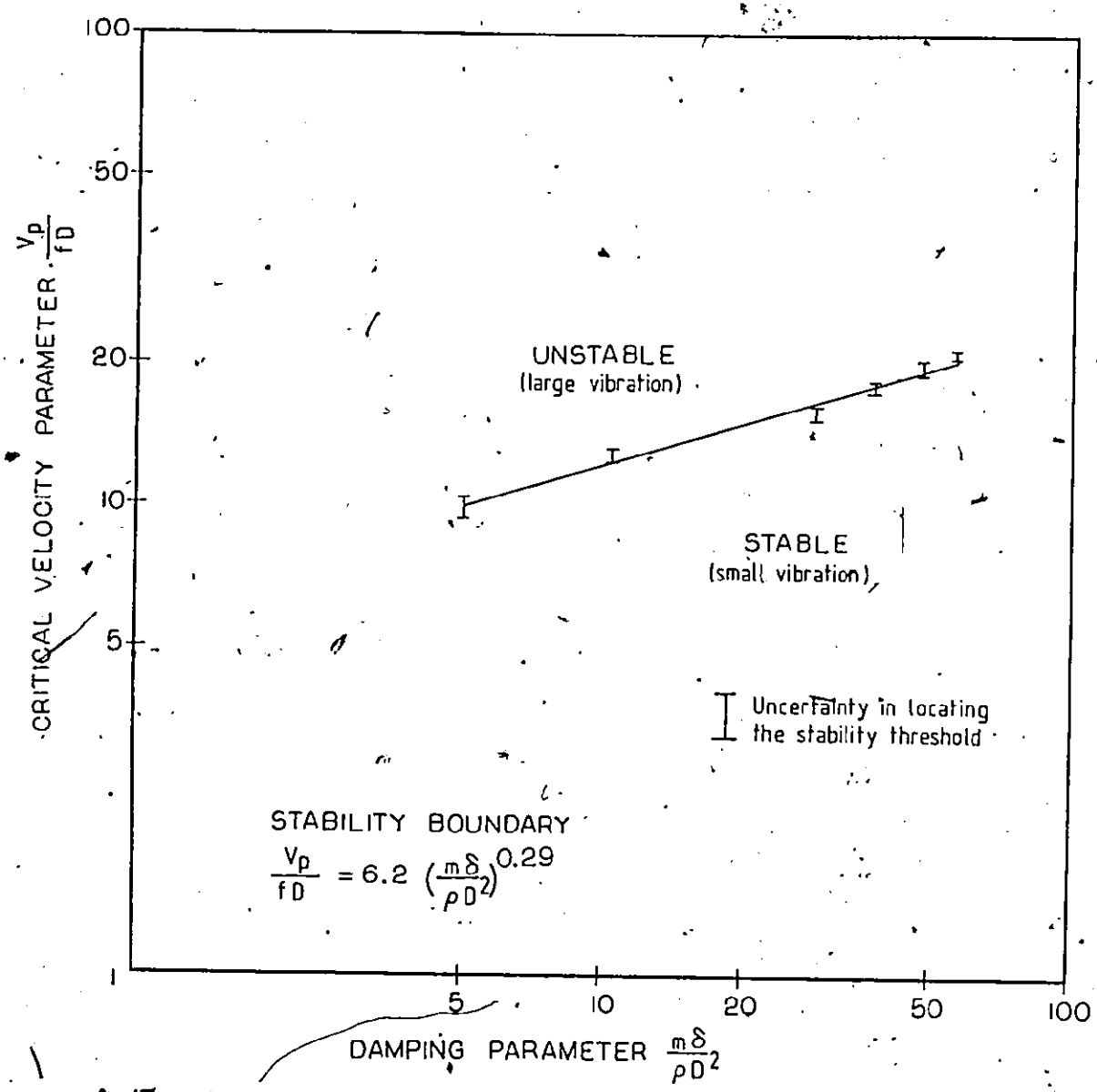
100
50
20
10
5
1
CRITICAL VELOCITY PARAMETER $\frac{V_p}{fD}$
UNSTABLE
(large vibration)
STABLE
(small vibration)
Uncertainty in locating the stability threshold
STABILITY BOUNDARY
$\frac{V_p}{fD} = 6.2 \left(\frac{m\delta}{\rho D^2}\right)^{0.29}$
5
10
20
50
100
DAMPING PARAMETER $\frac{m\delta}{\rho D^2}$

FIGURE 4.17

The two parameter ranges for which this 'stability boundary' has been obtained are:

Damping parameter $\frac{m\delta}{\rho D^2} = 5$ to 58

Velocity parameter $\frac{V_p}{fD} = 9.0$ to 22

The data used in plotting the 'stability boundary' is given in Table 4.5

As a result of keeping the tube mass constant for set no. 4 and tuning the tube to various values of damping, two other points are obtained for this set. The line fitted through these three points is shown in Figure 4.18. The data used are given in Table 4.6. The results obtained by Weaver and Grover [9] from his experiments on the same tube-array for constant tube mass and variable damping is also plotted in Figure 4.18. The two lines showed the same slope for the stability boundary. This boundary was defined by Weaver and Grover as

$$\frac{V_p}{fD} = 7.1 \left(\frac{m\delta}{\rho D^2}\right)^{0.21}$$

Figure 4.18 shows the difference in the boundary obtained from the present experiments using variable tube mass with constant damping and the old results obtained by Weaver and Grover using constant tube mass and variable damping.

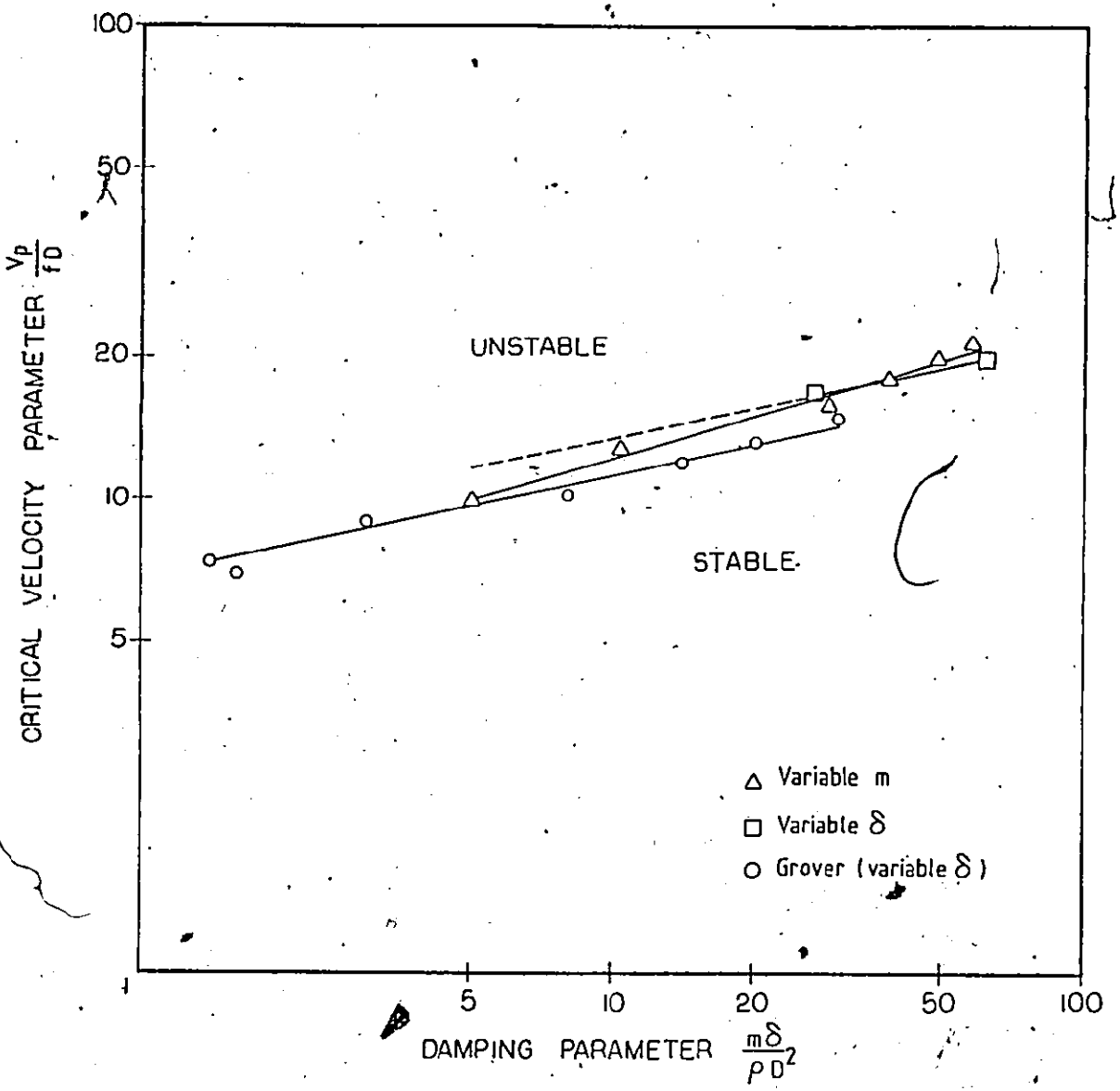
100
50
20
10
5
1
CRITICAL VELOCITY PARAMETER $\frac{V_p}{fD}$
UNSTABLE
STABLE
Variable m
Variable δ
Grover (variable δ)
5
10
20
50
100
DAMPING PARAMETER $\frac{m\delta}{\rho D^2}$

FIGURE 4.18

TABLE 4.5

SET NO.	TUBE MASS (grms.)	$\frac{m}{\rho D^2}$	$V_{p(cr.)}$ (m./sec.)	$\frac{m\delta}{\rho D^2}$	$\frac{V_p}{fD}$
1	48.0	200.00	5.05	5.000	9.94
2	99.1	416.91	6.45	10.42	12.70
3	270.6	1144.98	7.91	28.62	15.57
4	361.1	1528.64	8.92	38.21	17.55
5	461.5	1955.70	10.04	48.89	19.76
6	544.4	2303.35	10.70	57.58	21.06

TABLE 4.6

TUBE SET NO. 4

LOG DEC. δ	CRITICAL VELOCITY V_p (m/sec.)	$\frac{m\delta}{\rho D^2}$	$\frac{V_p}{fD}$
0.0174 (air)	8.35	26.60	16.44
0.0250	8.92	38.21	17.55
0.0400	10.04	61.15	19.76

f = 20.0 Hz.

D = 2.54 cm.

4.4.3 Discussion

The results obtained for the critical velocities from the present investigation show a new slope for the stability boundary. Connors' [4] stability threshold for a single-row of tubes is given by the 0.5 power law, in the form:

$$\frac{V_P}{fD} = 9.9 \left(\frac{m\delta}{\rho D^2}\right)^{0.5}$$

Weaver and Grover's [9] stability threshold for an array of tubes having the same geometry used for the present investigation has the form:

$$\frac{V_P}{fD} = 7.1 \left(\frac{m\delta}{\rho D^2}\right)^{0.21}$$

It is important to note that Weaver and Grover's fluidelastic stability boundary was obtained by varying the logarithmic decrement of damping. The present results show the fluidelastic stability boundary as a function of the mass ratio has the form:

$$\frac{V_P}{fD} = 6.2 \left(\frac{m\delta}{\rho D^2}\right)^{0.29}$$

This leads to a very important result. The mass ratio and logarithmic decrement of damping behave independently of each other. Thus, instead of the stability boundary being a line, it must be a surface, its equation is having the form:

$$\frac{V_P}{fD} = K \left(\frac{m}{\rho D^2}\right)^{0.29} \delta^{0.21}$$

Part of this surface is projected in a two-dimensional graph, as shown in Figure 4.19. This region is a combination of sets of lines having both slopes, i.e., 0.21 and 0.29. To avoid confusion the boundary of this projection is only shown including the present stability boundaries. The extreme lines of this boundary are restricted by the values of damping between 0.01 (obtained by extrapolating the boundary obtained for set no. 4) and 0.040, which are believed to be reasonable for practical design.

The available information on critical flow velocities for tube-arrays has been compiled by Shin and Wambsganss [2] in the form of a stability diagram and is reproduced in Figure 4.20. The results obtained by Weaver and Grover [9] with the present results have also been included in Figure 4.20.

Although nine points lie within the new suggested stability boundary and some other points are very close to this boundary, a comparison between the new results and the available ones still has little basis. Any change in the array geometry will in turn change the constant of proportionality K, and this shifts the stability boundary either above or below the suggested stability boundary. Also any change in the damping from those values used to obtain the extreme lines of this boundary will shrink or expand these two lines depending on the values of damping used. Because of these reasons, further experiments

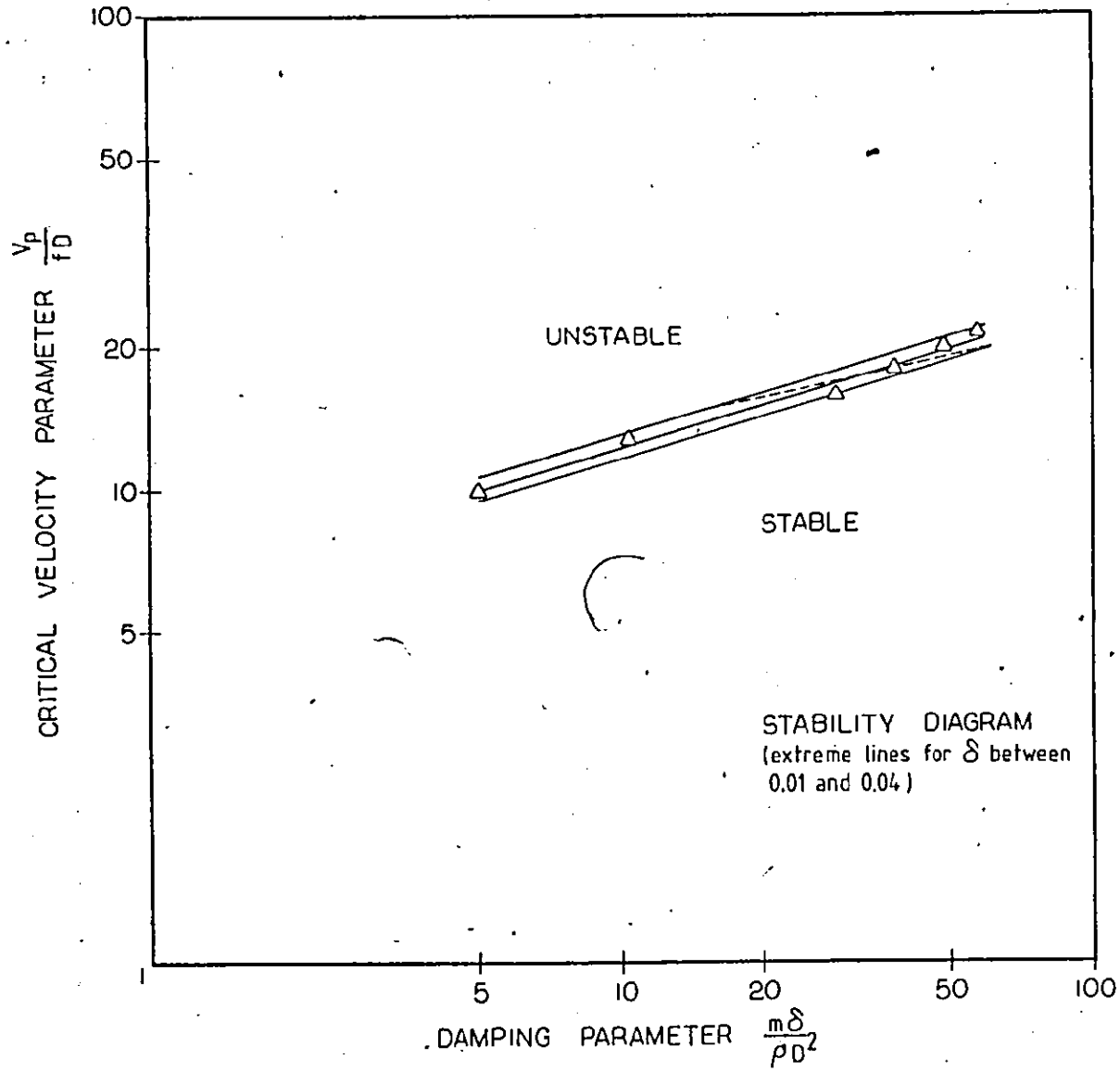
100
50
20
10
5
1
CRITICAL VELOCITY PARAMETER $\frac{V_p}{fD}$
UNSTABLE
STABLE
STABILITY DIAGRAM
(extreme lines for δ between 0.01 and 0.04)
5
10
20
50
100
DAMPING PARAMETER $\frac{m\delta}{\rho D^2}$

FIGURE 4.19

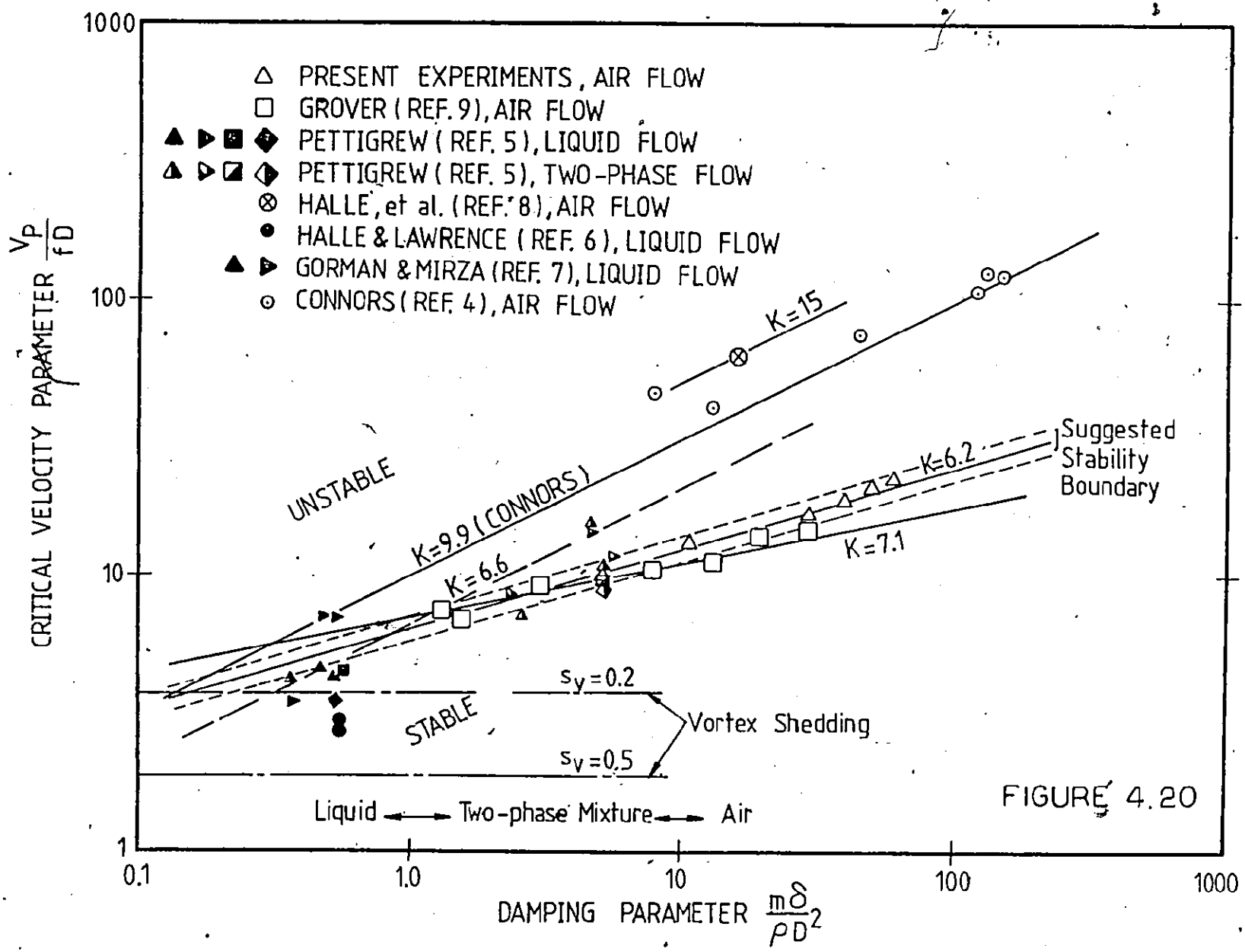
PRESENT EXPERIMENTS, AIR FLOW
GROVER (REF. 9), AIR FLOW
PETTIGREW (REF. 5), LIQUID FLOW
PETTIGREW (REF. 5), TWO-PHASE FLOW
HALLE, et al. (REF. 8), AIR FLOW
HALLE & LAWRENCE (REF. 6), LIQUID FLOW
GORMAN & MIRZA (REF. 7), LIQUID FLOW
CONNORS (REF. 4), AIR FLOW
CRITICAL VELOCITY PARAMETER $\frac{V_p}{fD}$
DAMPING PARAMETER $\frac{m\delta}{\rho D^2}$
1000
100
10
1
0.1
1.0
10
100
1000
UNSTABLE
STABLE
K=15
K=9.9 (CONNORS)
K=6.6
K=6.2
K=7.1
Suggested Stability Boundary
$s_v = 0.2$
$s_v = 0.5$
Vortex Shedding
Liquid ← → Two-phase Mixture ← → Air

FIGURE 4.20

along the same lines are required to generate a family of threshold boundaries for various geometries of tube-arrays.

CHAPTER 5

CONCLUSIONS

The present experiments were conducted in a low-speed wind-tunnel having 305 x 305 mm. working section. The tube-bundle was a parallel-triangular array of tubes having pitch/diameter = 1.375. The array was 18 rows deep with 5 tubes in each row. Nineteen identical tubes in the front of the array were movable and were especially designed so that their natural frequency and damping could be controlled precisely over a range of values. The remaining tubes were fixed tubes and were designed such that they could be conveniently removed from outside the wind-tunnel. Positions for as many as 9 rows of fixed tubes in the front of the tube-array were available in order to facilitate studying the effect of tube-bundle size on tube response.

The response of the tubes to different flow velocities was determined. The tubes responded randomly due to turbulence in the flow, followed by self-excited vibration or fluid-elastic vibration at the tube's natural frequency. The transition region from turbulence response to fluidelastic response defined the 'stability threshold'. The mode shape of vibration of the tube appeared to be predominantly in the transverse direction but the tube frequently oscillated within about $\pm$ 45 to this direction.

The effect of flow velocity on the fluid dynamic damping

was examined experimentally. The dynamic-damping increased with increasing flow velocity up to a maximum value, then dropped to a negligible value as the flow velocity reached the critical velocity of the tube. The first portion of the fluid dynamic damping-flow velocity curve was similar to the results recorded by some other authors. The location of a particular tube seems to have no effect on the fluid dynamic damping. The results obtained at the critical velocity confirm the use of the damping measured in still fluid as a measure of the damping at the onset of instability.

The results from the study of tube-bundle size on the fluidelastic stability threshold, show that the first tubes to become unstable in a particular tube-bundle will be in the first few rows, particularly in the third and fourth rows. That is, experiments on a tube-bundle with only five rows of tubes should be adequate for establishing the critical fluidelastic stability boundary for that array.

A fluidelastic stability boundary as a function of the mass ratio has been determined experimentally for the first time for the array. The results show a new slope for the fluidelastic stability boundary, and the periodic self-excited vibrations in the array as a function of the mass ratio has the form

$$\frac{V_p}{fD} = 6.2 \left(\frac{m\delta}{\rho D^2}\right)^{0.29}$$

This result coupled with the old result obtained by Weaver and Grover for the fluidelastic stability boundary as a function

of the damping only, show that the mass ratio and the damping behave independently of each other. Hence the fluidelastic stability boundary will be a surface rather than a line, its equation having the form:

$$\frac{V_P}{fD} = K \left(\frac{m}{\rho D^2}\right)^{0.29} \delta^{0.21}$$

where the constant of proportionality K depends on the geometry of the array. The new stability boundary agreed very well with some of the available information on the critical velocities for different tube arrays.

Although the present investigation has answered some very important questions, it has undoubtedly raised some other new questions for future research, such as:

(1) The mass ratio variation here has been obtained by changing the tube mass. In actual heat exchangers, the mass ratio varies principally because of fluid density. Heavy fluids will introduce further complications because of added mass and mode coupling effects. A comprehensive study of these should be undertaken.

(2) As the fluidelastic stability boundary is expected to vary with the geometry of the array, further experiments are required along the same lines to generate a family of threshold boundaries for various geometries of tube-arrays, especially for rotated square arrays where the fluidelastic vibration threshold is expected to be much sharper.

REFERENCES

1. Paidoussis, M. P., "Flow-induced Vibrations in Nuclear Reactors and Heat Exchangers, Practical Experience and State of Knowledge", Symposium on Practical Experiences with Flow-induced Vibration, Karlsruhe, Germany, Preprints I, pp. 01-39, Sept. 3-6, 1979.

2. Shin, Y. S. and Wambsganss, M. W., "Flow-induced Vibration in LMFBR Steam Generators: A State-of-the-Art Review", ANL-75-16, May, 1975.

3. Savkar, S. D., "A Survey of Flow-induced Vibrations of Cylindrical Arrays in Cross Flow", ASME Paper 76-WA/FE-21, 20 pp. (1976).

4. Connors, H. J., "Fluidelastic Vibration of Tube Arrays Excited by Cross Flow", Symp. on Flow-induced Vibration in Heat Exchangers, Winter Annual Meeting of ASME, New York, pp. 42-56, Dec., 1970.

5. Pettigrew, M. J. and Gorman, D. J., "Vibration of Heat Exchanger Components in Liquid and Two-phase Cross Flow", AECL-6184, presented at British Nuclear Energy Society Int. Conf. on Vibration in Nuclear Plant, Keswick, U.K., May 9-12, 1978.

6. Halle, H. and Lawrence, W. P., "Cross Flow-induced Vibration of Cylinders", Reactor Development Program Progress Report: April-May, 1973, ANL-RDP-16,pp. 3.10-3.11 (July 9, 1973).

7. Mirza, S. and Gorman, D. J., "Experimental and Analytical Correlation of Local Driving Forces and Tube Response in Liquid Flow Induced Vibration of Heat Exchangers", 2nd Conf. on Structural Mechanics in Reactor Technology, Berlin, Conf. 730942, Sec. F6/5, 1973.

8. Halle, H., Boers, B. L. and Wambsganss, M. W., "Fluid-elastic Tube Vibration in a Heat Exchanger Designed for Sodium-to-Air Operation", ASME J. Eng. for Power, Paper 75-PWR-B, 1975.

9. Weaver, D. S. and Grover, L. K., "Cross Flow-induced Vibrations in a Tube Bank - Turbulent Buffeting and Fluidelastic Instability", J. Sound and Vibration, Vol. 59, pp. 277-294, 1978.

10. Blevins, R. D., "Fluidelastic Whirling of a Tube Row", Trans. ASME J. Pressure Vessel Technol. 96, Series J, 4, pp. 263-267 (November, 1974).

11. Weaver, D. S. and Lever, J., "Tube Frequency Effects on Cross Flow-induced Vibrations in Arrays". Reprints for 5th Biennial Symp. on Turbulence, Univ. Missouri-Rolla, U.S.A. Paper IV.4, pp. IV. 4-1-IV. 4-8 (3-5 October, 1977).

12. Int. Symp. on Vibration Problems in Industry, Keswick, England, (U.K. Atomic Energy Authority at Windscale, N.P.L.), 1973.

13. Douma, J. H., "Field Experience with Hydraulic Structures", IUTAM/IAHR Symp. Flow-induced Struct. Vib., Karlsruhe, Germany, Springer-Verlag, New York Inc., N.Y. pp. 223-249, 1974.

14. Weaver, D. S., "On Flow-induced Vibrations in Hydraulic Structures and their Alleviation", Canadian J. of Civil Engg., Vol. 3, No. 1, pp. 126-137, 1976.

15. Sainsbury, R. N. and King, D., "The Flow-induced Oscillation of Marine Structures", Proc. Inst. Civ. Eng., pp. 269-299, 1971.

16. Symposium on "Fluid-solid Interaction", presented at ASME Winter Annual Meeting, Pittsburgh, Ed. J. E. Greenspon, Nov., 1967.

17. Proceedings of the Wind Effects on Buildings and Structures Conference, N.P.L., Teddington, England, June, 1963.

18. Benjamin, T. B., "The Threefold Classification of Unstable Disturbances in Flexible Surfaces Bounding Inviscid Flows", J. Fluid Mech., 16, pp. 436-450, 1963.

19. Naudascher, E., "From Flow Instability to Flow-induced Excitation", ASCE J. Hydraul. Div. 93 (HY4), pp. 15-40, 1967.

20. Marris, A. W., "A Review on Vortex Streets, Periodic Wakes, and Induced Vibration Phenomena", Trans. ASME J. Basic Eng., 86, Series D, 2, pp. 185-196 (June, 1964).

21. Owen, P. R., "Buffeting Excitation of Boiler Tube Vibration", J. Mech. Eng. Sci., 7, 4, pp. 431-439 (December, 1965).

22. Tritton, D. J., "Experiments on the Flow Past a Circular Cylinder at Low Reynolds Numbers", J. Fluid Mech. 6(4), 547-567, Nov., 1959.

23. Chen, Y. N., "Flow-induced Vibration and Noise in Tube-bank Heat Exchangers Due to von Karman Streets", J. Eng. Ind. 90(1), 134-146, Feb., 1968.

24. Grover, L. K., "Cross Flow-induced Vibration Deep Inside a Closely Packed Tube-bank", Ph.D Thesis, McMaster University, 1977.

25. Lienhard, J. H., "Synopsis of Lift, Drag and Vortex Frequency Data for Rigid Circular Cylinder", Bulletin 300, College of Engineering, Washington State University, 1966.

26. Chen, Y. N., "Flow-induced Vibrations in Tube Bundle Heat Exchangers with Cross and Parallel Flow", Symp. on Flow-induced Vibration in Heat Exchangers, Winter Annual Meeting of ASME, N.Y., pp. 57-58, Dec., 1970.

27. Bishop, R. E. D., and Hassan, A. Y., "The Lift and Drag Forces on a Circular Cylinder Oscillating in a Flowing Fluid", Proc. Royal Soc., Series A, 277, pp. 51-75, 1964.

28. Fitz-Hugh, J. S., "Flow-induced Vibration in Heat-Exchangers", Proc. Int. Symp. Vibration Problems in Industry, UKAFEA and NPL, Keswick, England, paper no. 427, 17 pp., April, 1973.

29. Brunn, H. H., and Davies, P. O. A. L., "An Experimental Investigation of the Unsteady Pressure Forces on a Circular Cylinder in a Turbulent Cross-flow", Journal of Sound and Vibration, Vol. 40(1),pp. 535-559, 1975.

30. Chen, Y. N., "Fluctuating Lift Forces of the Karman Vortex Streets on Single Circular Cylinders and in Tube Bundles, Part 3: Lift Forces in Tube Bundles", Trans. ASMEJ. Eng. Ind., 94, Series B, 2, pp. 623-628, May, 1972.

31. Funakawa, M. and Umakoshi, R., "The Acoustic Resonance in Tube Bank", Bull. JSME, 13, 57, pp. 348-355, March, 1970.

32. Morse, P. M., "Vibration and Sound", 2nd ed., McGraw Hill, p. 398, 1968.

33. Chen, Y. N., "Vibration in Tube Cluster Due to Bernard-Karman Streets", C. R. des 8e Journ. de l hydraul: Instability in Hydraulics and Fluid Mechancs, Lille, soc. Hydrotech. de France, Vol. 1, pp. 238-246 (8-10 June, 1964) (In French; English summary vol. 2, pp. 565).

34. Zdravkovich, M. M., and Nuttall, J. A., "On the elimination of Aerodynamic Noise in a Staggered Tube Bank", J. Sound Vibration 34(2), 173-177, May 22, 1974.

35. Hartlen, R. T., "Recent Field Experience with Flow-induced Vibration of Heat Exchanger Tubes", Proc. Int. Symp. Vibration Problems in Industry, UKAEA and NPL, Keswick, England, Paper No. 611, 20 pp, (10-12 April, 1973).

36. Roberts, B. W., "Low Frequency Aeroelastic Vibrations in a Cascade of Circular Cylinders", Inst. Mech. Eng., Mech. Eng. Sci. Monograph 4 (September, 1966).

37. Savkar, S. D., "A Note on the Phase Relationships Involved in the Whirling Instability in Tube Arrays, J. Fluids Engg., Dec. 1977/727.

38. Southworth, P. J., and Zdravkovich, M.M., "Effect of Grid-Turbulence on the Fluidelastic Vibrations of In-line Tube Banks in Cross Flow", J. of Sound and Vib., 39(4), pp. 461-469, 1975.

39. Blevins, R. D., "Flow-induced Vibration", Von Nostrand Reinhold Company, Toronto, pp. 218-220, 1977.

40. Chen, S. S., and Jendrzejczyk, J. A., "Dynamic Response of a Circular Cylinder Subjected to Liquid Cross Flow", ASME Paper 78-PVP-15, 1978.

APPENDIX A

INSTRUMENT CALIBRATION

1. Calibration of MTI-Capacitive Probe

The MTI-capacitive probe was calibrated by using precision blocks as shown in Figure A-1. The gap for the calibration was set using a micrometer and checked by a feeler-gauge. Both the MTI-probe and the micrometer were grounded first, and then the output of the capacitive probe (in thou.) was recorded using a Wayne-Kerr displacement bridge. The procedure was repeated by setting different gaps. The calibration curve has been plotted in Figure A-2. It is seen that the probe was linear for its full scale (0.010 in.) as specified by the manufacturer. (Note: As the MTI AS 1000 Distance and Vibration meter was used to conduct the experiments, this calibration was checked against the MTI bridge readings, and found to agree very well with the original calibration).

2. Calibration of the Movable-tube

As the MTI capacitive probe was installed close to the top end of the piano-wire outside the test section (see Figure A-3), a calibration was conducted to establish a relationship between the deflection of the tube at the middle and that recorded by the MTI capacitive probe. The arrangement is shown in Figure A-3, and the data obtained has been plotted in Figure A-4. It is evident that there is a linear relationship for the

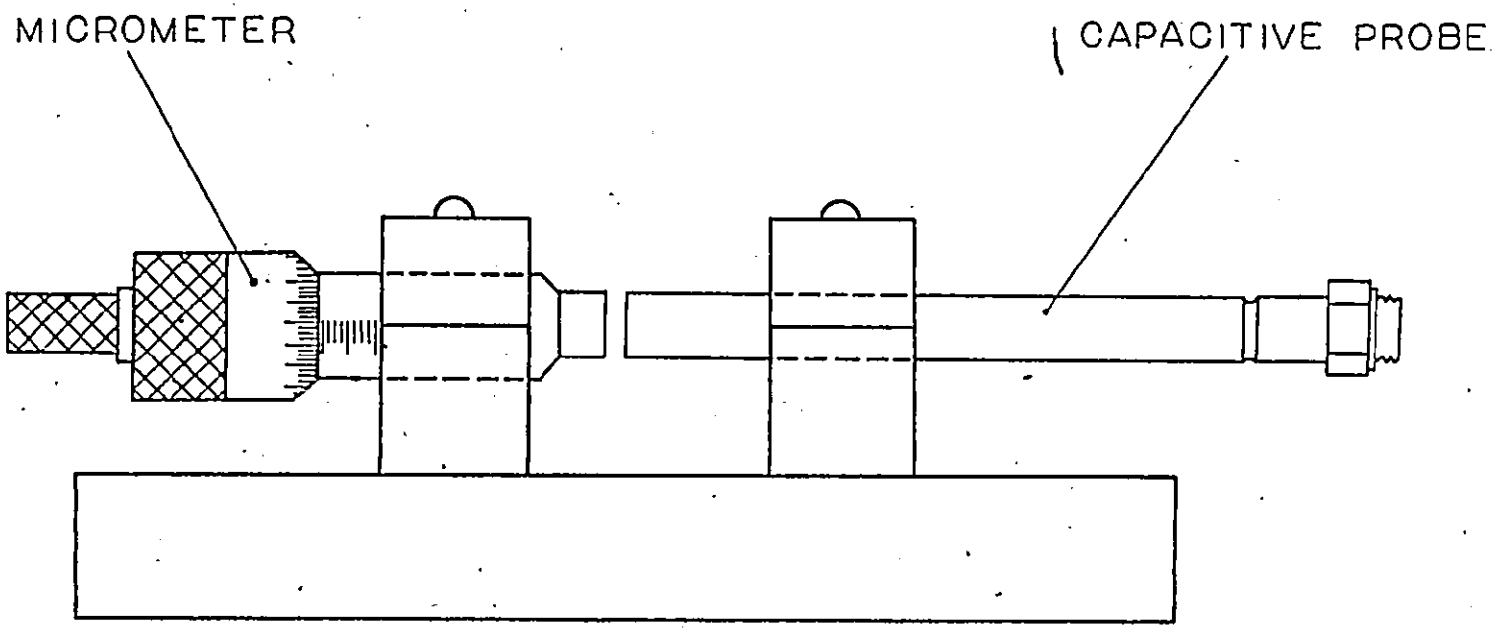

CALIBRATION OF MTI-PROBE

FIGURE A-1

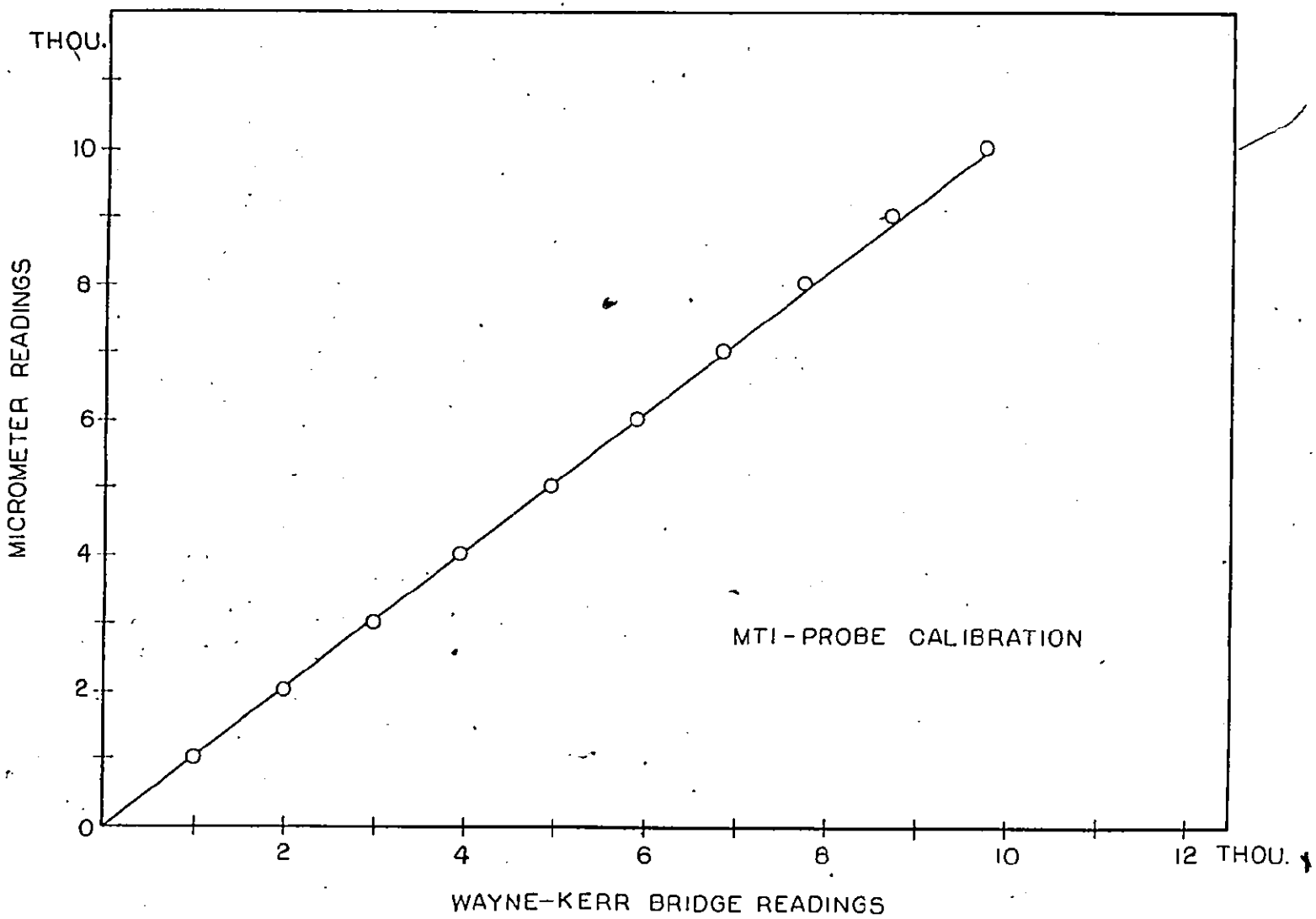
THOU.
10
8
6
4
2
0
MICROMETER READINGS
MTI-PROBE CALIBRATION
2
4
6
8
10
12 THOU.
WAYNE-KERR BRIDGE READINGS

FIGURE A-2

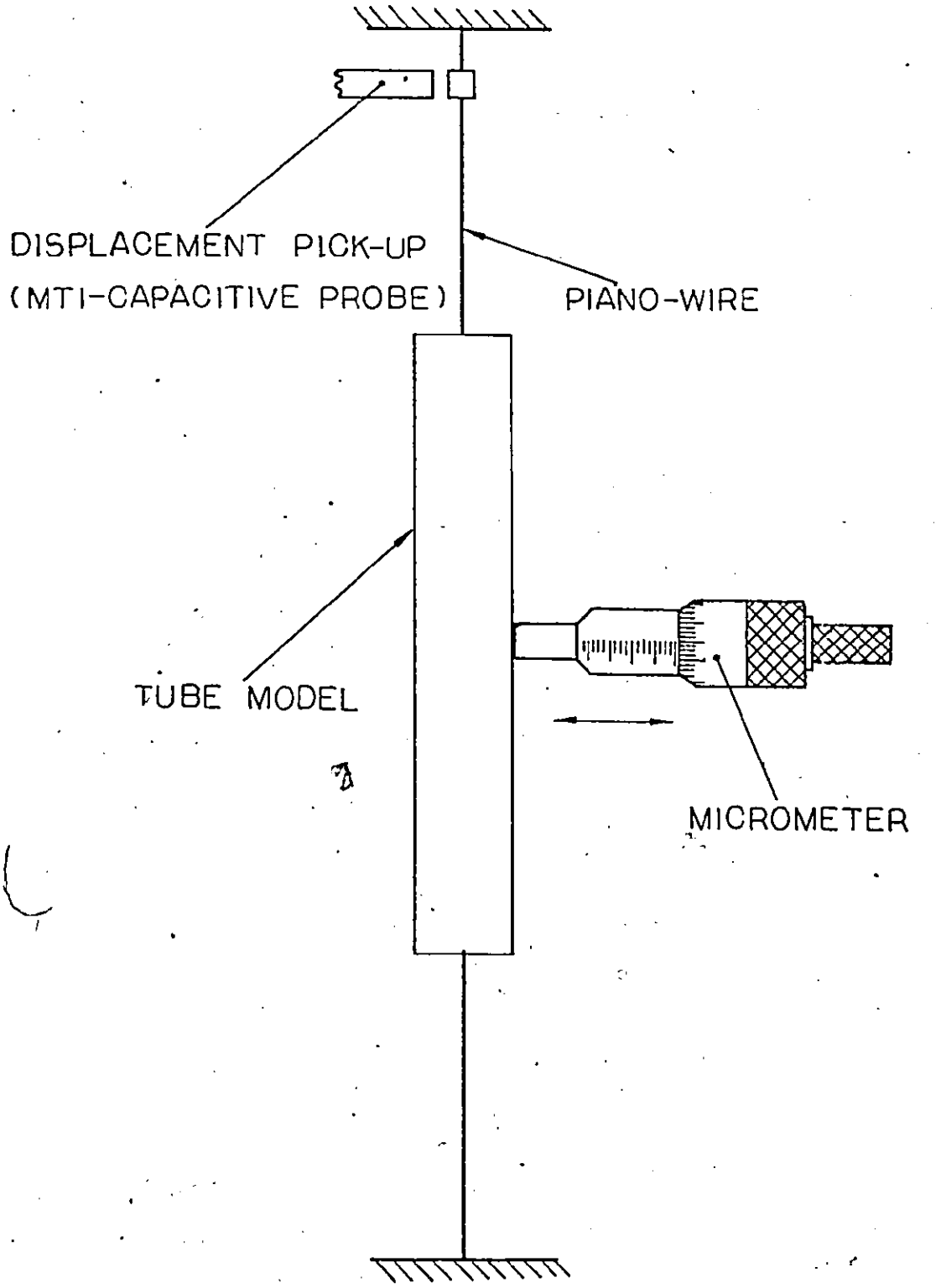

NOT TO SCALE

FIGURE A-3

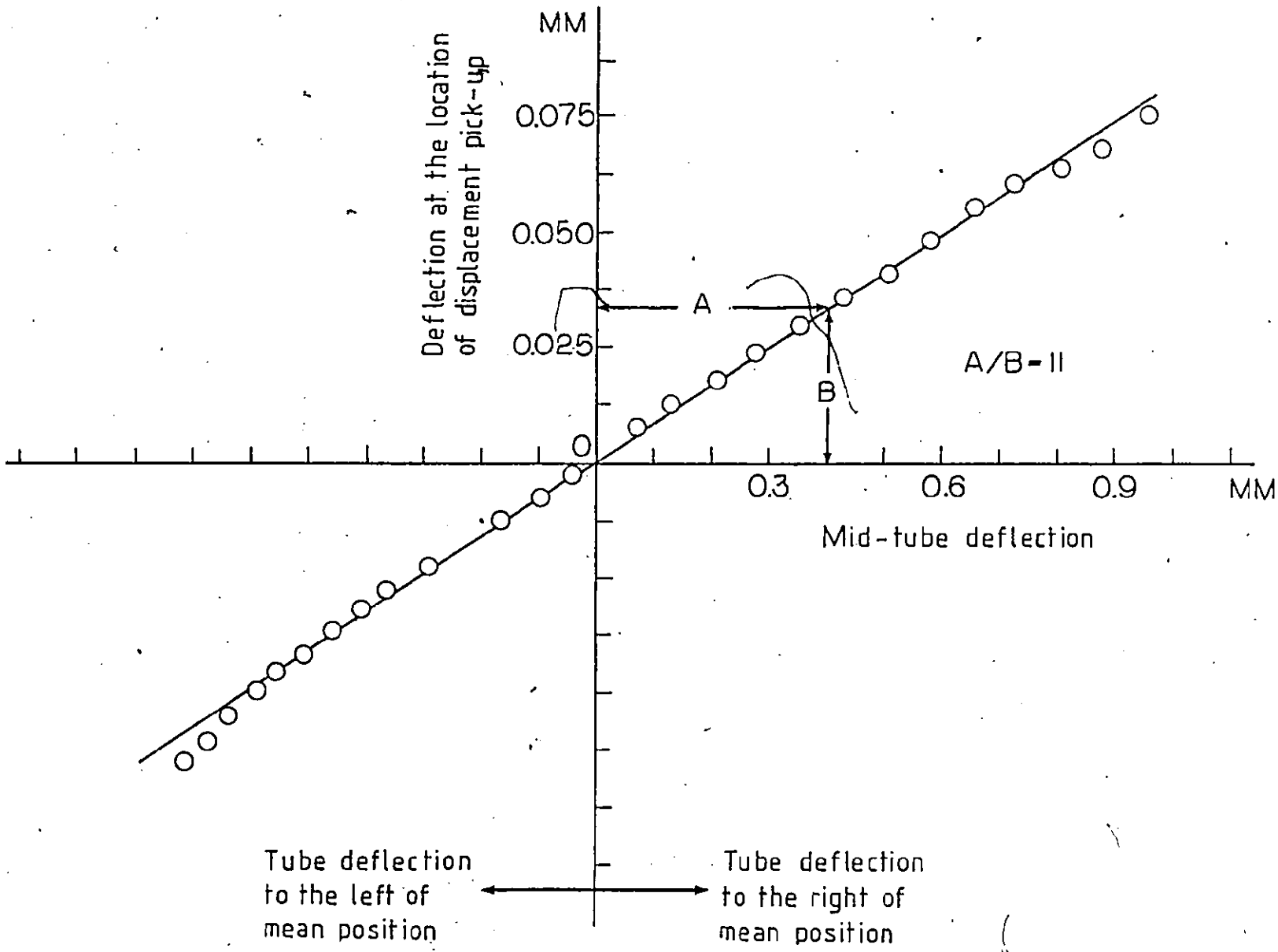
MM
0.075
0.050
0.025
0
Deflection at the location of displacement pick-up
A
B
A/B = 11
0.3
0.6
0.9
MM
Mid-tube deflection
Tube deflection to the left of mean position
Tube deflection to the right of mean position

FIGURE A-4

tube deflections up to approximately $\pm$ 0.7 mm. A ratio of 11 was found between the deflection of the tube at the middle and that at the probe position.

3. Calibrations of the Hot-wire Probes

A calibration nozzle giving a uniform flow field of good accuracy and a low turbulence potential core some 20 mm. in diameter was available in the department (see Figure A-5) for the calibration of hot-wire probes. The nozzle uses a contour, suitable for a wind-tunnel contraction design, the curvature being arranged to give a flat velocity profile at the exit. A pitot-probe and the hot-wire probe (to be calibrated) were mounted side by side at the exit of the nozzle. The blower was run at a constant speed and a steady air flow through the calibration nozzle was established. The outputs of the pitot-probe and hot-wire probe were recorded from an inclined manometer and a constant temperature anemometer respectively. The output of the hot-wire probe (volts) was plotted against the flow velocity (m./sec.). The procedure was repeated for a range of blower speeds and a complete calibration curve as shown in Figure A-6 was drawn. Figure A-7 shows another calibration curve for another probe used later in the experiments.

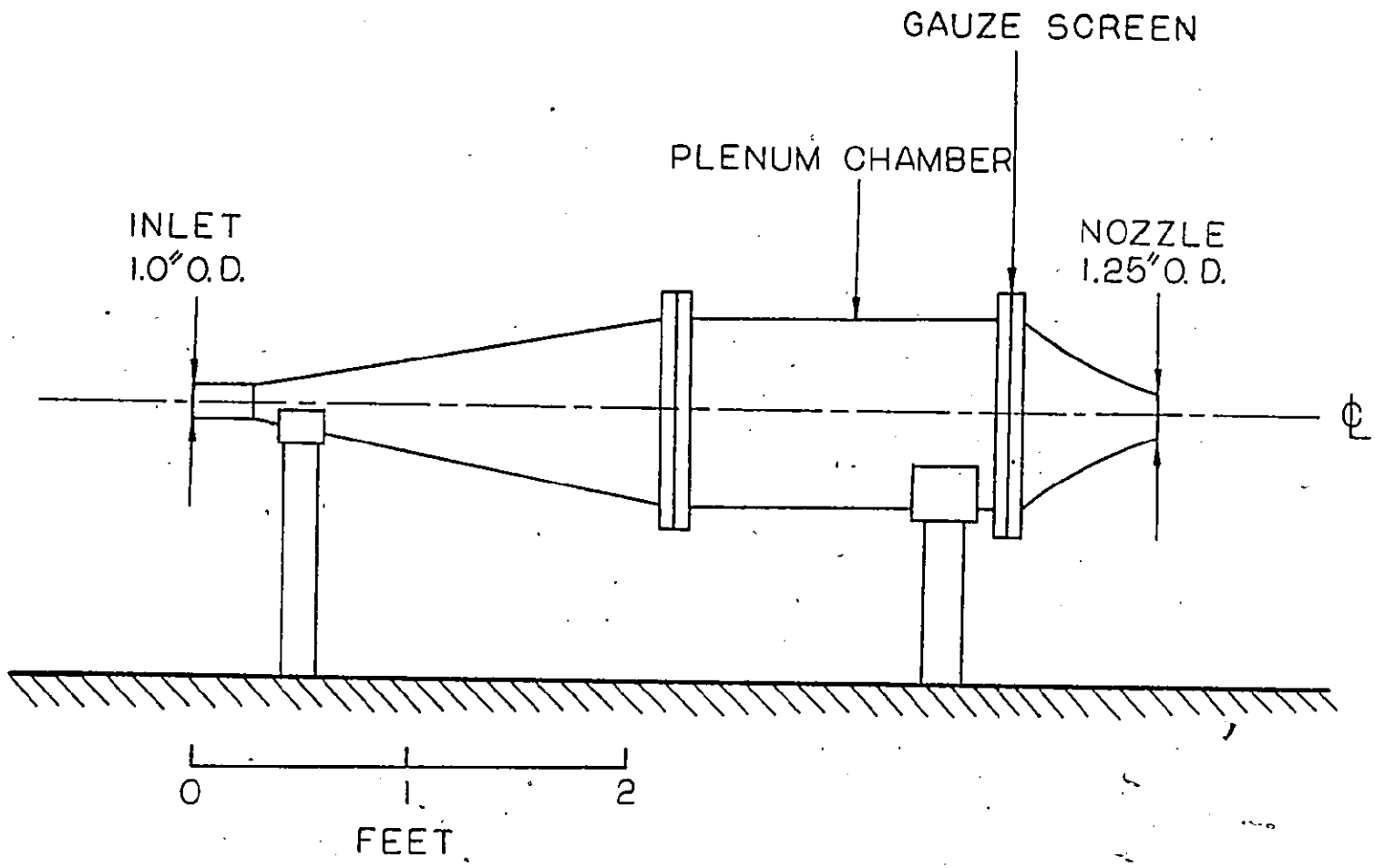

THE CALIBRATION NOZZLE

FIGURE A-5

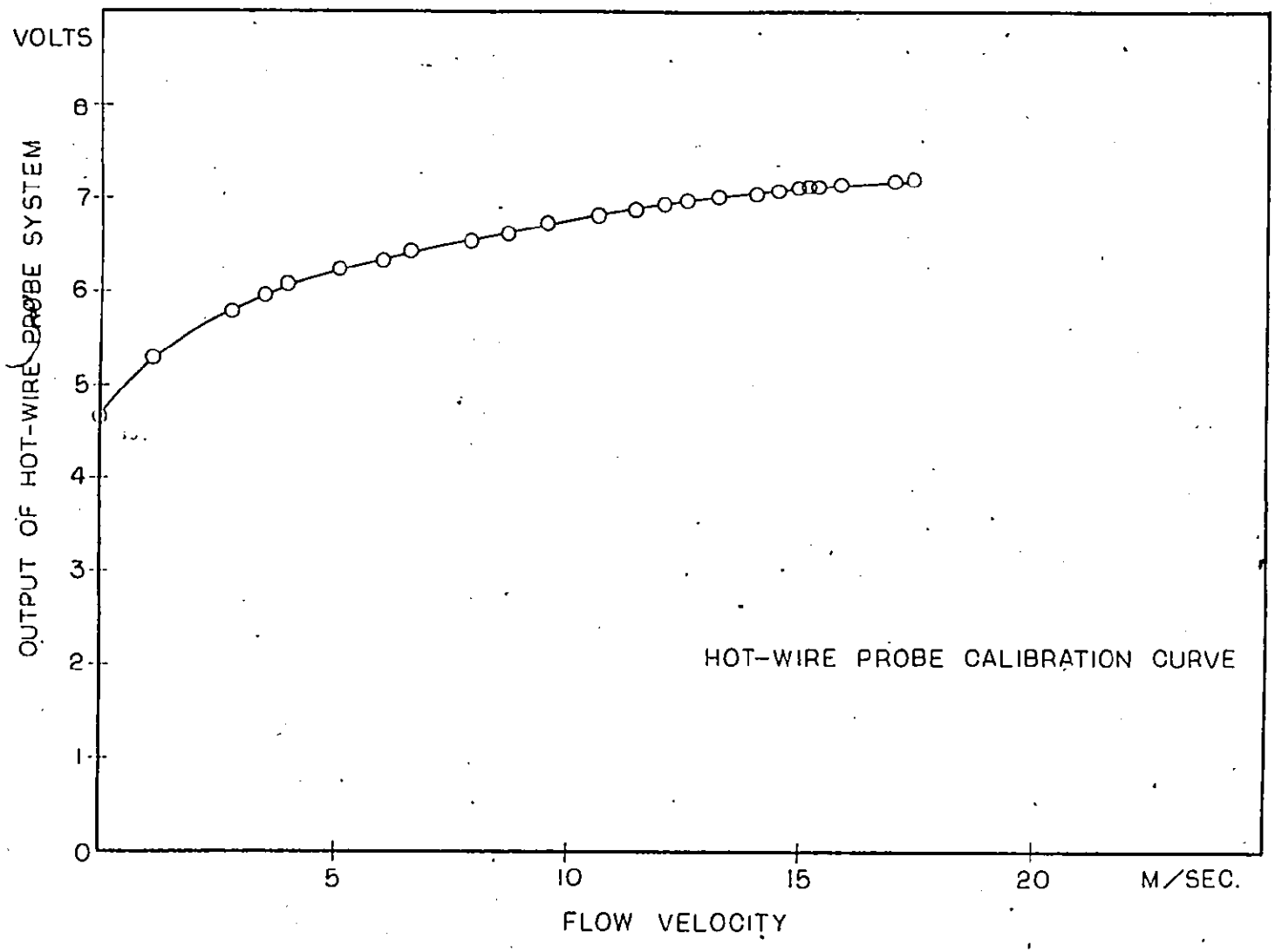
VOLTS
OUTPUT OF HOT-WIRE PROBE SYSTEM
0
1
2
3
4
5
6
7
8
5
10
15
20
M/SEC.
FLOW VELOCITY
HOT-WIRE PROBE CALIBRATION CURVE

FIGURE A-6

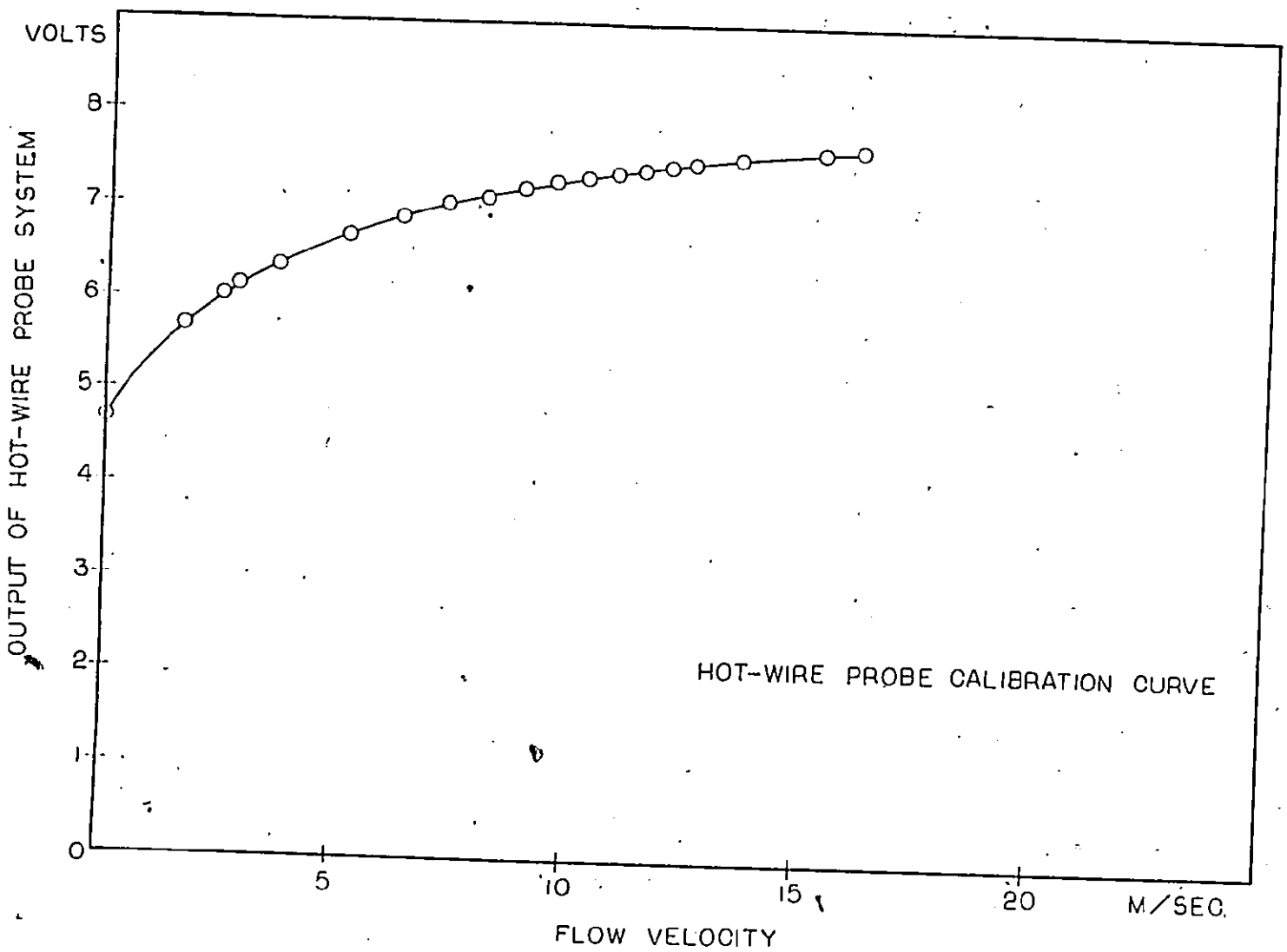
VOLTS
OUTPUT OF HOT-WIRE PROBE SYSTEM
8
7
6
5
4
3
2
1
0
5
10
15
20
M/SEC.
FLOW VELOCITY
HOT-WIRE PROBE CALIBRATION CURVE

FIGURE A-7

APPENDIX B

PIANO-WIRE TUBE-MODEL

As it was decided to use a tube sprung on a piano-wire, the feasibility of using the same model for different tube mass was examined.

The analytical model developed for this analysis is given in the following:

Analytical model

Strain in piano-wire due to displacement 'x' is

$$= \frac{(\ell^2+x^2)^{1/2} - \ell}{\ell}$$

$$= (1 + \frac{x^2}{\ell^2})^{1/2} - 1$$

$$= \frac{x^2}{2\ell^2}$$

the corresponding tensile force in the wire is:

$$T + A\ (E\ \frac{x^2}{2\ell^2}\ )$$

and the restoring force acting on mass 'm' will be

$$2[(T+AE\ \frac{x^2}{2\ell^2})\ \frac{x}{(\ell^2+x^2)^{1/2}}]$$

$$= 2[(T+AE\ \frac{x^2}{2\ell^2})\ \frac{x}{\ell}]$$

$$= \frac{2Tx}{\ell} + AE\ \frac{x^3}{\ell^3}$$

The equation of motion of mass 'm' thus becomes:

$$m\ddot{x} + 2\,T\,\frac{x}{\ell} + AE\,\frac{x^3}{\ell^3} = 0$$

which is a non-linear differential equation. It can be considered linear for small deflections 'x' and high initial tensile force T. The linearised equation (neglecting $AE\,\frac{x^3}{\ell^3}$ compared to $2\,T\,\frac{x}{\ell}$) is

$$m\ddot{x} + 2\,T\,\frac{x}{\ell} = 0$$

and for simple harmonic motion of mass 'm' the solution of this second order differential equation leads to:

$$f = \frac{1}{2\pi}\sqrt{\frac{2T}{m\ell}}$$

where f = the natural frequency of mass 'm' (mass of wire was neglected in this analysis as compared to tube mass).

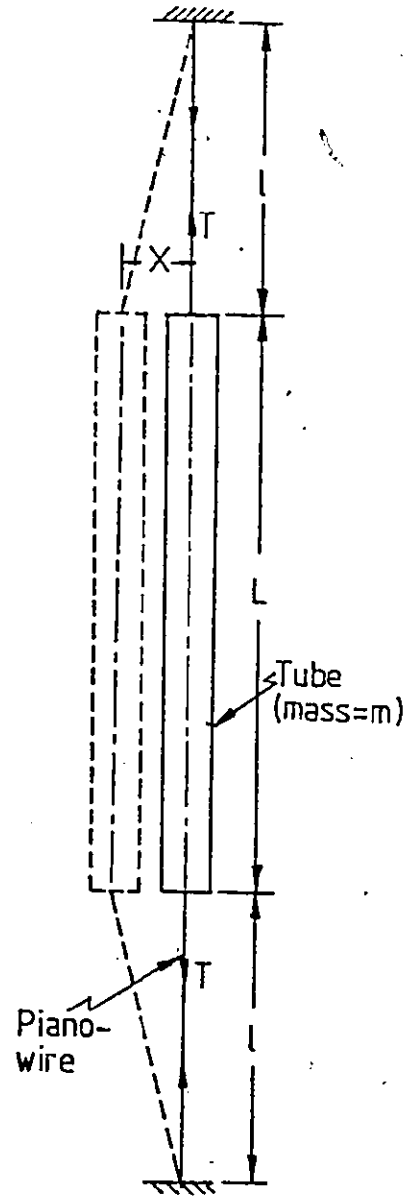

FIGURE B-1

Feasibility evaluation

With all sets of tubes, it was decided to use a commercially available 0.001 m. diameter piano-wire weighing 0.0066 kg/m., the tensile strength of this wire is 2.28×10^6 kN/m^2.

In all tests the natural frequency was held constant at 20 Hz, and the length ρ was fixed at 0.15 m. The mass 'm' of the tube was the parameter to be changed for the last set of the research. For the first set of tubes where m = 0.048 kg, we have:

$$f = \frac{1}{2\pi}\sqrt{\frac{2T}{m\ell}}$$

or

$$T = \frac{m\ell}{2}(2\pi f)^2$$

$$= \frac{1}{2}\,\frac{0.048}{9.8} \times 0.15\ (2\times3.14\times20)^2$$

$$= 5.80 \text{ kgs.}$$

The corresponding stress in the wire would be:

$$\sigma = \frac{T}{A}$$

$$= \frac{5.80\times4\times9.8}{\pi(0.001)^2}$$

$$= 72.395\times10^6 \text{ N/m}^2$$

$$= 0.07\times10^6 \text{ kN/m}^2$$

The strain in the wire, taking $E = 207\times10^6$ kN/m^2 for steel is:

$$\varepsilon = \frac{\sigma}{E}$$

$$= \frac{0.07\times10^6}{207\times10^6}$$

$$= 338.1\times10^{-6}$$

and for 0.15 m. length of wire, the wire at each end of the tube should be stretched by:

$$\delta = \varepsilon . \ell$$
$$= 338.1 \times 10^{-6} \times 0.15$$
$$= 50.88 \times 10^{-6} \text{ m.}$$

The same procedure was repeated for the other sets of tubes and the results obtained are given in Table B.1.

Summary and Conclusion

An analytical study of a tube sprung on a piano-wire has proven that such a tube-model is safe and feasible for all sets of tubes.

It is expected that this tube-model will give the desired parameter ranges and good control of the damping.

TABLE B.1

Set No.	Material	Tube Mass (kgs)	Tension, T (kgs)	Stress, σ $(KN/m^2)x10^6$	Strain, ε $x10^{-6}$	Elongation, δ (m.) $x\ 10^{-6}$
1	Aluminum	0.0480	5.80	0.072	338.1	50.58
2	Aluminum	0.0991	11.97	0.149	714.2	107.10
3	Steel (cold drawn)	0.2706	32.67	0.408	1955.8	293.37
4	Brass	0.3611	43.61	0.545	2612.5	391.87
5	Steel (cold drawn)	0.4615	55.72	0.698	3346.0	501.90
6	Steel (cold drawn)	0.5444	65.74	0.819	3926.0	588.90

Notice:

Tensile strength of the piano-wire is $2.28x10^6$ KN/m^2.

APPENDIX C

SPECIFICATIONS OF THE INSTRUMENTS EMPLOYED

1. Vibration Pick-up of a Movable Tube in the Array

(i) Capacitive probe

Mechanical Technology Incorporated (M.T.I.)

Type ASP-10 (0.010" full scale range, 0.250 mm).

(ii) Distance and vibration meter

M.T.I. Type AS1000

Supplier: The Mechanical Technology Incorporated Company, Latham, N.Y.

2. Fourier Analysis:

Spectrascope Real Time Analyzer Model SD335

It is a combination of the following sections:

(i) Analyzer Section

(ii) X-Y Display Oscilloscope Section

(iii) Averager and Storage Memory Section

Supplier: The Spectral Dynamics Corporation Company, San Diego, California.

3. Flow Measurements

(i) Pitot-static probe

Part No. PBC-18-G-16-KL

Supplier: United Electric Controls (Canada) Ltd., Mississauga.

(ii) Betz manometer

Supplier: Thermovolt Instruments Ltd., Toronto, S. No. 11248.

(iii) 90° miniature hot-wire probe

DISA Type 55P14

(iv) Hot-wire probe support

DISA Type 55H21

(v) Constant temperature anemometer

DISA Type 55A01

Supplier: DISA Elecktronic A/S,DK2730, Harlev, Denmark

4. Oscilloscope

Tektronix; Type 564, Storage Oscilloscope with Type 3A72 dual-trace amplifier and Type 2B67 time base.

5. Recorder

Visicorder Oscillograph, Model 2106, Honeywell test instruments Inc., Denver, Colorado. It is a direct writing 12-channel oscillograph that records at frequencies from D.C. to 13,000 Hz. The oscillograph uses a high-pressure mercury vapor lamp that emits high intensity ultra-violet light, which is reflected from miniature mirror galvanometers through a precision optical system into the recording paper.

6. Meter

Digital multimeter,

Model 3465A, Hewlett Packard

APPENDIX D

EFFECT OF TUBE-BUNDLE SIZE ON THE FLUIDELASTIC STABILITY THRESHOLD RESULTS

As it was mentioned previously in section 4.3, the effect of tube bundle size on the critical velocity of the monitored tube was determined. For the purpose of this study, the movable tubes marked from 1 to 6 and 10 to 13 (see Figure 4.1) were tuned to 20.0 Hz. These tubes were chosen so that the monitored tubes will be surrounded by tubes having the same conditions. The rest of the movable tubes were tuned to above 30.0 Hz., so that they would not interfere with the monitored tubes. The damping of the monitored tube was measured before each run of the experiment. The aluminum filler was used at the end supports to preserve the linear characteristics of the movable tube and to keep the damping constant. Three tubes were used for this study. Tube no. 1 in the first row, tube no. 2 in the second row, and tube no. 4 in the fourth row (see Figure 4.1). The amplitude response of the monitored tube was recorded by following the same procedure described in section 4.1. The stability threshold (critical velocity) was determined by using the point at which the slope of the displacement-velocity curve changes while noting that the general tube response changes from random to regular.

The results obtained for tube no. 1 are shown in Figures D-1, 2, 3. Although there is some doubt about the

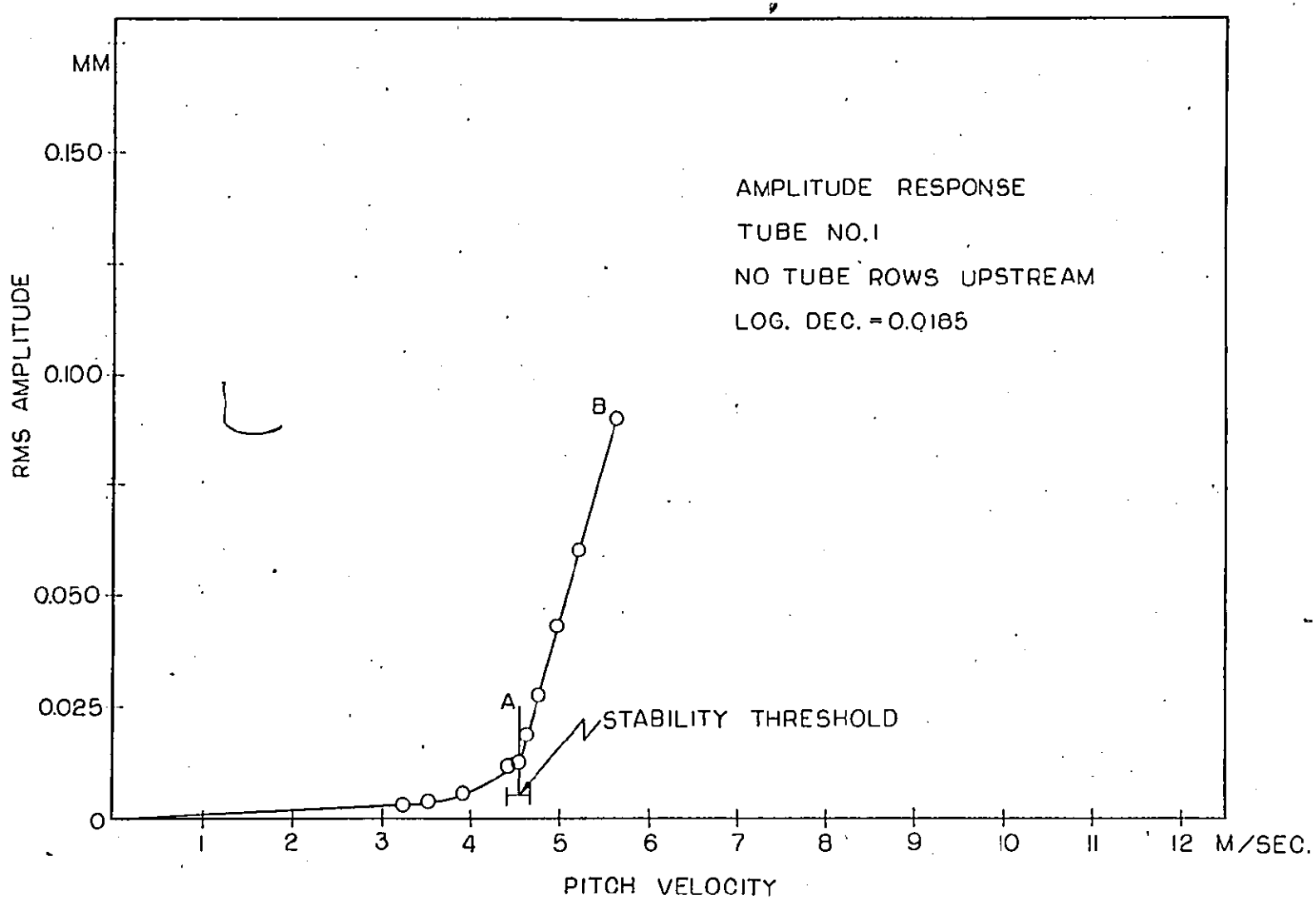
MM
0.150
0.100
0.050
0.025
0
RMS AMPLITUDE
AMPLITUDE RESPONSE
TUBE NO.1
NO TUBE ROWS UPSTREAM
LOG. DEC. = 0.0185
B
A
STABILITY THRESHOLD
1
2
3
4
5
6
7
8
9
10
11
12 M/SEC.
PITCH VELOCITY

FIGURE D-1.

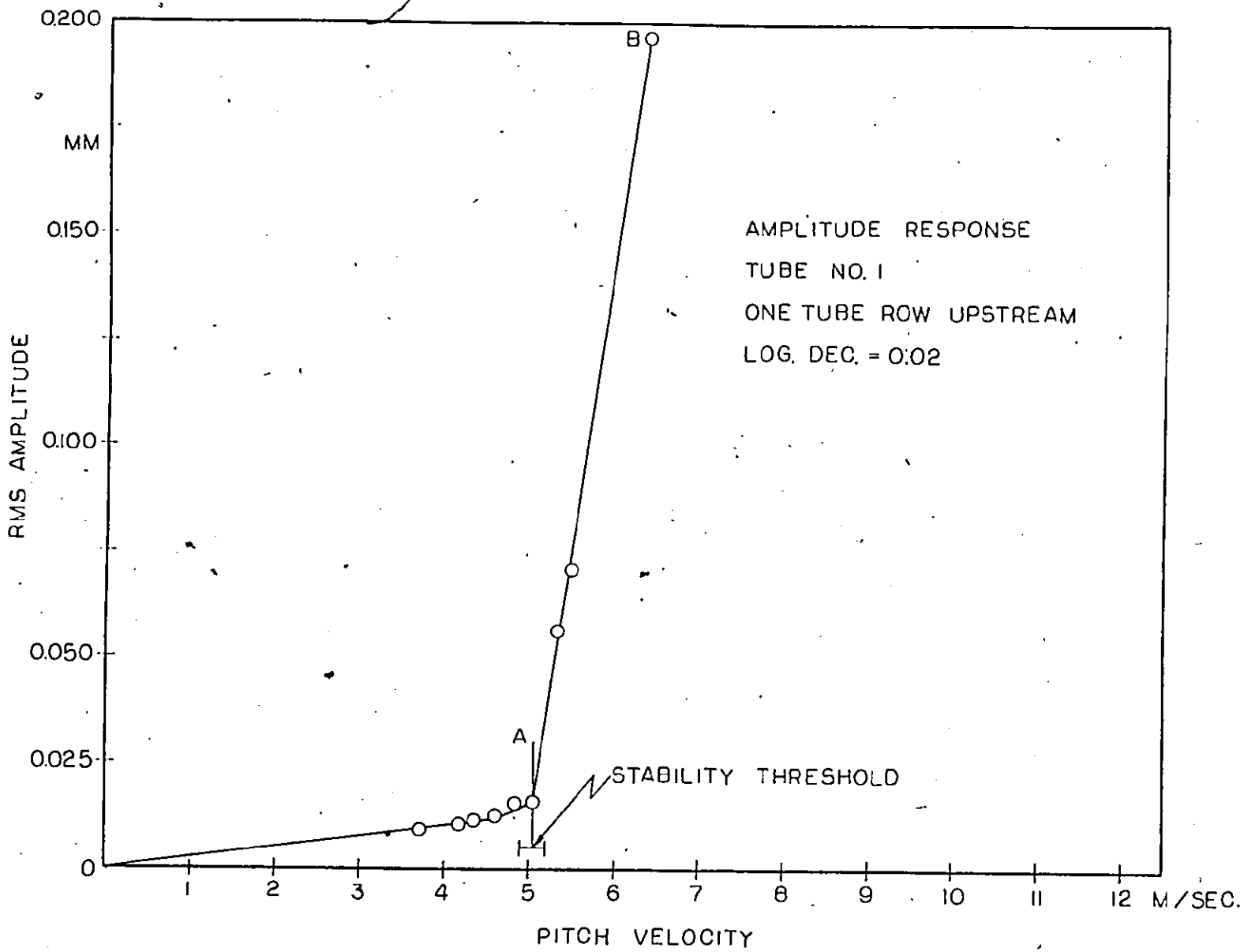
0.200
MM
0.150
0.100
0.050
0.025
0
RMS AMPLITUDE
B
A
AMPLITUDE RESPONSE
TUBE NO. 1
ONE TUBE ROW UPSTREAM
LOG. DEC. = 0.02
STABILITY THRESHOLD
1
2
3
4
5
6
7
8
9
10
11
12
M/SEC.
PITCH VELOCITY

FIGURE D-2

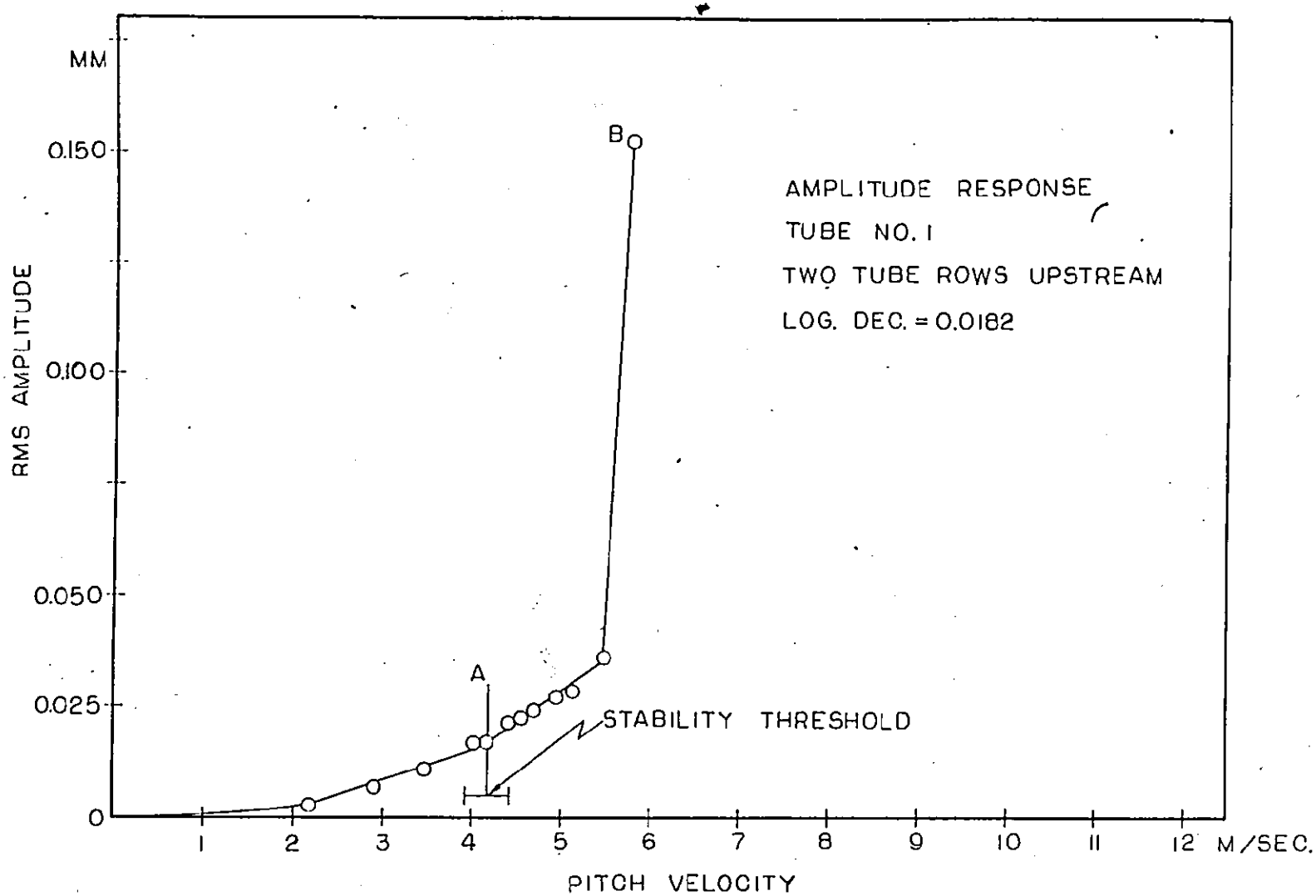
MM
0.150
0.100
0.050
0.025
0
RMS AMPLITUDE
B
A
AMPLITUDE RESPONSE
TUBE NO. 1
TWO TUBE ROWS UPSTREAM
LOG. DEC. = 0.0182
STABILITY THRESHOLD
1
2
3
4
5
6
7
8
9
10
11
12
M/SEC.
PITCH VELOCITY

FIGURE D-3

measured damping, these results showed a good agreement with those of tube no. 2 (see Figure 4.8) in the first second, and third rows.

The results obtained for the movable tube no. 2 as its location changes from the first to the seventh row are given in Figures D-4, 5, 6, 7, 8, 9, and 10. The result shown in Figure D-4 was obtained for tube no. 2 which was originally in the second row by removing the movable tube no. 1 and its row of stationary tubes from the first row. Figure D-11, shows a combination of the results obtained for the movable tube no. 2 as it moves from the first to the second row. It is easy to see the effect of turbulent buffeting, between the first and second row, on the amplitude build-up and an early take-off of the tube.

Figures D-12, 13, 14, 15, 16, 17 and 18 show the results obtained for the movable tube no. 4 from the fourth to the tenth row. While the stability threshold as defined by the point at which the slope of the displacement-curve changes was clear in most of the results obtained, the observation method was very helpful in others, such as those shown in Figures D-3, 8, 9, 10, 13 and 14 where the amplitude build-up was slow above the critical velocity.

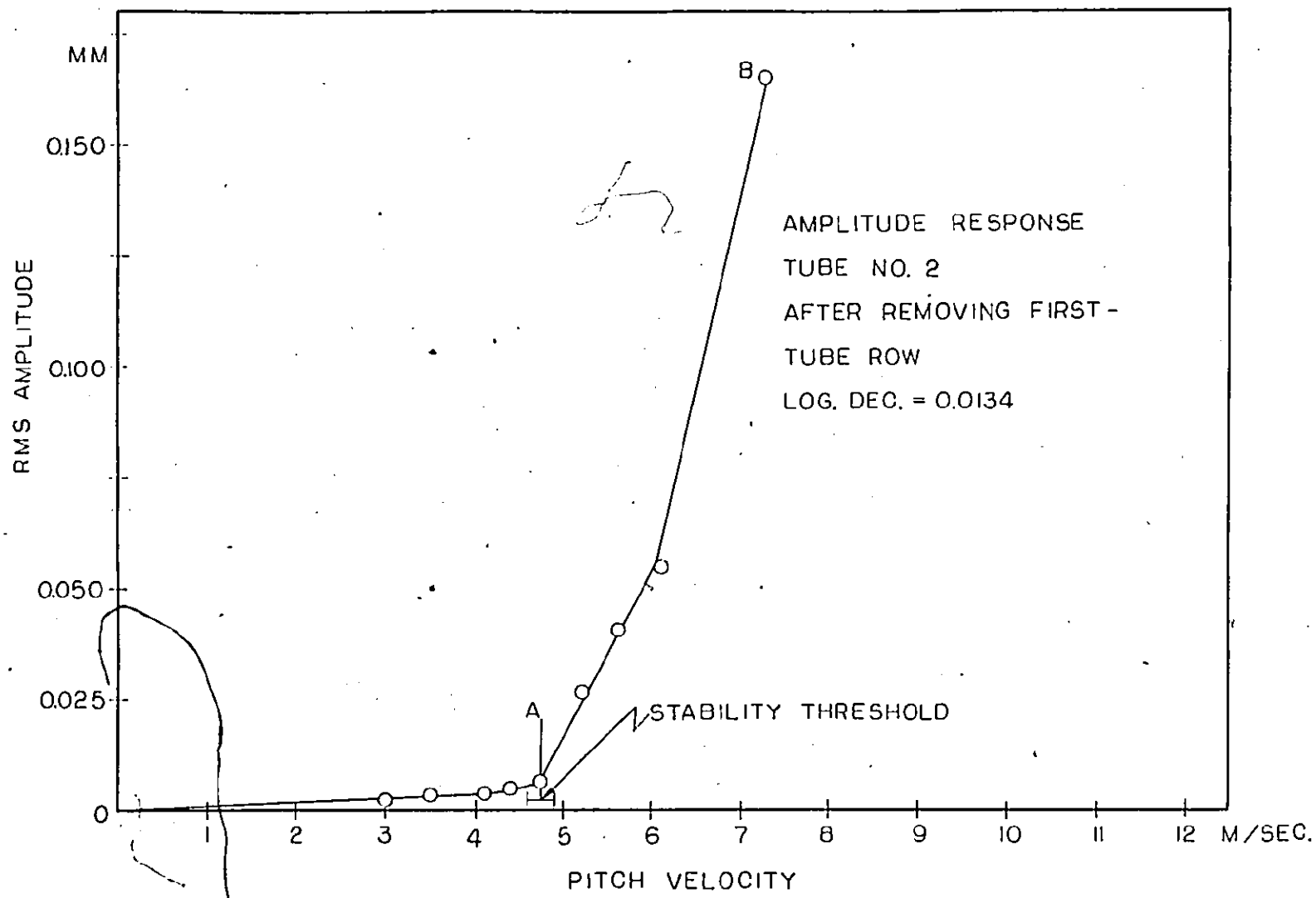
MM
0.150
0.100
0.050
0.025
0
RMS AMPLITUDE
B
A
AMPLITUDE RESPONSE
TUBE NO. 2
AFTER REMOVING FIRST-
TUBE ROW
LOG. DEC. = 0.0134
STABILITY THRESHOLD
1
2
3
4
5
6
7
8
9
10
11
12
M/SEC.
PITCH VELOCITY

FIGURE D-4

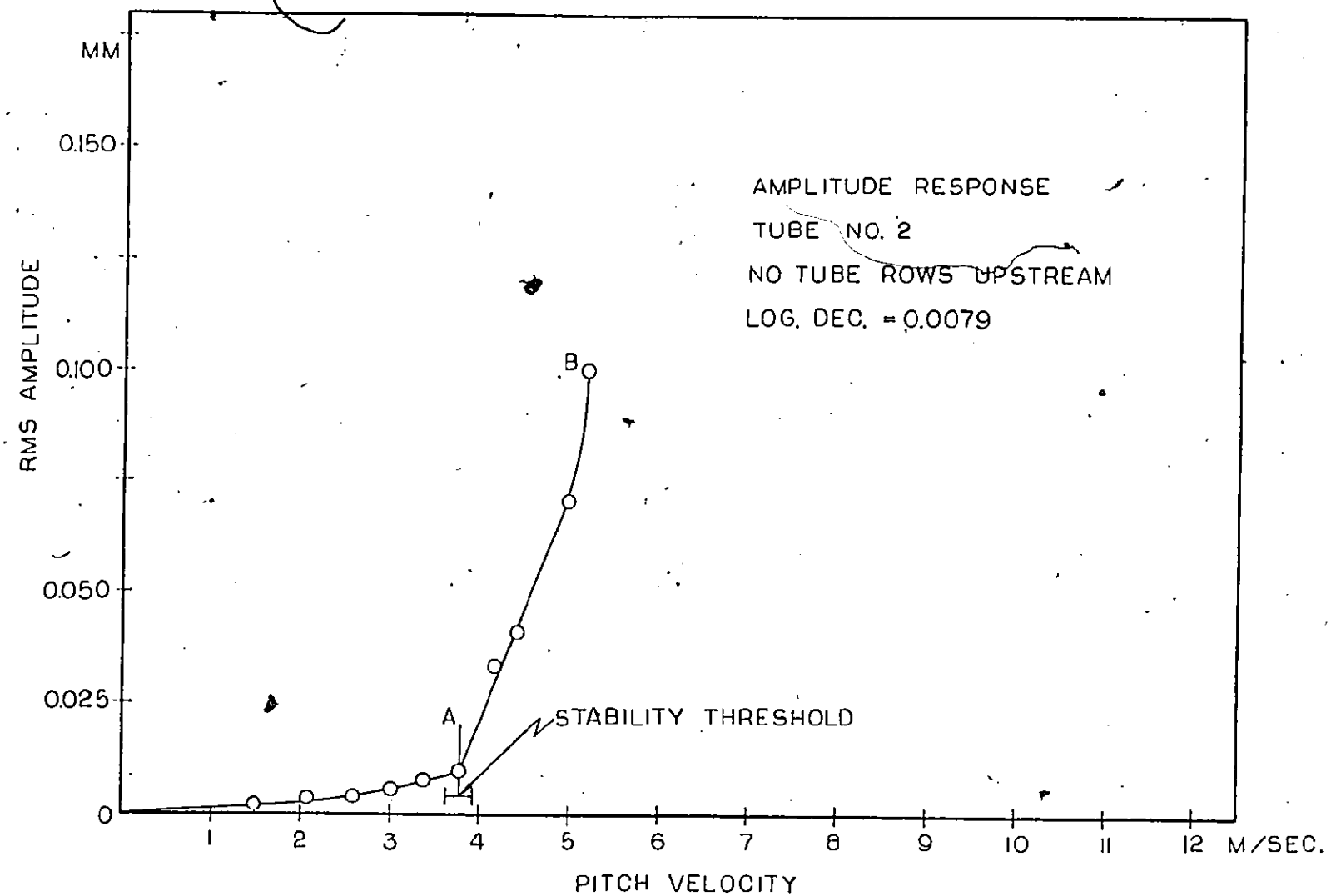
MM
0.150
0.100
0.050
0.025
0
RMS AMPLITUDE
AMPLITUDE RESPONSE
TUBE NO. 2
NO TUBE ROWS UPSTREAM
LOG. DEC. = 0.0079
B
A
STABILITY THRESHOLD
1
2
3
4
5
6
7
8
9
10
11
12
M/SEC.
PITCH VELOCITY

FIGURE D-5

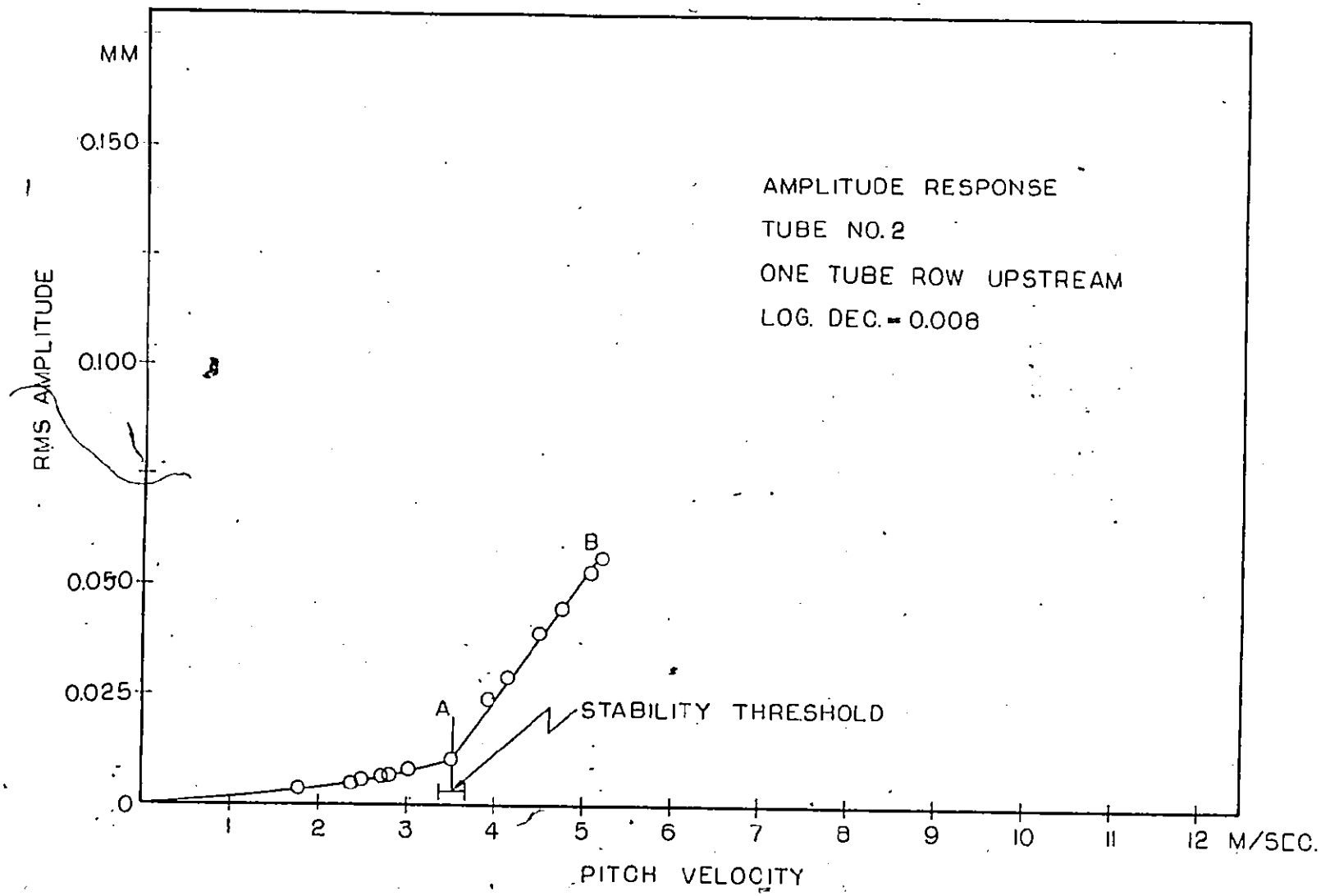
MM
0.150
0.100
0.050
0.025
0
RMS AMPLITUDE
AMPLITUDE RESPONSE
TUBE NO. 2
ONE TUBE ROW UPSTREAM
LOG. DEC. = 0.008
A
B
STABILITY THRESHOLD
1
2
3
4
5
6
7
8
9
10
11
12 M/SEC.
PITCH VELOCITY

FIGURE D-6

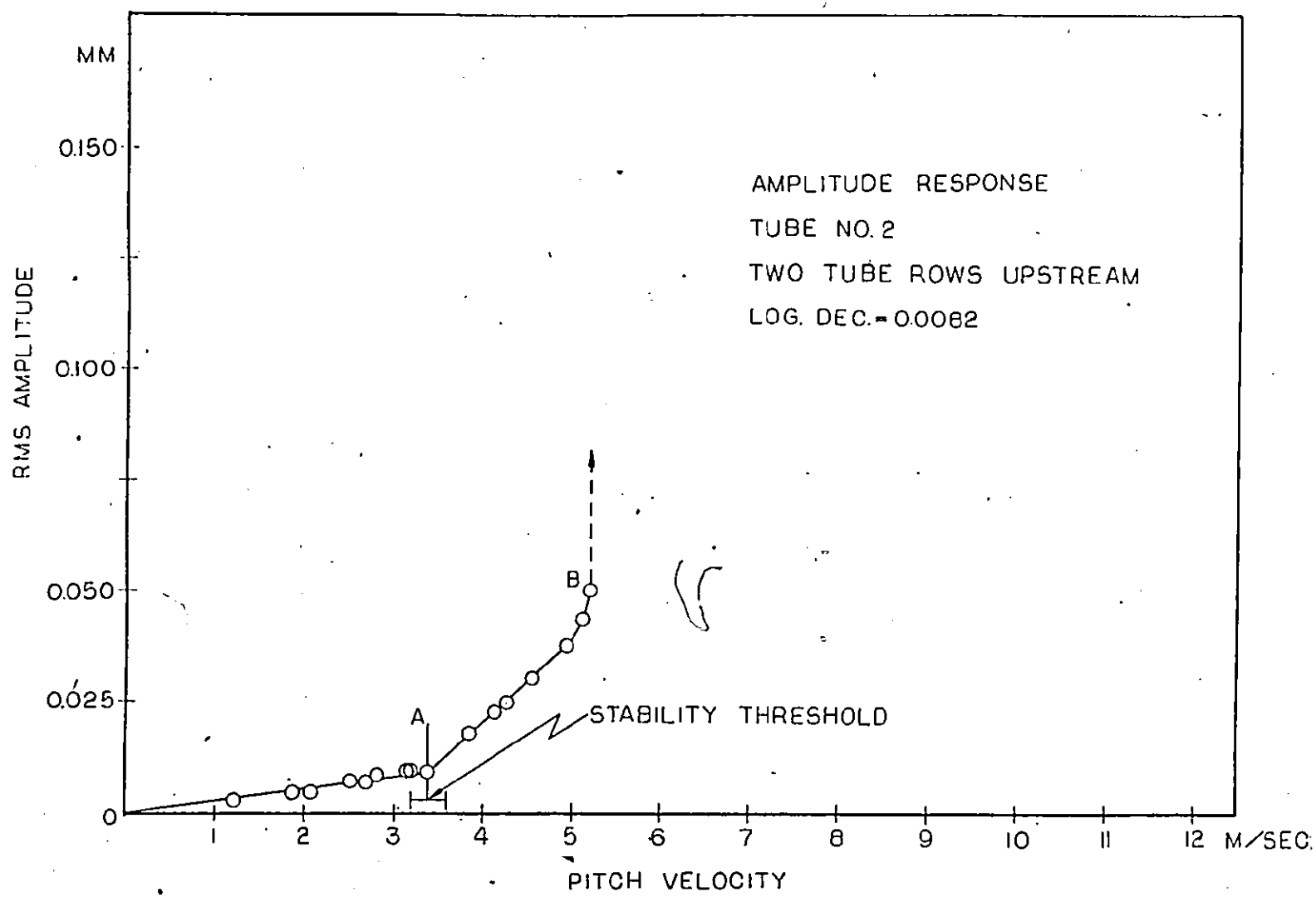
MM
0.150
0.100
0.050
0.025
0
RMS AMPLITUDE
AMPLITUDE RESPONSE
TUBE NO. 2
TWO TUBE ROWS UPSTREAM
LOG. DEC. = 0.0082
A
B
STABILITY THRESHOLD
1
2
3
4
5
6
7
8
9
10
11
12 M/SEC.
PITCH VELOCITY

FIGURE D-7

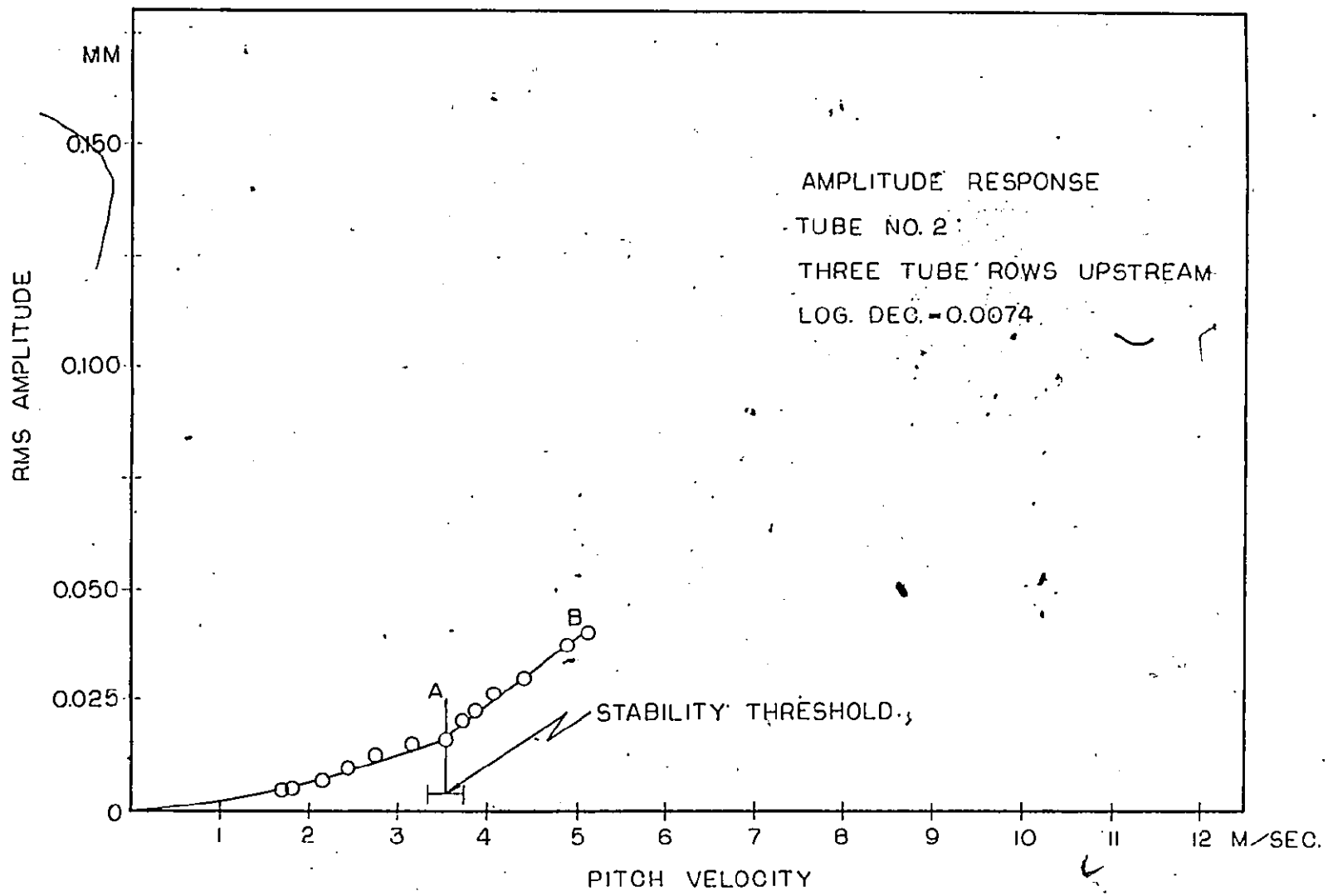
MM
0.150
0.100
0.050
0.025
0
RMS AMPLITUDE
AMPLITUDE RESPONSE
TUBE NO. 2
THREE TUBE ROWS UPSTREAM
LOG. DEC. = 0.0074
A
B
STABILITY THRESHOLD
1
2
3
4
5
6
7
8
9
10
11
12 M/SEC.
PITCH VELOCITY

FIGURE D-8

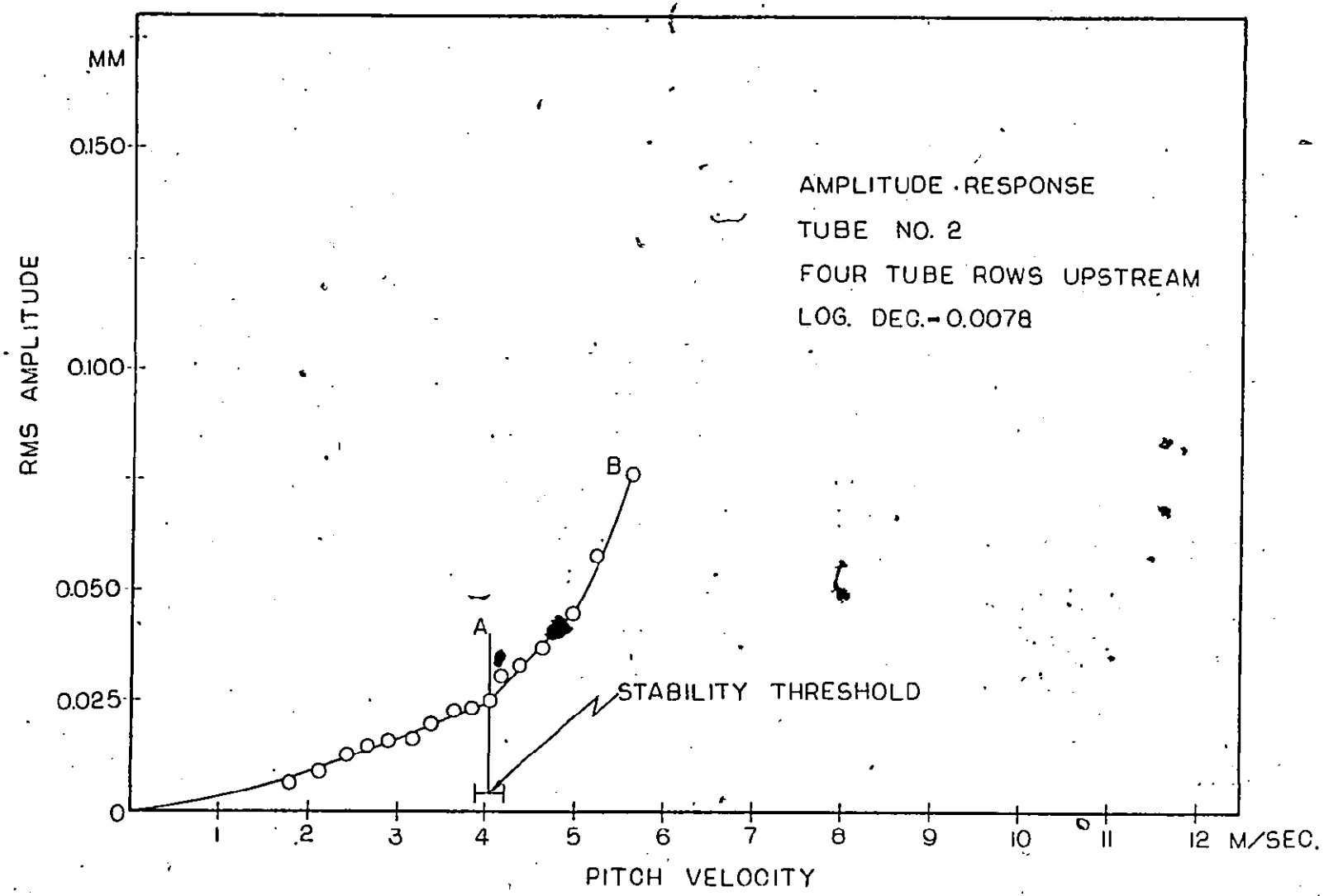
MM
0.150
0.100
0.050
0.025
0
RMS AMPLITUDE
AMPLITUDE RESPONSE
TUBE NO. 2
FOUR TUBE ROWS UPSTREAM
LOG. DEC.-0.0078
B
A
STABILITY THRESHOLD
1
2
3
4
5
6
7
8
9
10
11
12 M/SEC.
PITCH VELOCITY

FIGURE D-9

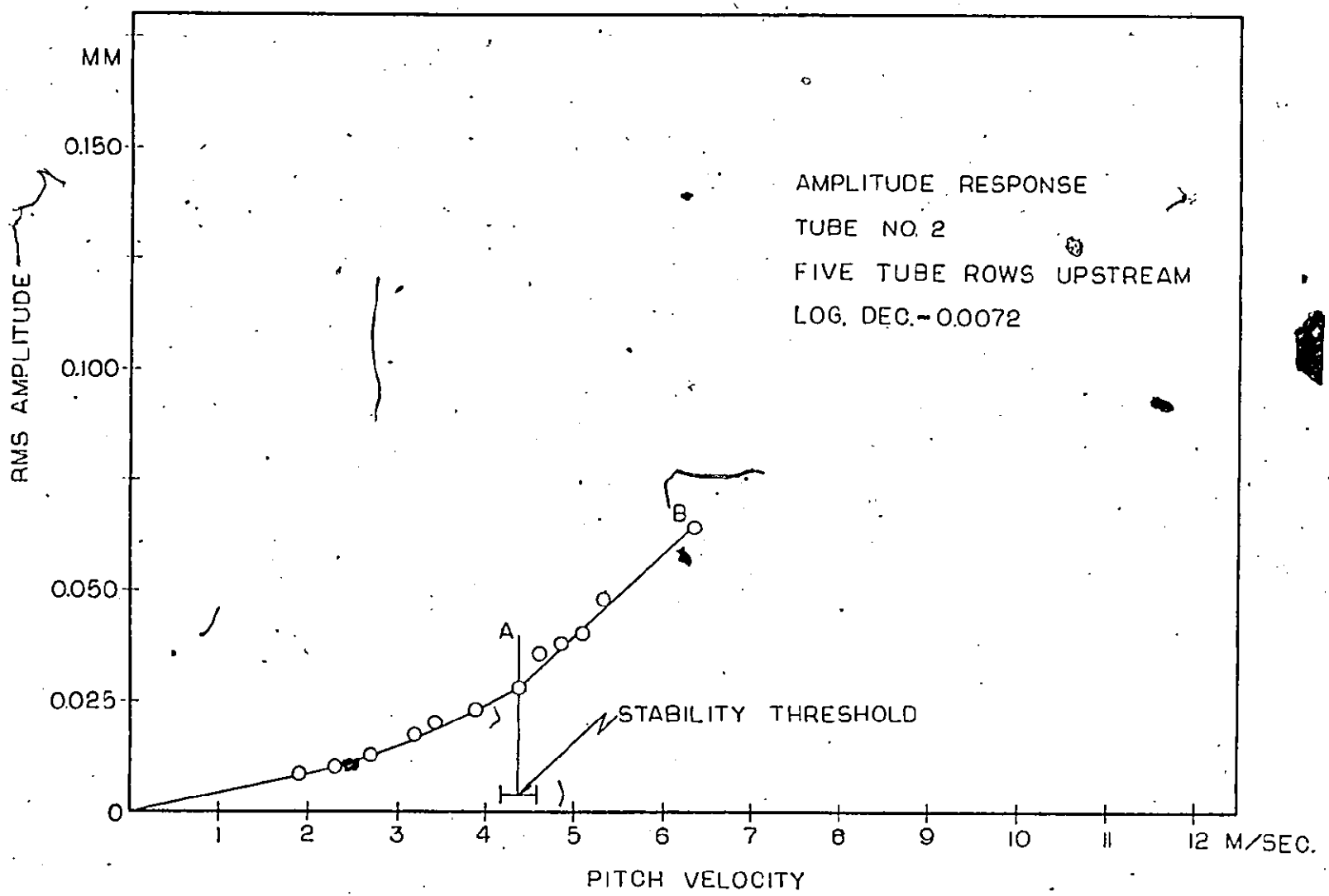
MM
0.150
0.100
0.050
0.025
0
RMS AMPLITUDE
AMPLITUDE RESPONSE
TUBE NO. 2
FIVE TUBE ROWS UPSTREAM
LOG. DEC.-0.0072
A
B
STABILITY THRESHOLD
1
2
3
4
5
6
7
8
9
10
11
12 M/SEC.
PITCH VELOCITY

FIGURE D-10

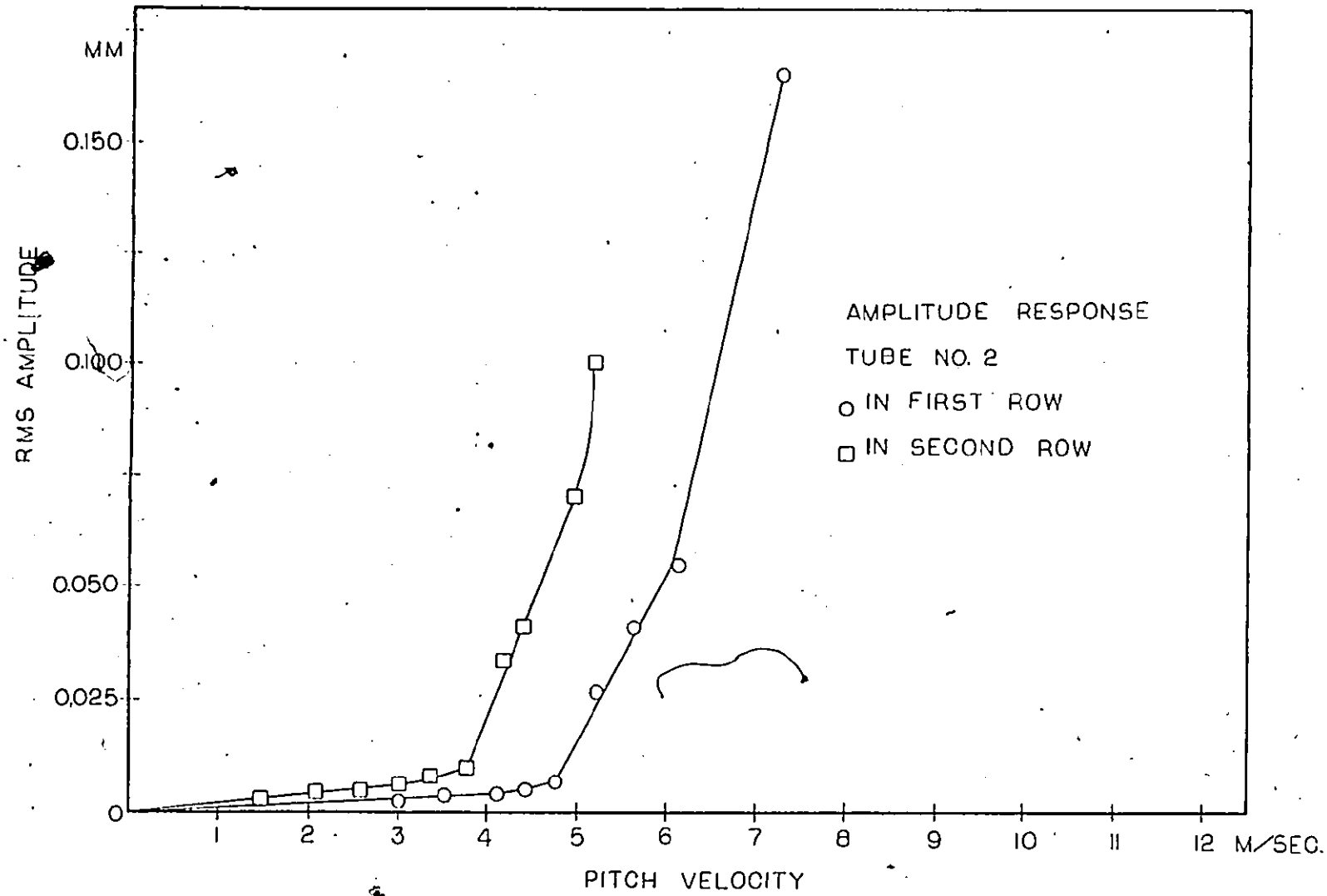
MM
0.150
0.100
0.050
0.025
0
RMS AMPLITUDE
1
2
3
4
5
6
7
8
9
10
11
12 M/SEC.
PITCH VELOCITY
AMPLITUDE RESPONSE
TUBE NO. 2
IN FIRST ROW
IN SECOND ROW

FIGURE D-11

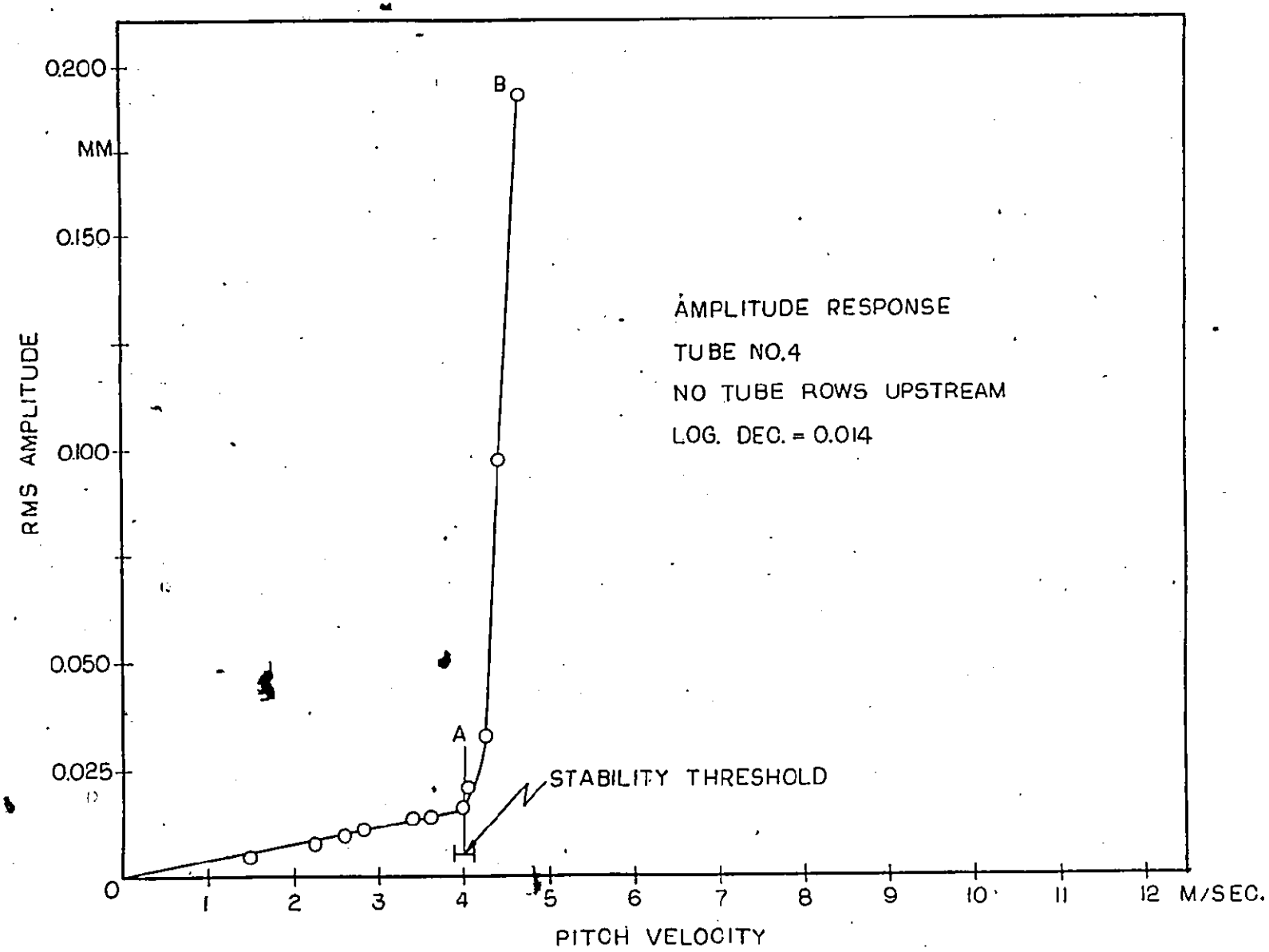
0.200
MM
0.150
0.100
0.050
0.025
0
RMS AMPLITUDE
B
A
AMPLITUDE RESPONSE
TUBE NO.4
NO TUBE ROWS UPSTREAM
LOG. DEC. = 0.014
STABILITY THRESHOLD
1
2
3
4
5
6
7
8
9
10
11
12
M/SEC.
PITCH VELOCITY

FIGURE D-12

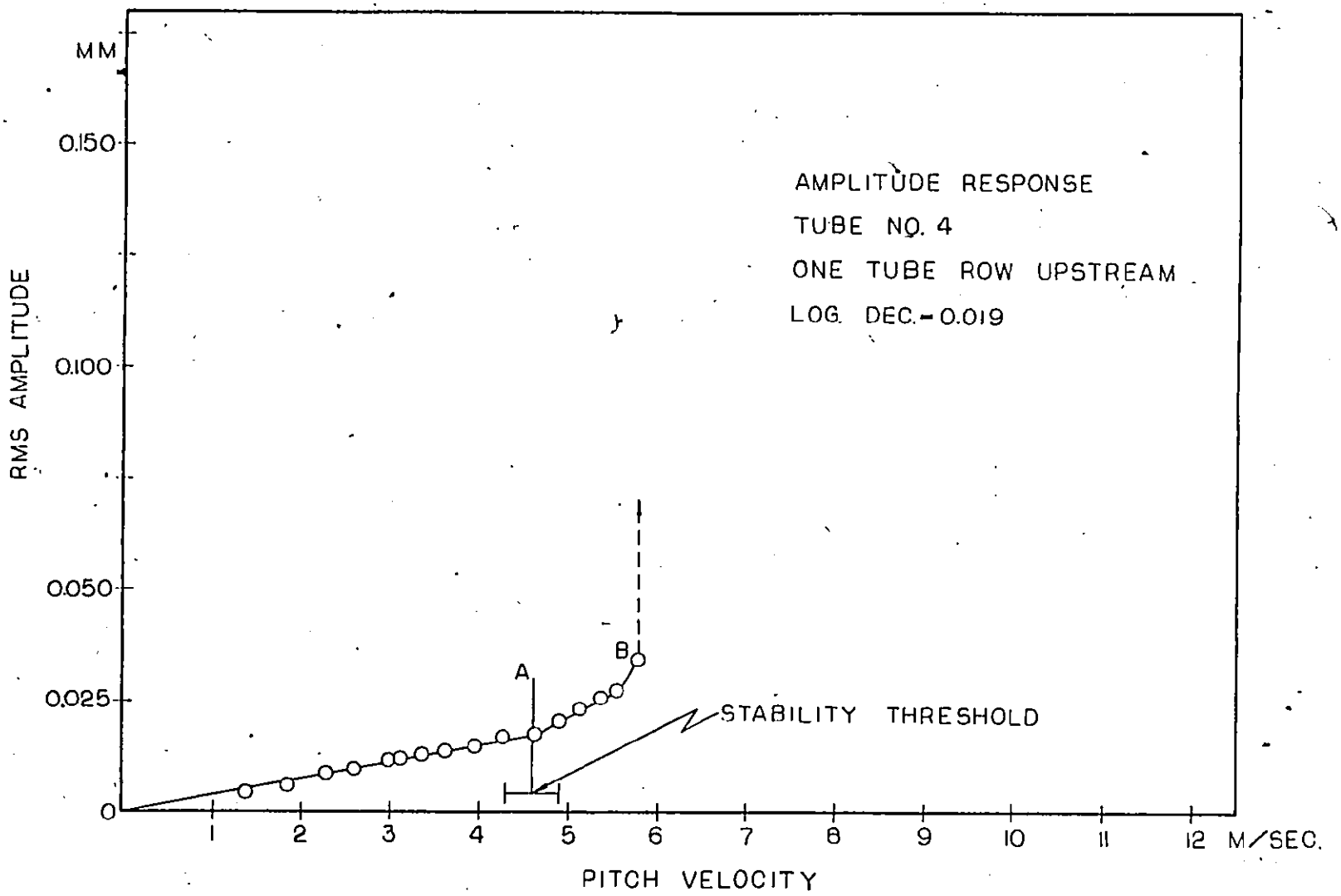
MM
0.150
0.100
0.050
0.025
0
RMS AMPLITUDE
AMPLITUDE RESPONSE
TUBE NO. 4
ONE TUBE ROW UPSTREAM
LOG. DEC. - 0.019
A
B
STABILITY THRESHOLD
1
2
3
4
5
6
7
8
9
10
11
12
M/SEC.
PITCH VELOCITY

FIGURE D-13

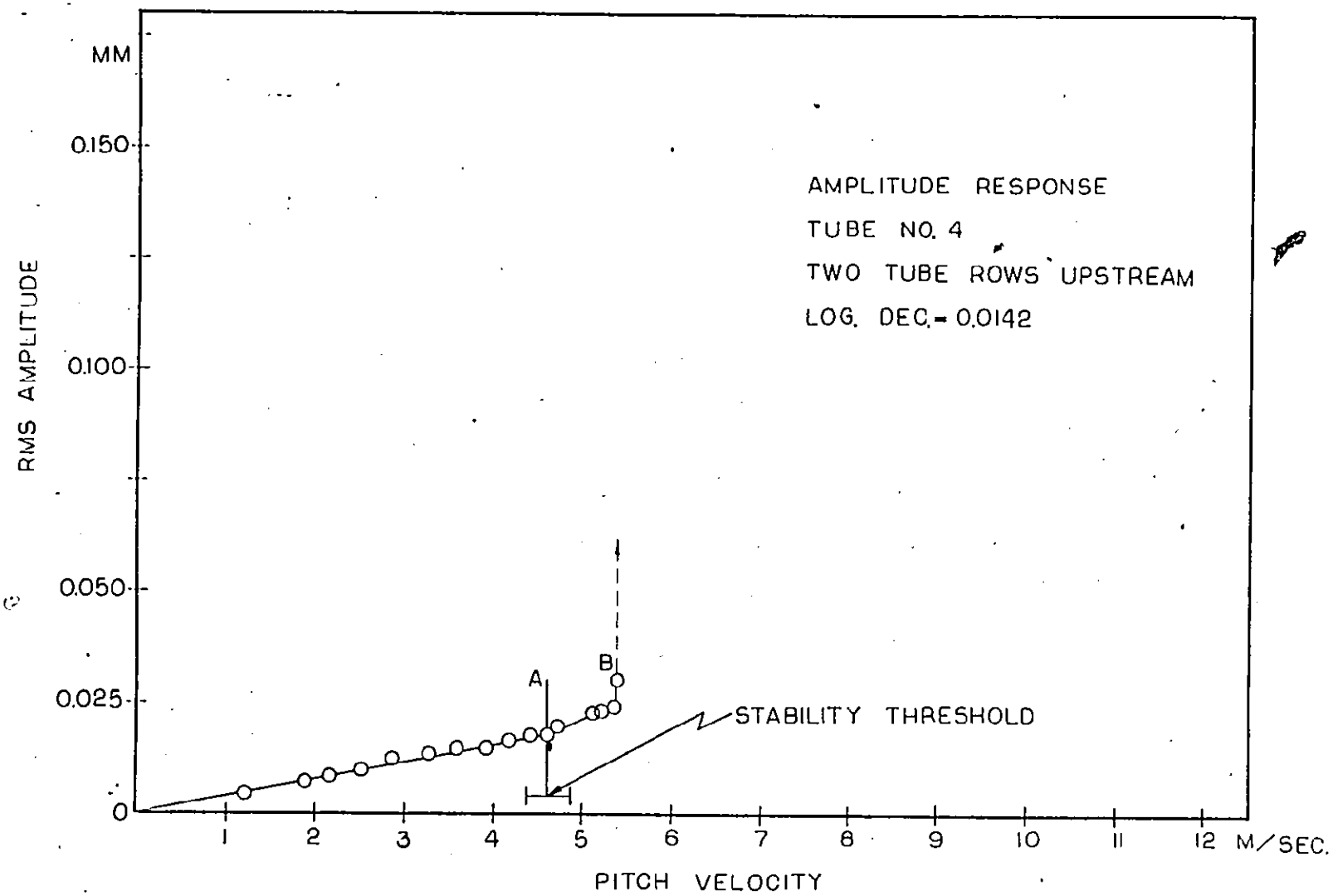
MM
0.150
0.100
0.050
0.025
0
RMS AMPLITUDE
AMPLITUDE RESPONSE
TUBE NO. 4
TWO TUBE ROWS UPSTREAM
LOG. DEC. = 0.0142
A
B
STABILITY THRESHOLD
1
2
3
4
5
6
7
8
9
10
11
12
M/SEC.
PITCH VELOCITY

FIGURE D-14

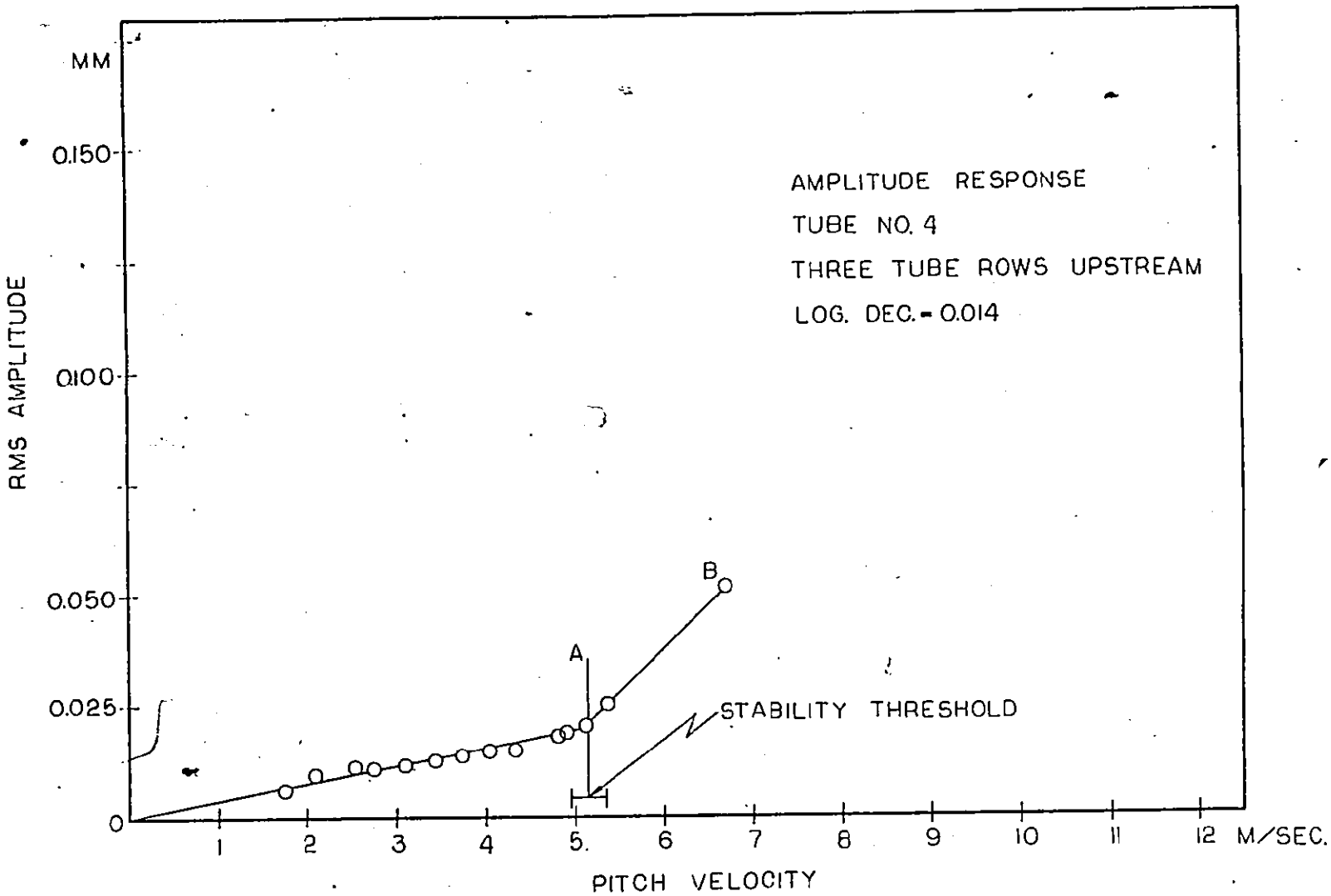
MM
0.150
0.100
0.050
0.025
0
RMS AMPLITUDE
AMPLITUDE RESPONSE
TUBE NO. 4
THREE TUBE ROWS UPSTREAM
LOG. DEC. = 0.014
A
B
STABILITY THRESHOLD
1
2
3
4
5.
6
7
8
9
10
11
12 M/SEC.
PITCH VELOCITY

FIGURE D-15

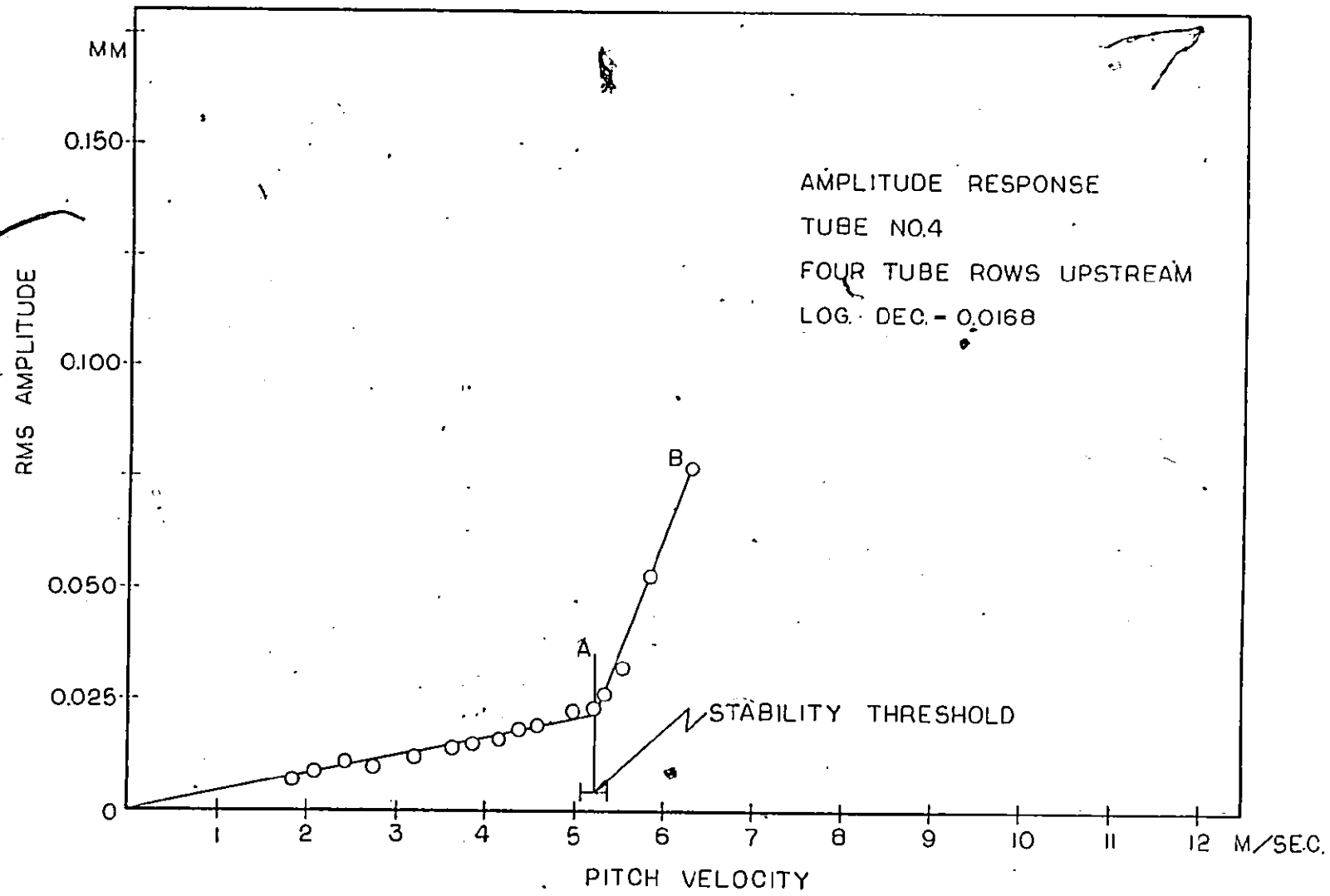
MM
0.150
0.100
0.050
0.025
0
RMS AMPLITUDE
AMPLITUDE RESPONSE
TUBE NO.4
FOUR TUBE ROWS UPSTREAM
LOG. DEC. - 0.0168
A
B
STABILITY THRESHOLD
1
2
3
4
5
6
7
8
9
10
11
12
M/SEC.
PITCH VELOCITY

FIGURE D-16

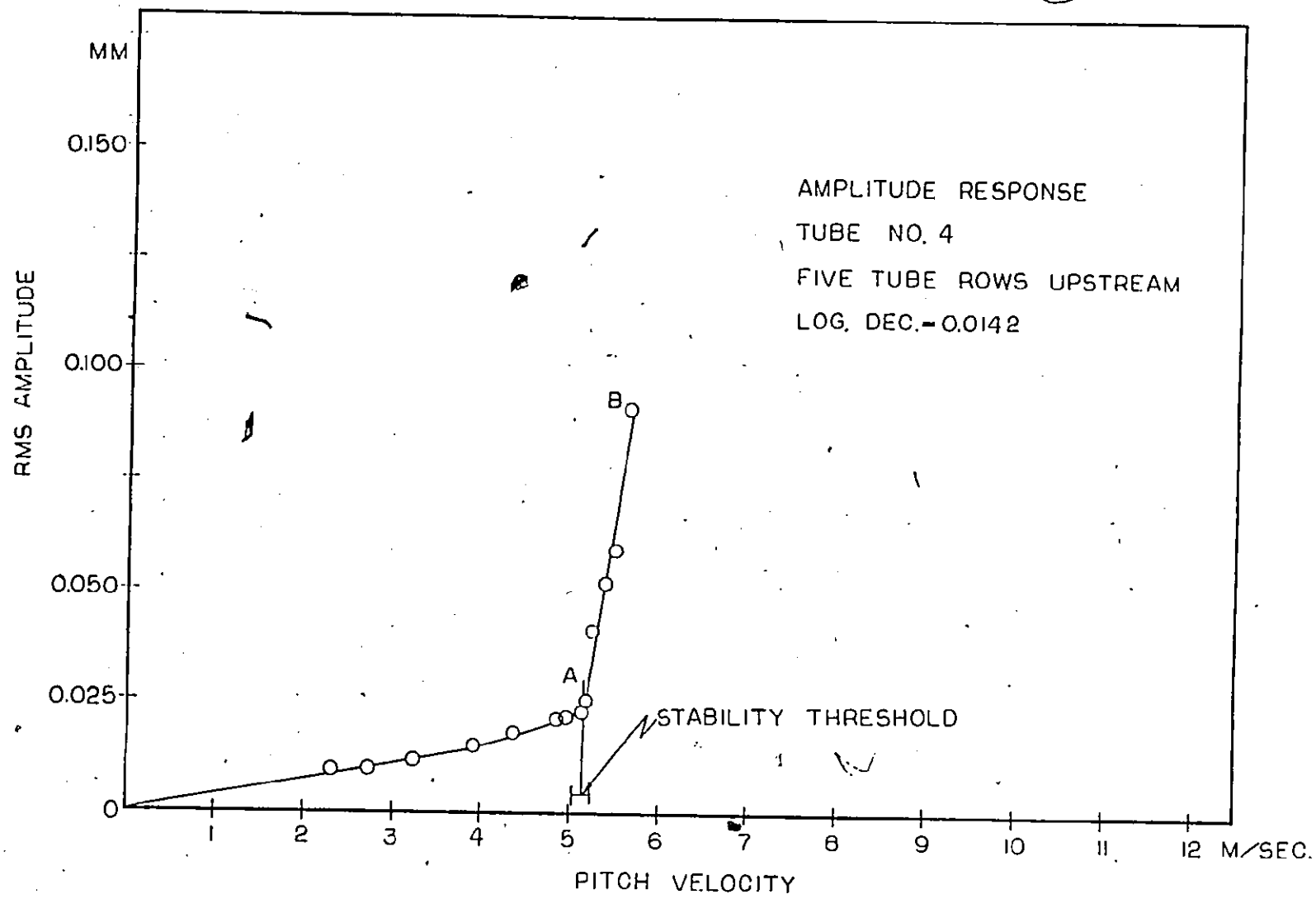
MM
0.150
0.100
0.050
0.025
0
RMS AMPLITUDE
AMPLITUDE RESPONSE
TUBE NO. 4
FIVE TUBE ROWS UPSTREAM
LOG. DEC.=0.0142
B
A
STABILITY THRESHOLD
1
2
3
4
5
6
7
8
9
10
11
12 M/SEC.
PITCH VELOCITY

FIGURE D-17

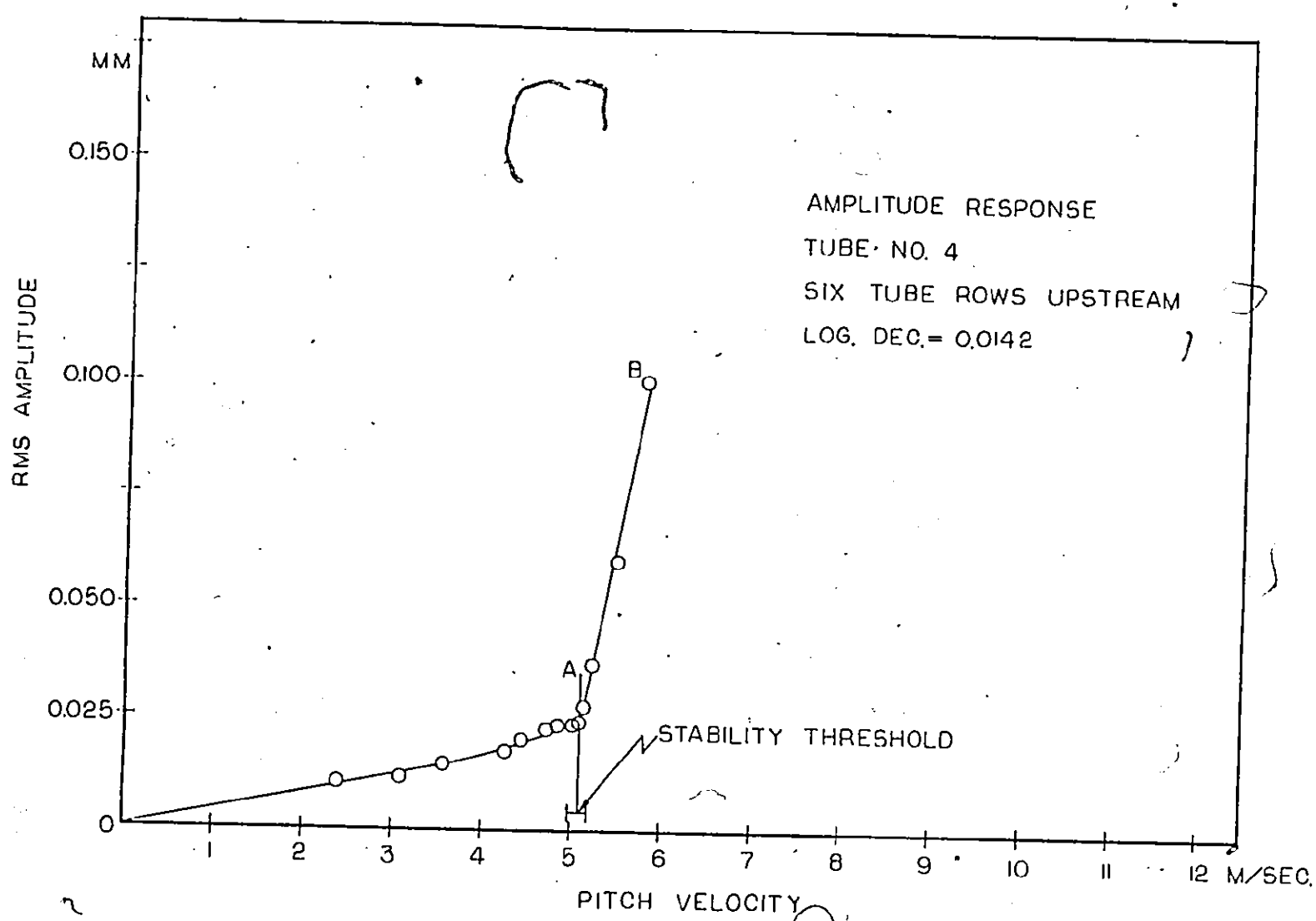
MM
0.150
0.100
0.050
0.025
0
RMS AMPLITUDE
AMPLITUDE RESPONSE
TUBE NO. 4
SIX TUBE ROWS UPSTREAM
LOG. DEC.= 0.0142
B
A
STABILITY THRESHOLD
1
2
3
4
5
6
7
8
9
10
11
12 M/SEC.
PITCH VELOCITY

FIGURE D-18